

**Stoichiometry and carbon dioxide yields from ethanol and
methanol oxidation in electrolysis and fuel cells**

by

Pasha Majidi

A thesis submitted to the School of Graduate Studies in partial fulfillment of

the requirements for the degree of

Doctor of Philosophy

Department of Chemistry

Memorial University

St. John's, Newfoundland

March, 2017

Abstract

With the heavy demand for sustainable fuel sources instead of fossil fuels, fuel cells employing alcohols are becoming more attractive. The high theoretical efficiency (97%) of direct ethanol fuel cells (DEFCs) based on proton exchange membrane (PEM) technology together with the high energy density and availability of bioethanol make DEFCs important as power sources. However, the low faradic efficiency of DEFCs, the poisoning of the anode by adsorbed carbon monoxide (COads) during ethanol oxidation and crossover of fuel from the anode to the cathode are major issues in DEFCs technology.

The main purpose of this research was to improve the faradic efficiency of DEFCs. Therefore, different potential waveforms were applied to an ethanol electrolysis cell with aqueous ethanol supplied to the anode and nitrogen at the cathode, in order to increase the yield of carbon dioxide and therefore increase cell efficiency relative to operation at a fixed potential.

Also, we have developed a novel electrochemical method to measure the average number of electrons generated during oxidation of ethanol to carbon dioxide. The method is based on quantitative oxidation of fuel that crosses through the membrane to avoid the errors that would otherwise result from crossover. It is useful for rapid screening of catalysts, and allows performances (polarization curves) and n-values to be determined simultaneously under well controlled transport conditions. This method was also used for determination of n values for a cell in anode polarization mode and a real fuel cell.

Acknowledgments

I would first like to express my sincere gratitude to my supervisor Dr. Peter Pickup for his continuous support throughout my program. His patience, motivation, enthusiasm and immense knowledge have made my PhD an enjoyable and unforgettable experience. I could not have asked for a better advisor for my program.

I would like to thank my supervisory committee, Dr. Graham Bodwell and Dr. Christina Bottaro for the advice, support and time they have dedicated throughout my program.

I acknowledge the support staff especially the staff members of C-CART and the technicians working out of the Department of Chemistry. I would also like to thank the administration and physical science store staff for their help. I thank Dr. Reza Moghaddam and Dr. Ehab El-Sway for sharing their knowledge with me. I also thank Pickup group for all of their supports as well.

I would like to extend my sincere gratitude to the funding agencies that made my program possible: School of Graduate Studies, the Chemistry Department and NSERC.

I would like to thank all of my friends in Newfoundland during my PhD for their supports and companions. Most importantly, my deepest appreciation to my parents and brothers who helped and encouraged me during my PhD. They are whom taught me the true value of hard work and its price. I thank all my family members and friends in Canada as well, especially Shirin Khosravaneh (my aunt), Mikhael Missakabo and Fred Batterman for their daily supports in my life.

Finally, I would like to dedicate my thesis to all scientists and people around the world whom devoted their lives and knowledge to enhance mankind understandings about the world.

People such as Pythagoras, Socrates, Nasir al-Din al-Tusi, Galileo Galilei, Sir Isaac Newton, Antoine Lavoisier, Carl Fredrick Gauss and so many other great names who devoted their lives to shed light on our darkness.

Table of Contents

| | |
|--|-----|
| Abstract | ii |
| Acknowledgments | iii |
| List of Tables | ix |
| List of Figures | xi |
| List of Abbreviations | xiv |
| List of Symbols | xvi |
| Introduction | 1 |
| 1.1 Introduction | 2 |
| 1.2 Proton Exchange Membrane (PEM) Fuel Cell | 7 |
| 1.2.1 Nafion Membrane | 8 |
| 1.3 Direct Methanol Fuel Cells (DMFCs) | 13 |
| 1.4 Direct Ethanol Fuel Cells (DEFCS) | 15 |
| 1.4.1 Oxygen Reduction Reaction (ORR) | 17 |
| 1.4.2 Ethanol Oxidation Reaction (EOR) | 18 |
| 1.4.3 Effect of Pt alloys on EOR | 20 |
| 1.4.4 Incomplete EOR | 23 |
| 1.4.5 Fuel Crossover | 25 |
| 1.5 Fuel Cell Performance | 27 |
| 1.6 Project goal | 35 |

| | |
|--|----|
| References..... | 37 |
| Experimental | 49 |
| 2.1. Chemicals and Materials | 50 |
| 2.2 Preparation of electrodes and Nafion membranes..... | 50 |
| 2.3. Electrochemical Measurements..... | 51 |
| 2.4. CO ₂ Analysis Instrumentation | 52 |
| 2.4.1. Nondispersive Infrared (NDIR) Carbon Dioxide Detector ⁵⁻⁷ | 52 |
| 2.5 Methanol analysis | 53 |
| References,..... | 55 |
| Improving Carbon Dioxide Yields and Cell Efficiencies for Ethanol Oxidation by Potential | |
| Scanning..... | 56 |
| 3.1 Introduction..... | 58 |
| 3.2 Experimental | 62 |
| 3.2.1 Chemicals and materials | 62 |
| 3.2.2 The cell | 63 |
| 3.2.3 CO ₂ analysis | 63 |
| 3.3 Results and discussion..... | 64 |
| 3.3.1 Potential cycling vs. fixed potential at ambient temperature | 64 |
| 3.3.2 Effects of potential limits at ambient temperature | 70 |
| 3.3.3 Operation at elevated temperatures | 75 |

| | |
|---|-----|
| 3.3.4 PtRu Anode Catalyst..... | 79 |
| 3.4 Conclusions..... | 83 |
| References,..... | 84 |
| Sinusoidal Potential Cycling Operation of a Direct Ethanol Fuel Cell to Improve Carbon | |
| Dioxide Yields | 88 |
| 4.1 Introduction..... | 90 |
| 4.2 Experimental | 91 |
| 4.3 Results and discussion..... | 92 |
| 4.4 Conclusions..... | 100 |
| References..... | 101 |
| Determination of the Average Number of Electrons Released During the Oxidation of Ethanol | |
| in a Direct Ethanol Fuel Cell..... | 104 |
| 5.1. Introduction..... | 106 |
| 5.2. Experimental | 108 |
| 5.3. Modeling | 109 |
| 5.4. Results and discussion..... | 112 |
| 5.4.1. Methanol oxidation | 112 |
| 5.4.2. Ethanol oxidation | 118 |
| 5.5. Conclusions..... | 121 |
| References..... | 122 |

| | |
|---|-----|
| Determination of the Efficiency of Methanol Oxidation in a Direct Methanol Fuel Cell..... | 125 |
| 6.1 Introduction..... | 126 |
| 6.2 Experimental | 130 |
| 6.3 Result and discussion | 130 |
| 6.3.1 Crossover mode..... | 130 |
| 6.3.2 Anode polarization mode | 135 |
| 6.3.3 Operation of the cell as a fuel cell..... | 140 |
| 6.4 Conclusion | 143 |
| References..... | 145 |
| Summary and future work..... | 148 |
| 7.1 Summary | 149 |
| 7.2 Future work | 150 |
| References,..... | 152 |

List of Tables

| | |
|--|----|
| 3.1 Summary of data for the electrolysis of 0.1 M ethanol at ambient temperature at a Pt black anode under potential cycling conditions. The lower potential limit was 0.1 V. | 72 |
| 3.2 Summary of data for the electrolysis of 0.1 M ethanol at ambient temperature at a Pt black anode under potential cycling conditions. The upper potential limit was 0.9 V. ^a Power consumption for an EEC. Not meaningful when negative cell potentials were employed. ^b Values differ from those in Table 3.1 because this is a different data set for a different MEA. | 74 |
| 3.3 Effects of temperature on cell performance parameters for the electrolysis of 0.1 M ethanol at ambient temperature at a Pt black anode for potential cycling between 0.1 V and 0.7 V at 10 mV s ⁻¹ | 77 |
| 3.4 Average currents and CO ₂ yields for the electrolysis of 0.1 M ethanol at 80 °C at a Pt black anode under sweep (10 mV s ⁻¹) and hold, and potential cycling (100 mV s ⁻¹) conditions. The lower potential limit was 0.1 V. (-) results too uncertain to report | 78 |
| 3.5 Average currents and CO ₂ yields for the electrolysis of 0.1 M ethanol at 80 °C at a PtRu black anode under sweep (10 mV s ⁻¹) and hold, and potential cycling (10 mV s ⁻¹) conditions. The lower potential limit was 0.1 V | 81 |
| 4.1 Summary of data for operation of a DEFC at 80 °C at constant potential and under AC potential cycling conditions. Currents and yields are averages after 900 s of operation. | 97 |

| | |
|--|-----|
| 5.1 Apparent n_{av} values from two point fits to eq. 13 with a high flow rate of 0.5 mL min ⁻¹ as a function of the second (lower) flow rate, for 0.1 M methanol and ethanol solutions at 50 °C | 117 |
| 5.2 n_{av} and I_{lim} results, from currents at 0.02 and 0.5 mL min ⁻¹ , for ethanol oxidation under a variety of operating conditions. Averages with standard deviations are for 2 or 3 measurements on different days | 120 |
| 6.1 Theoretical and experimental results for I_{lim} , $C_{exhaust}$ and n_{av} for 50 and 100 mM MeOH at two different flow rates at 50 °C and 0.7 V | 134 |
| 6.2 Theoretical and experimental results for I_{lim} , $C_{exhaust}$ and n_{av} for 21.9 mM and 111 mM MeOH at two different flow rates at 50 °C and 0.7 V for the cell in anode polarization mode | 137 |
| 6.3 Theoretical and experimental results for I_{lim} , $C_{exhaust}$ and n_{av} for 21.9 mM MeOH at different flow rates at 50 °C and 0.35 V for the cell in anode polarization mode | 139 |
| 6.4 Theoretical and experimental results for I_{lim} , $C_{exhaust}$ and n_{av} for 21.25 mM MeOH at two different flow rates at 50 °C for a fuel cell with two different potentials | 142 |

List of Figures

| | | |
|-------------|--|----|
| 1.1 | Schematic diagram of MEA for the PEMFC that is used in this project | 8 |
| 1.2 | Chemical structure of Nafion | 9 |
| 1.3 | Grotthus mechanism | 11 |
| 1.4 | Proton conductivity in PEM | 12 |
| 1.5 | A schematic representations of distance of sulfonic groups in PEM. ³ | 13 |
| 1.6 | A schematic of a DEFC | 16 |
| 1.7 | Simplified mechanism for CO oxidation into CO ₂ | 21 |
| 1.8 | CO and M (Pt) molecular orbital formation | 22 |
| 1.9 | The methanol crossover in a DMFC | 26 |
| 1.10 | Schematic polarization curve for a DEFC | 29 |
| 1.11 | Current-Potential cure for the reaction 1.34, assuming $\alpha=0.5$. ⁴ | 31 |
| 1.12 | Tafel plots for fast and slow electrochemical reactions. ⁵ | 32 |
| 1.13 | Schematic of the electrode reactions | 34 |
| 2.1 | Illustration of the three modes of cell operation | 52 |
| 2.2 | Gas chamber tube of a NDIR CO ₂ monitor consisting of an IR lamp, optical filter and IR detector | 56 |
| 3.1 | Schematic diagram of the electrolysis cell and CO ₂ analysis system | 61 |
| 3.2 | Current vs. time plots for electrolysis of 0.1 M ethanol at ambient temperature at a Pt black anode using a linear potential sweep from 0.1 V vs. DHE with a potential hold at the upper limit of 0.9 (dashed), and potential cycling between 0.1 and 0.9 V (solid). Sweep rate = 10 mV s ⁻¹ | 65 |

| | |
|--|------|
| 3.3 CO ₂ concentration vs. time plots for the electrolyses shown in Fig. 2. Data for sweep and hold (dotted) and potential cycling (solid) are shown. Lower potential = 0.1 V; Upper potential = 0.9 V. | 66 |
| 3.4 Apparent CO ₂ yields vs. time for electrolysis of 0.1 M ethanol at a Pt black anode during potential cycling between 0.1 V and 0.7 V at ambient temperature, 50 °C and 80 °C. | .767 |
| 3.5 Current vs. time plots for electrolysis of 0.1 M ethanol at 80 °C at a PtRu black anode using a linear potential sweep from 0.1 V vs. DHE with a potential hold at the upper limit of 0.6 V (dashed), and potential cycling between 0.1 and 0.6 V (solid). Sweep rate = 10 mV s ⁻¹ | 80 |
| 3.6 CO ₂ concentration vs. time plots for the electrolyses shown in Fig. 5. Data for sweep and hold (dashed) and potential cycling (solid) are shown. Lower potential = 0.1 V; Upper potential = 0.6 V. | 80 |
| 4.1 Cell potential (solid) and current (dotted) vs. time plots for operation of a DEFC at 80 °C under AC potential cycling conditions. Potential bias = 0.4 V; frequency = 0.1 Hz; amplitude = 0.1 V rms | 92 |
| 4.2 CO ₂ concentration vs. time plots for the combined anode and cathode exhaust streams from a DEFC at 80 °C at a constant potential of 0.4 V (dotted) and under AC potential cycling conditions (solid; bias = 0.4 V; frequency = 0.1 Hz; amplitude = 0.1 V rms | .94 |
| 4.3 Polarization curve (■; current averaged over 1 min after 4 min at each potential) and current vs. potential for AC potential cycling (dotted; potential | |

| | |
|--|-----|
| bias = 0.4 V; frequency = 0.1 Hz; amplitude = 0.1 V rms. | .96 |
| 4.4 Theoretical relationships between faradaic efficiency and CO ₂ yield at acetaldehyde (AL): acetic acid (AA) ratios of 1.0 (solid), 0.5 (dotted), and 0 (dashed) | .98 |
| 5.1 Schematic cross-sections of the cell along the fuel flow field (top) and across a channel in the fuel flow field (bottom) | 110 |
| 5.2 Polarization curves for oxidation of 0.1 M methanol (□) and 0.1 M ethanol (■) at 50 °C | 113 |
| 5.3 Calculated (eq. 13 with $I_{lim}/C_0 = 0.3 \text{ A M}^{-1}$) current vs. flow rate curves and experimental data for 0.1 M methanol at 50 °C | 114 |
| 5.4 Calculated (eq. 5.9) concentration profiles for selected flow rates with $C_0 = 0.1 \text{ M}$, $I_{lim} = 30 \text{ mA}$ and $n_{av} = 6$ | 115 |
| 5.5 Current vs. flow rate for oxidation of 0.1 M ethanol at 50 °C (points) and best fit curve calculated by using eq. 13 with $I_{lim}/C_0 = 0.198 \text{ A M}^{-1}$ and $n_{av} = 4.23$ | 118 |
| 6.1 Illustration of the three modes of cell operation used in chapter 6 | 129 |
| 6.2 Anode polarization curves for the oxidation of 111 mM and 21.9 mM methanol at 50°C in the cell configurations in Fig. 6.1B. The methanol flow was 0.5 mL min ⁻¹ | 136 |
| 6.3 Fuel cell polarization curves for the oxidation of 21.25 mM methanol at 50°C in the cell configurations in Fig. 6.1C. The methanol flow was 0.5 mL min ⁻¹ . The cathode was purged with air. | 141 |

List of Abbreviations

| | |
|-------|---------------------------------|
| AA | Acetic acid |
| AAL | Acetaldehyde |
| AC | Alternating current |
| AFC | Alkaline fuel cell |
| AOR | Alcohol oxidation reaction |
| CFP | Carbon fiber paper |
| CV | Cyclic voltammetry |
| DAFC | Direct alcohol fuel cell |
| DEFC | Direct ethanol fuel cell |
| DFAFC | Direct formic acid fuel cell |
| DHE | Dynamic hydrogen electrode |
| DMFC | Direct methanol fuel cell |
| EEC | Ethanol electrolysis cell |
| EOR | Ethanol oxidation reaction |
| EW | Equivalent weight |
| FCEB | Fuel cell electronic bus |
| HFC | Hydrogen fuel cell |
| HOR | Hydrogen oxidation reaction |
| IR | Infrared |
| LSV | Linear sweep voltammetry |
| MEA | Membrane and electrode assembly |

| | |
|-------|------------------------------------|
| MOR | Methanol oxidation reaction |
| NDIR | Nondispersive infrared |
| OCP | Open circuit potential |
| ORR | Oxygen reduction reaction |
| PEFC | Polymer electrolyte fuel cell |
| PEM | Proton exchange membrane |
| PEMFC | Proton exchange membrane fuel cell |
| RT | Room temperature |

List of Symbols

| | |
|----------------------|--|
| α | Charge transfer coefficient |
| δ | Diffusion layer thickness |
| C | Concentration |
| D | Diffusion coefficient |
| E° | Standard potential |
| E | Potential |
| E_{rev} | Reversible cell potential |
| ε_{rev} | Theoretical efficiency |
| ε_E | Potential efficiency |
| ε_F | Faradic efficiency |
| ε_{cell} | Efficiency of the cell |
| F | Faraday constant |
| f | Flux |
| G | Gibbs free energy |
| H | Enthalpy |
| h | The height of the flow channel |
| I | Intensity of the light striking the detector |
| I_0 | Measured intensity of the light |
| I_{lim} | The limiting current |
| i | Current |
| i_0 | Exchange current |

| | |
|----------|---|
| j | Current density |
| k | System dependent constant |
| l | The thickness of the membrane |
| η | Overpotential |
| n | Electrons transferred in a reaction |
| n_{av} | Average number of electrons released in fuel oxidation reaction |
| N | Moles of product |
| u | Flow rate |
| Q | Charge |
| R | Gas constant |
| S | Entropy |
| σ | Conductivity |
| τ | Efficiency |
| t | Time |
| T | Temperature |
| V_0 | Volume |
| x | Distance through the flow field |
| w | The width of the flow plate |

Chapter 1

Introduction

1.1 Introduction

Humankind is facing many challenges with the use of fossil fuels. The first and foremost is global warming due to greenhouse gases such as carbon dioxide (CO₂). CO₂, which is the main product of the consumption of gasoline and other fossil fuels, can increase the temperature of our planet's atmosphere.¹ Also, the exploitation and purification of fossil fuels may cause other environmental problems. Therefore, it is reasonable to search for alternative kinds of energy sources. One attractive alternative source of clean energy production is fuel cells. In fuel cell technology, which has been a prime focus of many research groups around the world, the electrochemical oxidation of a fuel such as hydrogen,²⁻⁴ methanol,⁵⁻⁸ or ethanol⁹⁻¹¹ is the source of energy production. Although energy generation from methanol and ethanol are relatively new, energy production from hydrogen in fuel cells has been studied for a long time.

The idea of energy production from the electrochemical oxidation of hydrogen was developed by William Grove in 1839, who demonstrated that when hydrogen and oxygen were fed to two platinum electrodes in a separated electrolyte, current was produced.¹²

Ludwig Mond and Carl Langer developed experiments with a hydrogen fuel cell that generated 6 A per square foot at 0.73 V. They used an electrolyte soaked up by a porous non-conducting material.¹³ Although more than 150 years have passed since Grove's and Mond's fuel cells, until recently there have been only a few efforts for the commercialization of fuel cells. In the first half of the 20th century, there were some individual attempts to evolve the idea of fuel cells and power production from fuel cells. For instance, Francis Bacon demonstrated a fuel cell with a hydrogen / oxygen redox system using alkaline electrolytes and nickel electrodes in 1932.¹² Harry Karl Ihrig made a tractor with a 20-horsepower (15 kW)

fuel cell in the same year.¹⁴ However, the turning point in the fuel cell industry was the early 1960s, when NASA utilized a polymer electrolyte membrane fuel cell (PEMFC) for the Gemini space program and an alkaline fuel cell (AFC) for the Apollo program for energy production purposes.^{15, 16} Since 1961, fuel cells have been used as supplementary power sources in many space programs. However, despite these developments, no market was found for fuel cells. In the last decade of the 20th century, due to global warming awareness, resource problems, and international rules such as Zero Emission Mandates, authorities forced industries to switch to electric vehicles (EVs) with a supplementary fuel-cell power source. At the end of the 1990s, many vehicle companies around the globe started to develop fuel cell-EVs as their products. Today, not only is energy production from fuel cells growing for transportation but fuel cells have also become energy sources for residential heat and power.^{17,}

18

Most of the fuel cells described earlier were based on solid polymer electrolytes. Proton exchange membrane fuel cells (PEMFCs) are a type of solid polymer fuel cell that can produce high power densities. The key part of a PEMFC is a proton-exchange membrane that is responsible for the movement of hydrogen ions from the anode to the cathode. Oxidation of fuel at the anode produces hydrogen ions (H^+). The membrane that is placed between the electrodes allows hydrogen ions to migrate from the anode to the cathode (proton conduction). This structure allows a simple and compact fuel cell for energy production.

By the end of the 1960s, the DuPont Company developed a perfluorosulfonic acid membrane called “Nafion[®]”. Nafion has many advantages such as higher conductivity and greater lifespan other ion-exchange membranes.^{19, 20} Due to these superior characteristics, Nafion has become the main part of PEMFCs. Moreover, due to the high durability of Nafion

membrane in acidic media, direct alcohol fuel cells (DAFCs) have become an alternative source in the production of clean energy.²¹

The hydrogen fuel cell (HFC) is the first fuel cell that was studied. The simple anodic and cathodic reactions of HFCs at high thermodynamic potential (1.23 V) have made HFCs fashionable systems for power and heat production. For instance, in the United States, legislators authorized the National Fuel Cell Bus program in 2006 to address the demands for commercialization of fuel cell electric buses (FCEBs). In the summer of the same year, 18 FCEBs were operative at six different locations in the U.S.²² For the Winter Olympics of 2010, the BC transit system used a fleet of 20 New Flyer buses with the Ballard fuel cells. In China, Korea and Japan, many automotive industries are developing their transportation systems with fuel cell technologies.²³ Despite the hazardous issues involved with hydrogen storage, use of liquid hydrogen can make HFCs a reliable alternative heating source. Some studies in the UK are showing that utilizing fuel cells that are powered by hydrogen from gas networks can decrease the cost of heat generation at peak demand times.^{17, 24}

Direct alcohol fuel cells (DAFCs) have the same structure as hydrogen fuel cells. A membrane (Nafion) divides two electrodes from each other. However, instead of the oxidation of hydrogen at the anode, the oxidation of low molecular weight alcohols such as methanol, ethanol and recently ethylene glycol takes place at the anode²⁵⁻²⁷ in DAFCs. During the same process, the reduction of oxygen happens at the cathode.

Energy and current production from direct methanol fuel cells (DMFCs) has been at the centre of studies for a long time. The energy density of methanol is 6.09 kWh kg⁻¹. This value, which is reasonably close to the energy density of gasoline (10 kWh kg⁻¹), can make methanol an attractive alternative power source.²⁸ In DMFCs, oxidation of methanol to carbon

dioxide and hydrogen ions occurs at the anode. Then, protons migrate from the anodic solution to the cathodic through the ion-exchange membrane (Nafion). At the cathode, the reduction of oxygen to water takes place. The thermodynamic reversible potential of methanol oxidation is close to the equilibrium potential of hydrogen:



However, in comparison to oxidation of hydrogen, methanol oxidation to carbon dioxide has very sluggish kinetics.²⁹ This is largely due to the formation of carbon monoxide at the surface of the platinum catalyst, which is called the poisoning of platinum by carbon monoxide.³⁰ Many research groups have studied the methanol oxidation reaction (MOR) to enhance the direct oxidation of methanol to carbon dioxide without formation of intermediate species such as carbon monoxide.³¹⁻³⁴ According to many studies, platinum (Pt) alloys with secondary metals such as Ru,^{35, 36} Sn,^{37, 38} and Rh^{39, 40} can decrease platinum poisoning. Poisoning of platinum is not the only issue for DMFCs. Also, use of methanol in fuel cell has been the centre of debate due to its toxicity, since methanol is a hazardous compound for human life and nature. Although the lethal dose of methanol for humans is not known, some studies report that the lethal dose is about 100 mL, while some others report a lethal dose as 15 mL of 40% methanol.⁴¹

Presently, due to the disadvantages of methanol that were discussed, energy production from the ethanol oxidation reaction (EOR) and direct ethanol fuel cells (DEFCs) is of growing interest. One of the reasons is related to the high energy density of ethanol. With an energy density of ca. 8 kWh kg⁻¹ (even higher than the energy density of methanol), ethanol has become a promising fuel for the production of clean energy. Also, unlike the transportation and storage of hydrogen, the transportation and storage of ethanol is less hazardous. Moreover,

ethanol can be produced from a wide range biomass and renewable sources, such as feedstocks like corn, grape, sugar cane, sunflowers, and potatoes.

Although there are advantages to use of ethanol, oxidation of ethanol to carbon dioxide is very complex.^{42, 43} Ethanol oxidation involves two commonly accepted pathways. In both pathways, formation of acetaldehyde has a key role. The first pathway involves formation of adsorbed acetaldehyde and then further oxidation of acetaldehyde to acetic acid (partial oxidation of ethanol to acetic acid). In the second pathway, the cleavage of the bond between the carbons in adsorbed acetaldehyde leads to the formation of adsorbed CH_x and CO . Formation of adsorbed CO is followed by oxidation of adsorbed CO to carbon dioxide (complete oxidation of ethanol to carbon dioxide). In the complete oxidation of ethanol to carbon dioxide, the C-C bond in adsorbed acetaldehyde needs to be broken at the surface of platinum. As a result of this C-C bond cleavage, CO and CH_x are formed and cover the surface of the catalyst. Although both carbon monoxide and CH_x oxidize to carbon dioxide at high enough potentials, it has been reported that CH_x at the surface of platinum can also be reduced to methane.^{44, 45} The complete oxidation of ethanol to carbon dioxide generates more electrons than methanol oxidation (12 and 6 electrons for ethanol and methanol, respectively). This high electron generation by ethanol oxidation (EOR) makes DEFC an interesting source for energy production for many proposes such as stationary and portable power sources.^{46, 47}

Acetaldehyde and acetic acid are by-products of the EOR. Therefore, due to the low electron generation in the formation of acetaldehyde (2 electrons) and acetic acid (4 electrons), the efficiency of DEFCs decreases drastically. One of the main aims of ethanol oxidation studies is to find platinum-alloy catalysts to favour the ethanol oxidation through the complete

pathway. These catalysts should also decrease the poisoning of platinum by carbon monoxide.⁴⁸⁻⁵⁰

Although the efficiency of the EOR is an immense issue in DEFCs, crossover of ethanol from the anodic solution to the cathode is another challenge.⁵¹ Ethanol crossover decreases the efficiency of EOR due to the loss of fuel. Also, at the cathode, formation of adsorbates and products by chemical reactions between ethanol and oxygen can affect the electrochemical reduction of oxygen. Moreover, crossover of ethanol to the cathode can cause a “mix-potential”, which leads to a decrease in the cathode potential and cell voltage.⁵² The purpose of thesis reported in this thesis was to find solutions to these problems.

1.2 Proton Exchange Membrane (PEM) Fuel Cell

A fuel cell is a device that converts the chemical energy of a fuel to electricity and heat without combustion. PEMFCs are based on a solid thin layer assembly. The most important parts of a PEMFC is the membrane and electrode assembly (MEA). Fuel cell MEAs have three major components: an anode, a cathode and an electrolyte membrane. At the anode, oxidation of fuel takes place. As a result of the oxidation reaction, electrons are produced and moved from the anode to the cathode via the external circuit. At the cathode, with the presence of the oxidant (O_2) and electrons, reduction occurs. The main role of the membrane is to separate the anode and cathode reactants. Also, the membrane allows the migration of ions (protons that are generated during fuel oxidation) from the anode to the cathode. As discussed earlier, PEMs are the main membranes used widely in DEFCs or DMFCs.⁵³ A schematic diagram of a MEA for a PEMFC is shown in Figure 1.1.

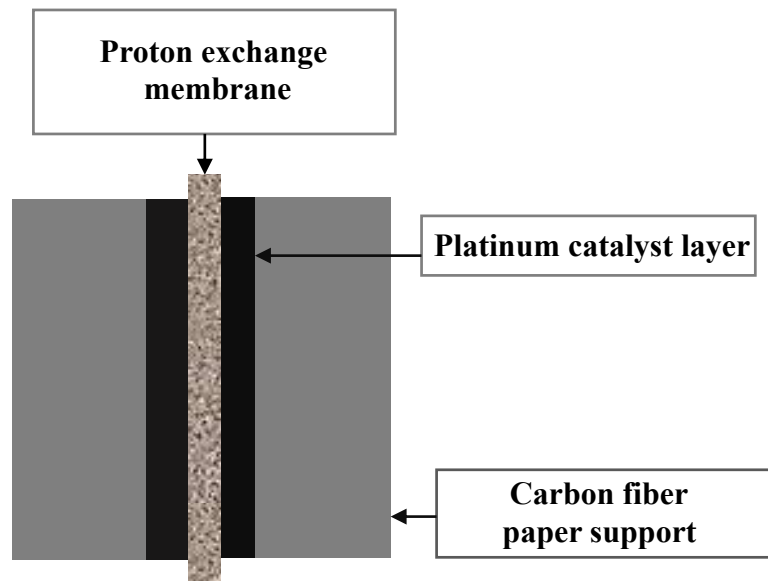


Figure 1.1 Schematic diagram of an MEA for the PEMFC that was used in this project.

1.2.1 Nafion Membrane

Because all of the experiments in this thesis were conducted with a fuel cell with a Nafion membrane, the main focus in this section will be on Nafion and its structure. Nafion is one of the most widely used membranes in PEMFCs. It has two moieties: a hydrophobic backbone (tetrafluoroethylene) as a continuous phase (polymer moiety) and a sulfonic acid ($-\text{SO}_3\text{H}$) domain which provides hydrophilic regions. The hydrophilic regions act as a water reservoir, while the hydrophobic domain is essential for the stability of Nafion. Figure 1.2 shows the chemical structure of Nafion.

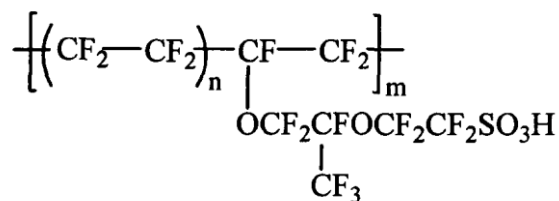


Figure 1.2 Chemical structure of Nafion.

The equivalent weight (EW) or ion exchange capacity of Nafion is defined as grams of dry Nafion per mole of acid groups (sulfonic acid groups) when the polymer is in the acid form.^{54, 55} The relation between EW and n is $\text{EW} = 100n + 446$, where 100 (g/mol) is the molar mass of the tetrafluoroethylene subunit ($-\text{CF}_2\text{CF}_2-$) and 446 (g/mol) is the molar mass of the perfluorovinyl ether sulfonic acid side chains, $\text{C}_7\text{F}_{13}\text{O}_5\text{SH}$. For instance, for a Nafion 117 film, the number 117 refers to 1100 EW ($n=14$) and a thickness of 0.007 inches. In the case of Nafion 115, the number 115 indicates 1100 EW and thickness 0.005 inches.

The main role of the hydrophilic moiety is to transport protons (H^+) from the anode to the cathode. In order to provide high performances, the membrane should have a high proton conductivity, be impermeable to oxygen and fuel (methanol or ethanol), possess a high chemical stability, and also be an electrical insulator.^{12, 56, 57} Generally, a membrane should have excellent characteristics for all of these aspects. However, most PEM (including Nafion) are good in only some of these properties and not all, and contribute significantly to the efficiency losses in fuel cells.

As mentioned above, a key parameter of a PEM is its ability to conduct protons through the membrane. For instance, consider the following oxidation reaction at the anode of a hydrogen fuel cell with a Nafion membrane,



Protons that are produced at the anode must pass through the membrane to reach the cathode. At the cathode, the reduction of oxygen in the presence of electrons and protons takes place. The ability of Nafion to shuttle protons from the anode to the cathode is dependent on the water and acidic content of the Nafion. To understand how these depend on proton exchange, some explanation is needed.

Generally, proton transfer in a PEM occurs through water conduction. When a proton is introduced into an aqueous solution, it leads to the formation of a hydrogen bond with water molecules in the solution. When a new hydrogen bond is formed, the surrounding bonds are weakened (proton defect). As a result of this protonic defect, a contraction of hydrogen bond occurs in the vicinity of the defect. This process leads to movement of a proton from one water molecule to the next water molecule in the solution. This is called the Grotthuss mechanism.⁵⁸

In this mechanism, introduction of a proton would be followed with the formation of a hydrogen bond between the proton and water molecules (Eigen ion, $H_9O_4^+$). This positively charged ion can lose a proton via a cleavage of hydrogen bond to the neighboring water molecule (Zundel ion). As a result, the extra proton moves thorough the solution. The same process occurs in PEMs (Figure 1.3).^{55, 56, 59-61}

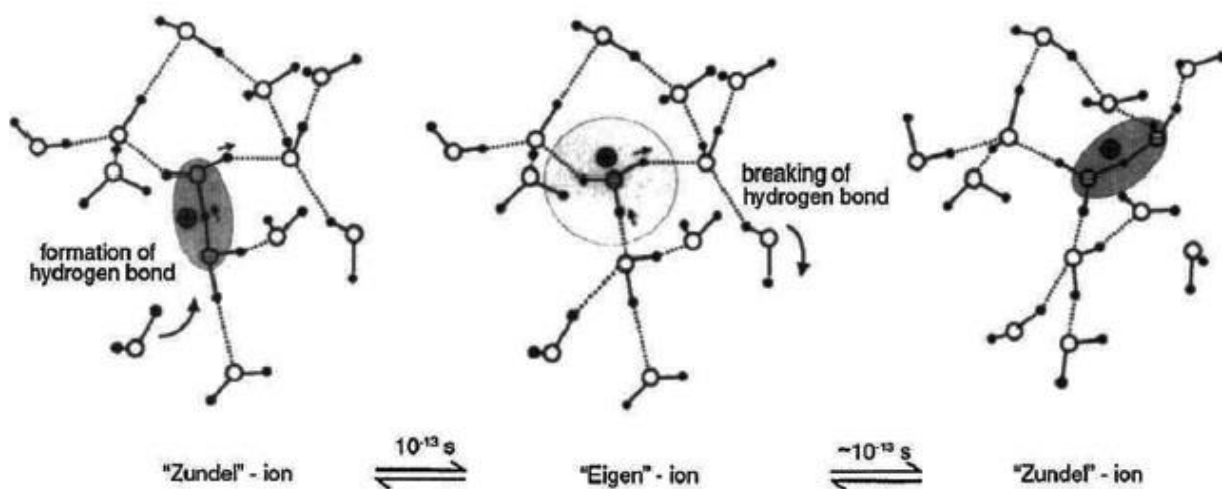


Figure 1.3 Grotthuss mechanism adopted with permission.⁵⁹

In Nafion, proton mobility not only can be explained by the Grotthuss mechanism but also it can be assisted by the diffusion of the hydrogen atom of the sulfonic acid groups.⁶² Therefore, acidic strength governs how easily a proton dissociates from the sulfonate counter-ion. For the dissociation of a proton, which is bound and immobilized in dry Nafion, the presence of water molecules is crucial.⁶³ Water molecules increase the hydrogen dissociation from the sulfonic acid and at the same time, enhance proton transport (from the oxidation of fuel) through the membrane. The ratio of water molecules per sulfonic acid group is expressed by λ . It has been reported that when $\lambda = 3$, effective dissociation of protons occurs. Nonetheless, for complete dissociation, the water content must be higher ($\lambda > 6$), with the ideal λ for Nafion 117 at ambient temperature being $16 < \lambda < 20$.^{64, 65} Based on the role of water molecules in proton transport, it is expected that with higher water contents in the membrane, the conductivity of the membrane would increase. However, with high numbers of water molecules, the sulfonate groups become more diluted. As a result, the conductivity of the membrane would decline.⁶⁶ Thus, the water content of the membrane is an important factor influencing the efficiency of PEM fuel cells (PEMFCs).

Another important factor that governs proton mobility in Nafion is the structure of the polymer (tetrafluoroethylene backbone). As mentioned earlier, the hydrophilic regions (sulfonic acid groups) swell in the presence of water molecules. The swelling of the membrane leads to the formation of channels that allow protons to move through the membrane.⁶⁷

Figure 1.4, below, represents this process.

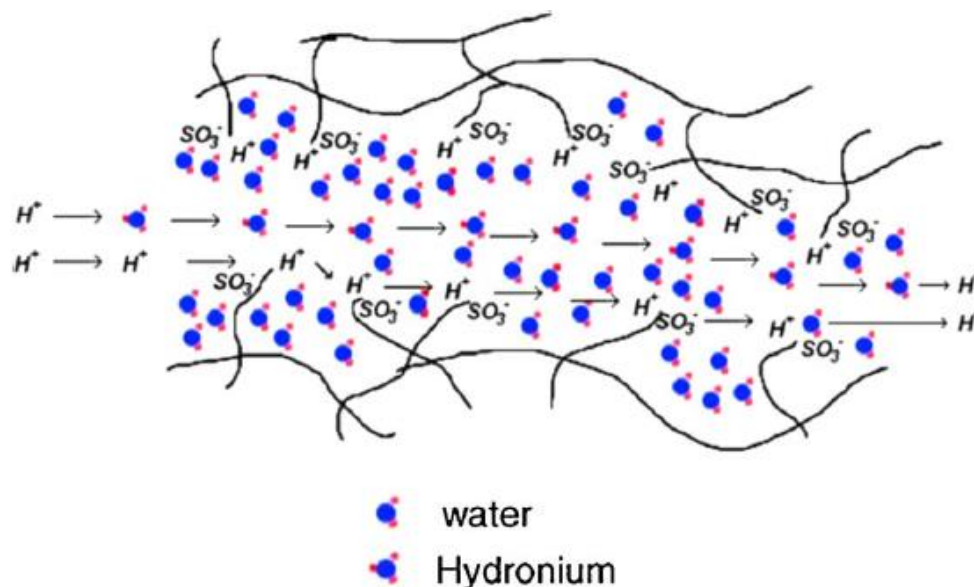


Figure 1.4 Proton conductivity in PEM.⁶⁷

While protons are crossing the membrane via the hydrophilic region, the hydrophobic regions of Nafion maintain structural integrity. Finally, the distance between sulfonic acid groups in the membrane can affect proton mobility. High numbers of sulfonic acid groups, which would lead to low gaps inside the membrane, would increase the conductivity of the membrane due to the fact that more shuttles are provided for introduced protons to traverse through the membrane (see Figure 1.5).^{64, 68-70}

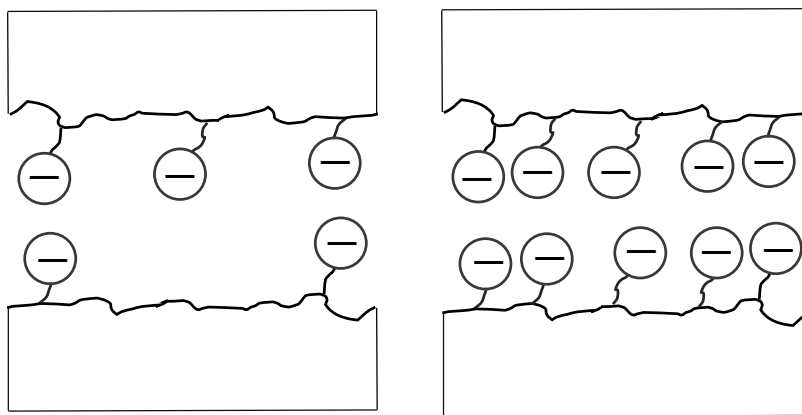


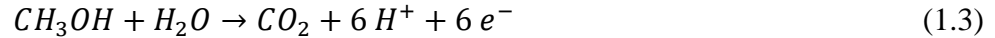
Figure 1.5 Schematic representations of distance between sulfonic acid groups in a PEM (left: Nafion with low numbers of sulfonic acid groups, right: Nafion with high numbers of sulfonic acid groups). Adopted from reference 13.

It is important to note that some other factors, such as temperature and the chemical structure of the polymer chain of the membrane, can also affect proton mobility. The study of these parameters was beyond the scope of this thesis.

1.3 Direct Methanol Fuel Cells (DMFCs)

Although hydrogen in fuel cells is one of the important new means of energy generation, it suffers from many difficulties. Hydrogen storage and transportation are the main problems for fuel cells that use hydrogen as a fuel. Thus, the search for non-hazardous fuels is essential. Alcohols are one of the alternative sources for energy production in FCs. Among those, methanol was the first alcohol to be used in the fuel cell industry. Unlike hydrogen, methanol is liquid at room temperature, and it can be stored easily. Moreover, methanol can be produced from many natural sources, such as feedstocks. Finally, by the usage of methanol in fuel cells, the design and structure of such cells would become smaller than HFCs.^{24, 71-73}

At the anode side of a direct methanol fuel cell, the oxidation of aqueous methanol to carbon dioxide occurs at the surface of a platinum based catalyst. At the cathode, the reduction of oxygen to water takes place. The anodic and cathodic reactions of a DMFC are,



And the overall reaction is,



However, during the complete oxidation of methanol, formation of adsorbed intermediates such as CO can cover the surface of the catalyst, which can inhibit further methanol oxidation to carbon dioxide. Thus, the CO layer at the surface of Pt must be oxidized. Oxidation of CO to CO₂ needs a hydroxyl group (at the surface of platinum) from water dissociation. These multiple steps in the mechanism decrease the kinetics of the methanol oxidation reaction (MOR) greatly in comparison to the hydrogen oxidation reaction (HOR) in hydrogen fuel cells.^{29, 34, 74}

Also, the incomplete oxidation of methanol may lead to the formation of formic acid and formaldehyde, which are the by-products of methanol oxidation. The incomplete oxidation of methanol generates fewer electrons than complete oxidation (4 or 2 electrons for formic acid and formaldehyde, respectively).⁷⁵ Therefore, due to the lower electron production

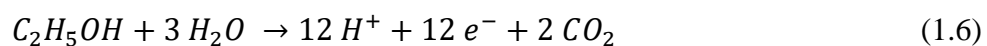
of incomplete oxidation, the efficiency of DMFCs would decrease dramatically in comparison to the complete oxidation of methanol to carbon dioxide.

A major problem of DMFC is methanol crossover from the anode to the cathode. Even at very low concentrations, methanol can cross the membrane. Methanol at the cathode can react chemically with oxygen. This chemical reaction does not produce any Faradaic current, and consumes oxygen; therefore, the efficiency of the cell is decreased.

1.4 Direct Ethanol Fuel Cells (DEFCS)

Oxidation of ethanol can be a good alternative source of energy. Among renewable alcohols, ethanol has some advantages over the others. First, the energy density of ethanol is ca 8.0 kWh kg⁻¹ which is greater than methanol and close to the energy density of gasoline, 6 kWh kg⁻¹ and 10 kWh kg⁻¹, respectively. Moreover, ethanol is a less toxic alcohol that can be produced from a variety of feedstocks such as corn, sugar cane, straw, cotton and other biomass. The high energy density of ethanol corresponds to 12 e⁻ per molecule for the total electrochemical oxidation reaction. To convert this amount of electron generation to energy, electrochemical oxidation of ethanol (EOR) should occur at the anode, while an oxidant gas such as oxygen reduces at the cathode. Pt and Pt alloys can be good electrodes for electrochemical reactions of ethanol.^{76, 77}

The following equation describes the complete electrochemical oxidation of ethanol at the anode:



At the cathode reduction of oxygen takes place as in eq. 1.4. Since, $E^{\circ}_{\text{CO}_2/\text{EtOH}} = +0.084 \text{ V}$ and $E^{\circ}_{\text{H}_2\text{O}/\text{O}_2} = +0.1.229 \text{ V}$ vs. the standard hydrogen electrode, $\Delta E = E^{\circ}_{\text{H}_2\text{O}/\text{O}_2} - E^{\circ}_{\text{CO}_2/\text{EtOH}} = 1.145 \text{ V}$ for the cell.

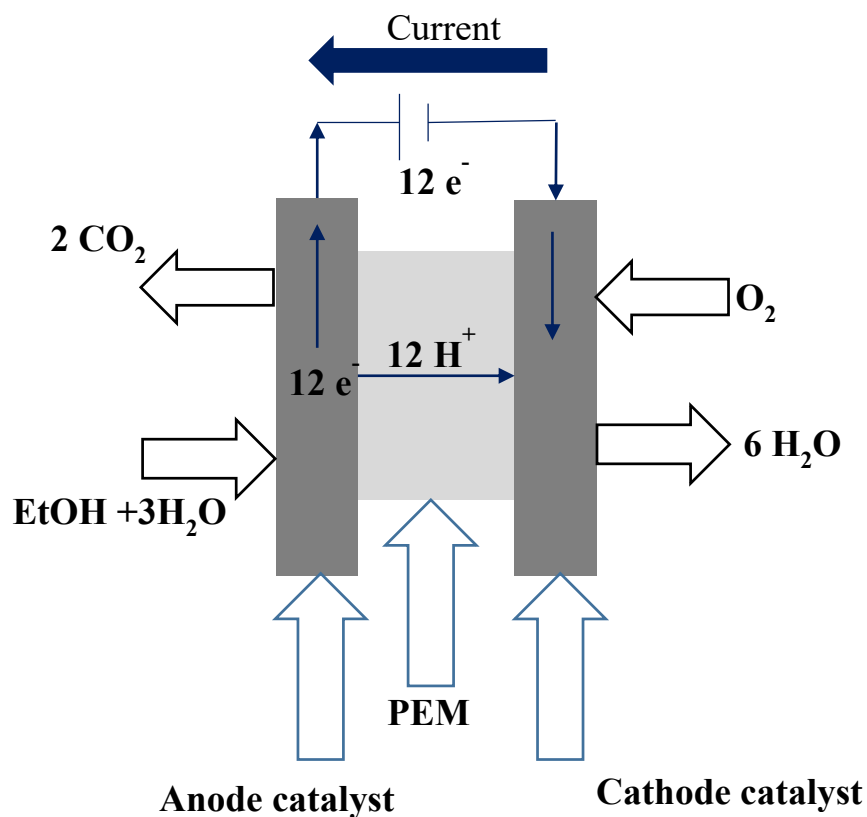
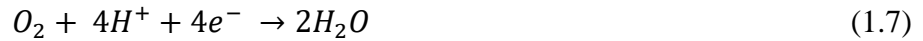


Figure 1.6 Schematic of a DEFC

However, due to the slow kinetics of the anodic and cathodic reactions, high over voltages are necessary for electrochemical oxidation of ethanol.⁷⁸ In addition, incomplete oxidation will decrease the energy density of ethanol. Acetic acid and acetaldehyde are the two main products of incomplete oxidation of ethanol. Hence, it is essential to study complete and incomplete EOR reactions.

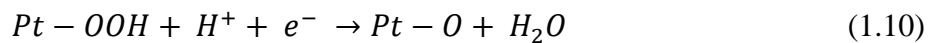
1.4.1 Oxygen Reduction Reaction (ORR)

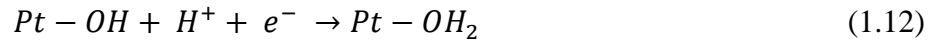
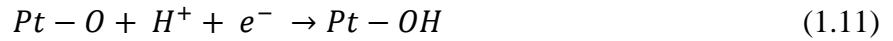
In DEFCs, O₂ is used as the oxidant. Electrochemical reduction of O₂ is a multielectron reaction that can take place through two different pathways, as shown in equations 1.7 and 1.8.



The first pathway, in which water is the result of oxygen reduction, is the favorable reaction in DEFCs. This can be attributed to two major reasons. Firstly, the standard potential at equilibrium (E^0) for first pathway is higher than the standard potential of the second pathway, 1.23 V and 0.67 V vs. SHE, respectively. This is a very important factor due to the fact that the reversible cell potential (E_{rev}^0) is equal to the difference between potentials of the anode and cathode ($E_{rev}^0 = E_{cathode} - E_{anode}$). Hence, the higher the $E_{cathode}$, the higher cell performance. Secondly, the peroxide production in the second pathway at the cathode can damage the membrane.^{79, 80}

Platinum is the best single component catalyst for the ORR. Which pathway is followed is dependent on the lattice structure of the surface Pt. It has been reported that the four electrons pathway is favourable for platinum with (100) and (110) structures. On the other hand, Pt (111) is selective for the two electrons pathway.⁸¹⁻⁸³ The ORR via the four electron pathways occurs as follows,⁸⁴

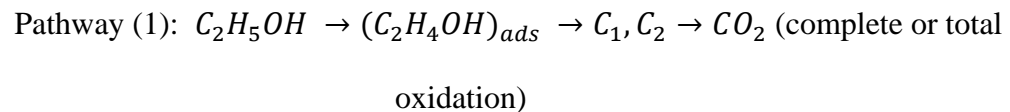




Due to the high cost of platinum and also the sluggish kinetics of the ORR, many studies have focused on finding alternative catalysts. It has been reported that Pt alloys with transition metals such as Co, Cr, and Ni enhanced the ORR and decrease the cost of the catalyst.⁸⁵⁻⁸⁷ It is important to note that the ORR efficiency can also be affected by ethanol crossover from the anode to the cathode. The presence of ethanol at the cathode leads to chemical reactions that do not produce any current. Also, there is a mixed potential at the cathode and intermediates from ethanol oxidation can poison the cathode.

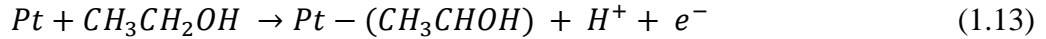
1.4.2 Ethanol Oxidation Reaction (EOR)

For oxidation of ethanol to carbon dioxide, cleavage of the C-C bond must take place. Platinum, is one of the most favourable catalyst for this. At the anode, before the breakage of the bond between carbons, ethanol must be adsorbed at the Pt surface. However, adsorption of ethanol may follow different pathways that lead to distinct products such as, carbon dioxide, acetic acid, acetaldehyde and other compounds. Generally, the adsorption and then oxidation of ethanol on platinum in acidic media can be summarized in two parallel paths.^{88, 89}



Pathway (2): $C_2H_5OH \rightarrow (C_2H_4OH)_{ads} \rightarrow CH_3CHO \rightarrow CH_3COOH$ (partial or incomplete or oxidation).

As can be seen, the first step of both pathways is absorption of ethanol at the Pt surface. In this step, ethanol loses one proton and one electron:



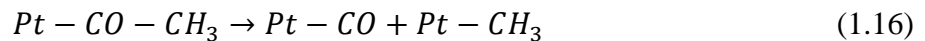
The second step is almost the same for complete and incomplete oxidation, where Pt-(CH_3CHOH)_{ads} releases the second electron and proton:



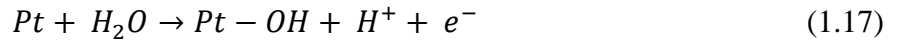
At this point, acetaldehyde can desorb as a product, or dehydrogenation continues to form an adsorbed acetyl group as shown in eq. 1.15:



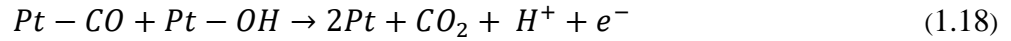
At low potentials, adsorbed acetaldehyde plays a key role in both the complete and incomplete oxidation of ethanol. In pathway (1), after the formation of an adsorbed acetyl group on Pt from adsorbed acetaldehyde rupture of the C-C bond occurs. As a result, an adsorbed methyl group and carbon monoxide are formed on Pt (eq. 1.16). Both of these intermediates cause catalyst poisoning:



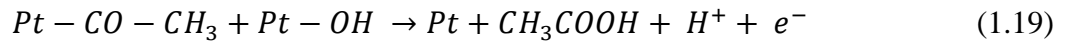
Once carbon monoxide is formed, adsorption of ethanol on the Pt would be inhibited. Thus, further oxidation of adsorbed species would be slow. At high enough potentials, dissociation of water occurs according to the following reaction:



Adsorbed hydroxyl groups on Pt are needed for CO oxidation,



Following formation of the adsorbed acetyl group (eq. 1.16), adsorbed hydroxyl can react with it instead of rupture of the C-C bond and acetic acid can form (partial or incomplete oxidation),



In the partial oxidation pathway, formation of acetic acid is the end of the EOR for DEFCs, since it can not be oxidized further at attainable anode potentials. Therefore, searching for conditions under which pathway (1) becomes dominant is crucial. Conditions are also needed to inhibit the formation of poisoning species such as carbon monoxide.^{45, 90}

1.4.3 Effect of Pt alloys on EOR

Although platinum is a good catalyst for the EOR, it is highly susceptible to poisoning by carbon monoxide during ethanol oxidation. Another drawback is the high cost of platinum for commercialization of DEFC. Therefore, searching for catalysts that increase the efficiency of the EOR, and also decrease cost is crucial.

Platinum poisoning by carbon monoxide is illustrated in Figure 1.5. Carbon monoxide, which is an intermediate during the EOR, can be adsorbed at Pt in both linear and bridged forms. The interaction between platinum and carbon monoxide is very strong and it needs high potentials to oxidize CO to CO₂. As mentioned in the last section, oxidation of adsorbed CO to CO₂

requires a hydroxyl group on the platinum adjacent to Pt-CO. Formation of a hydroxyl group on the Pt involves dissociative adsorption of a water molecule. Since formation of CO on the platinum occurs at lower potentials than the formation of Pt-OH, most of the platinum sites are already poisoned by CO before dissociation of water molecules and formation of Pt-OH (illustrated in Figure 1.7, below).

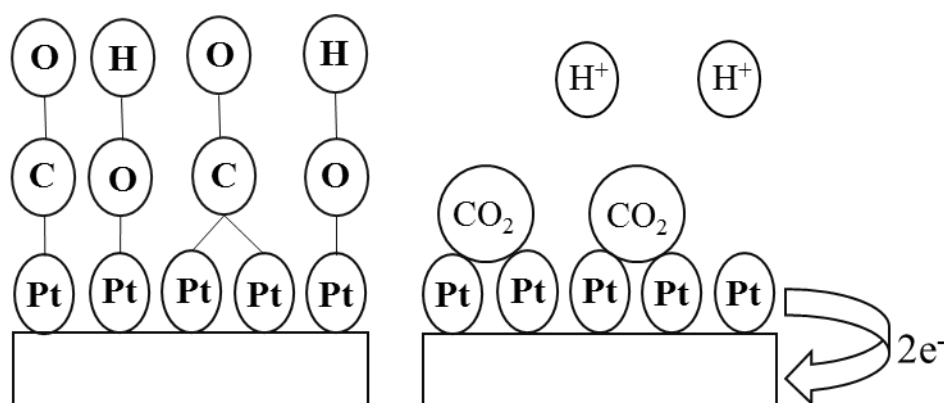
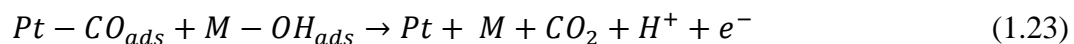
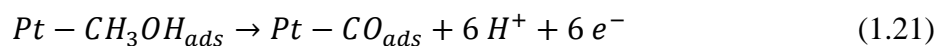


Figure. 1.7 Simplified mechanism for CO oxidation into CO₂.

One of the most studied methods for oxidation of CO to CO₂, is the development of catalysts based on Pt alloys such as PtRu^{91, 92}, PtSn^{93, 94}, and PtRh.^{95, 96} Use of platinum alloys as catalyst for EOR can shift dissociative adsorption of ethanol to lower potentials, and Pt-OH may be formed earlier so that CO can be oxidized to CO₂. The mechanism of carbon monoxide oxidation to carbon dioxide by platinum alloys can often be explained by a bifunctional mechanism and/or the ligand effect.⁹⁶⁻⁹⁸

In the bifunctional mechanism, Pt alloys with secondary or tertiary metals are capable of decreasing the dissociative adsorption potential of water. Hence, the overpotential that is needed to oxidize adsorbed CO to CO₂ would be altered to lower values. This leads to the

availability of sufficient sites for adsorption of –OH groups. The close proximity of the adsorbed CO and OH species increases the kinetics of the CO oxidation to CO₂. The ethanol oxidation mechanism at binary alloys composed of Pt and a second metal (M) that can activate H₂O at low potentials is described by equations 1.20 to 1.23;



As mentioned above, the bond between platinum and carbon monoxide is very strong, and, the strength of this interaction makes it difficult to oxidize carbon monoxide to CO₂. The tenacity of Pt-CO can be explained by the molecular orbital theory of platinum (M) and carbon monoxide. As can be seen from Figure 1.8, a M-CO bond consists of two main components;

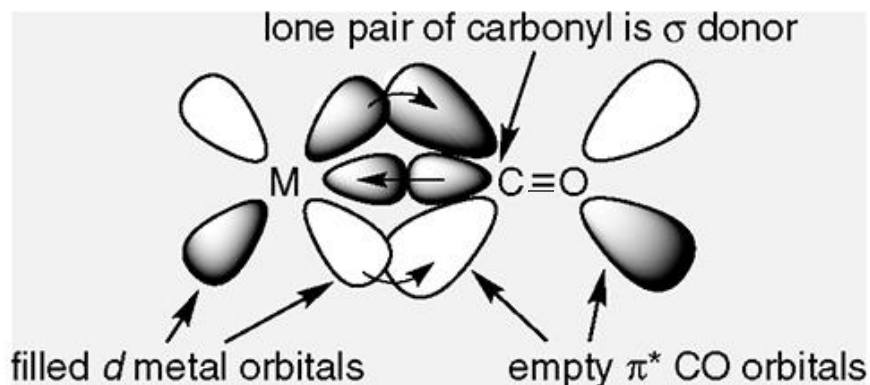


Figure. 1.8 CO and M (Pt) molecular orbital formation.⁹⁷

First, a σ bonding interaction occurs due to overlap of a filled lone pair on the carbon atom with an empty Pt (M) orbital ($d\sigma$). This leads to electron density transfer from the CO molecule to the metal centre. Second, there is a π bonding interaction takes place due to overlap of filled platinum d orbitals with the $2\pi^*$ antibonding molecular orbital of the CO molecule. As a result, Pt-CO becomes a stable intermediate and it is difficult to oxidize CO to CO₂. However, introduction of secondary metal to platinum (Pt) alloys can cause weakening of the Pt-CO bond (ligand or electronic effect). In the Pt alloys, a modification of the empty electron density of Pt takes place, with a shift of the Fermi energy level with respect to the energy of the CO molecular orbital.⁹⁷ In such a situation the interaction of the Pt-CO bond loses its stabilizing effect. Many research groups have studied the effect of Pt alloys on the EOR reactions. It has been reported that Pt-based catalysts that can enhance the kinetics of the EOR reaction.^{98,99}

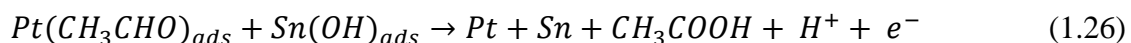
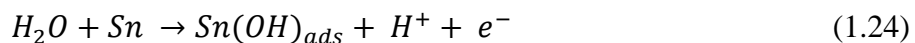
1.4.4 Incomplete EOR

Incomplete ethanol oxidation will produce many undesirable products that will decrease the efficiency of a DEFC. Quantification and measurement of these by-products have been studied by many research groups. For instance, differential mass spectroscopy (DEMS)^{92,100-101}, *in situ* Fourier transform infra red spectroscopy (FTIRS)^{88,78,102}, NMR spectroscopy¹⁰³ and also some chromatography techniques^{100,104} have been used to determine the product distribution of the EOR reaction. Although some studies have been shown that acetic⁴³ and acetaldehyde⁴⁵⁻⁴⁶ are

the main by-products of the EOR, formation of ethyl acetate¹⁰⁵, methane¹⁰⁶ and ethane¹⁰⁶⁻¹⁰⁷ have been also reported. Moreover, ethane-1,1-diol¹⁰⁵, ethoxyhydroxyethane¹⁰⁵, and formic acid^{105,108} have also been observed as minor products.

Complete oxidation of ethanol is a very complex reaction. Based on some reports,^{44, 104} it is suggested that the production of CO₂ primarily results from an acetaldehyde intermediate (incomplete EOR) and only small amounts of CO₂ are produced from the direct oxidation from ethanol (complete EOR).

As mentioned earlier, the use of Pt alloys can significantly increase the performance of the cell. PtRu and PtSn have been shown to give the best performance and the best power density for EOR in DEFCs. However, it has also been shown that when Ru or Sn is introduced into the platinum structure, the selectivity towards CO₂ is significantly decreased (in comparison to pure Pt)⁹⁴. Beyhan et al.⁹⁵ demonstrated that the introduction of Sn into a Pt electrode lowered both the yields of CO₂ and acetaldehyde, while significantly increasing the acetic acid yield. This suggests that in order to adsorb dissociated ethanol on the surface and break the C-C bond, adjacent Pt sites are needed. When the C-C bond in ethanol is not cleaved, adsorbed acetaldehyde covers the surface and by the bifunctional mechanism, the Sn activates H₂O forming OH_{ads}, and the acetaldehyde and OH_{ads} react to form acetic acid.⁸⁹



Neto et al¹⁰¹ reported the same effect on partial oxidation of ethanol by a PtRu alloy. They mentioned that although Ru can oxidize adsorbed species to carbon monoxide according to the bifunctional mechanism, the main effect is on the activity of the partial oxidation of ethanol to acetic acid.

To bring this section to a proper end, it is important to note that the development of new anode catalysts is a very complicated procedure, as a balance between performance and selectivity is needed. As the performance of a catalyst is increased, it is generally found that the selectivity towards complete oxidation is decreased¹⁰², and vice versa. As Pt catalysts are typically the best for selectivity towards CO₂, one of the objectives for improving catalyst technology is to increase the performance of the electrode while leaving the CO₂ yield unchanged.

1.4.5 Fuel Crossover

Fuel crossover in the cell is a great challenge for the efficiency of DMFCs and DEFCs. Generally, fuel crossover (methanol and ethanol crossover) is the phenomenon whereby fuel permeates through the membrane from the anode to the cathode. Not only does crossover waste fuel, but the reaction between fuel and oxidant also forms products (undesirable products) that decrease current generation and cell efficiency.

In this project, the crossover of methanol and ethanol in a DMFC and DEFC were studied. Due to the fact that the reactions that are involved in methanol crossover are simpler than those in ethanol crossover, the current section focuses only on methanol crossover.

As mentioned in the previous section, the Nafion membrane needs to be hydrated for proton conduction. During proton transport through the membrane, water molecules also move

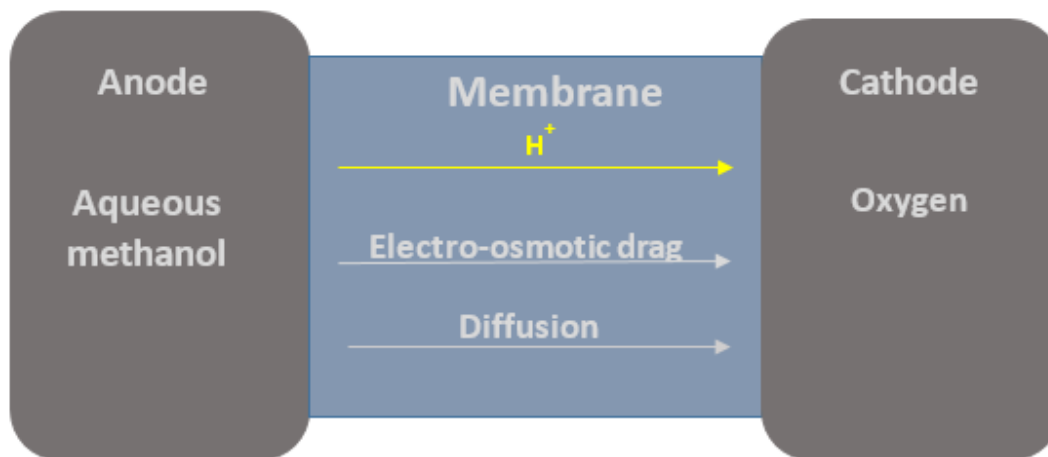


Figure. 1.9 Methanol crossover in a DMFC.

through the membrane, a process which is called “electro-osmotic drag”. Due to the high solubility of methanol in water, methanol molecules will crossover with water molecules in the membrane by electro-osmotic drag. However, electro-osmotic drag is not the only source of methanol crossover. At the anode side, when methanol is in contact with the membrane, methanol diffuses via the membrane to the cathode (due to the methanol concentration gradient between the anode and cathode). Figure 1-9 depicts these two phenomena.

There are several factors that can effect the crossover of methanol. It has been reported that the methanol crossover rate increases with increasing temperature.¹⁰³ Also, the same trend occurs with increasing methanol concentration.^{104, 109, 110} Use of a thicker membrane is one solution to limit methanol crossover. It has been shown that increasing the membrane thickness and also use of membranes of higher equivalent weight (EW), decrease MeOH crossover.¹¹⁰ However, when the thickness of the membrane is increased, its resistance to

proton transport become an issue. A thicker membranes cause high ohmic loss in the cell voltage and the efficiency of the FC declines.

The structure of the membrane can also affect methanol crossover.¹¹¹ Nafion is the most widely used membrane material in DMFCs. Generally, methanol crossover and proton permeability increase with an increase in the number of sulfonic groups in the membrane.¹¹⁰ Therefore, finding membranes other than Nafion or the synthesis of other polymeric membranes is vital to overcoming methanol crossover in DMFCs.

Methanol crossover is not the only type of crossover in DMFCs. Oxygen can also traverse from the cathode compartment to the anode side via the membrane. Oxygen crossover is a serious disadvantage for the efficiency of DMFCs. Oxygen solubility increases with elevation in the hydrophobicity of the membrane and also increases with the number of water molecules in the membrane.⁸⁵ The effect of oxygen crossover in DMFCs or DEFC is beyond the scope of this project.

1.5 Fuel Cell Performance

To understand how a DEFC performs, it is important to review the basics of fuel cell thermodynamics and electrochemistry. Generally, in a power source system, the open circuit potential (OCP) describes the electrical output of the cell. To put it simply, the OCP is the potential difference in the cell when there is no current flow and it is one of the most important parameters when describing the behaviour of the cell. When the cell is operating under thermodynamically reversible conditions, the potential difference between electrodes is called

the “reversible cell potential” (E_{rev}). However, in a fuel cell conditions, there are differences in the OCP and E_{rev} . The E_{rev} can be calculated from thermodynamic data under standard conditions:

$$\Delta G^0 = -1325 \text{ kJ mol}^{-1} ; \Delta H^0 = -1366 \text{ kJ mol}^{-1}$$

This gives the E_{rev} at equilibrium:¹¹²

$$E_{rev} = \frac{\Delta G^0}{nF} = \frac{1325 \times 10^3}{12 \times 96485} \quad (1.27)$$

$$= E^0_{cathode} - E^0_{anode} = 1.144 \text{ V} \quad (1.28)$$

Where $F = 96485 \text{ C}$ is the Faraday constant and $n = 12$ is the number of electrons exchanged per molecules for complete oxidation of ethanol to carbon dioxide. From the Gibbs free energy (equation 1.27), the energy density ($E\rho$) of ethanol is;

$$E\rho = \frac{\Delta G^0}{3600 M} \quad (1.29)$$

M is molar mass of methanol,

$$E\rho \approx 8 \text{ kWh kg}^{-1}$$

The theoretical energy efficiency of an ethanol fuel cell under standard conditions is defined as the ratio between the Gibbs free energy (ΔG^0) and the enthalpy of combustion (ΔH^0);

$$\epsilon_{rev} = \frac{\Delta G^0}{\Delta H^0} \quad (1.30)$$

$$\Delta G^0 = \Delta H^0 - T\Delta S^0 \quad (1.31)$$

$$= 1 - \frac{T\Delta S^0}{\Delta H^0} = \frac{1325}{1366} = 0.97$$

However, under experimental conditions not only does the energy efficiency drop dramatically, but the OCP also decreases (the OCP is always less than E_{rev} in a fuel cell). These losses from the ideal value (E_{rev}) are due to three main factors as illustrated in the schematic curve of cell potential (voltage) versus cell current of a DEFC shown in Figure 1.1

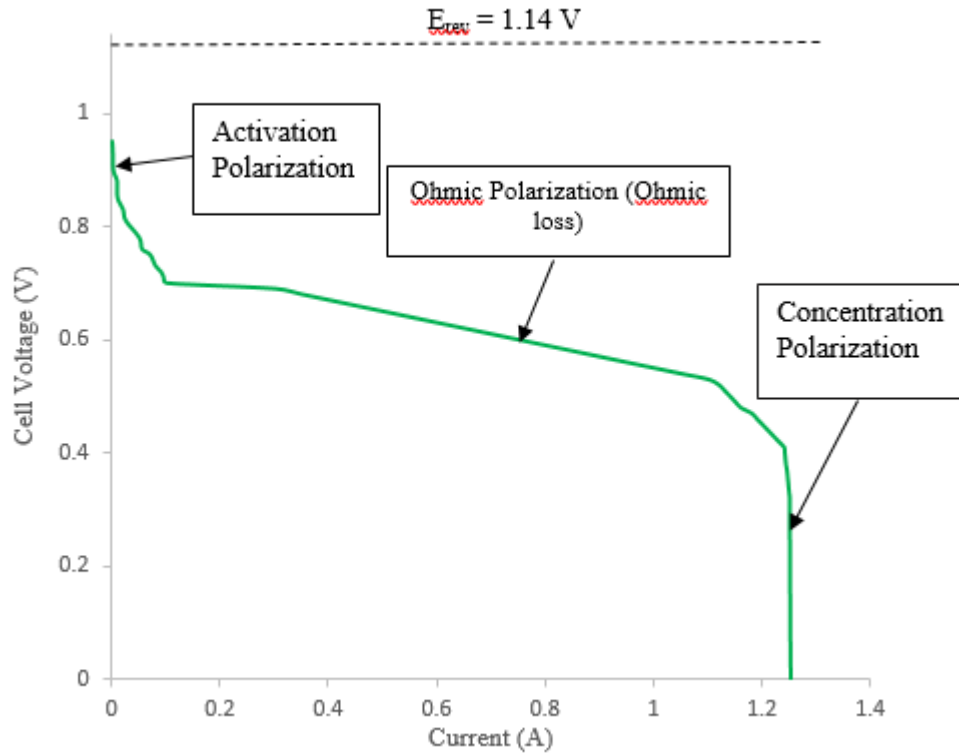


Figure. 1.10 Schematic polarization curve for a DEFC.

As can be seen from this figure, the OCP is lower than the reversible cell potential ($E_{rev} = 1.14 \text{ V}$). This potential loss can be related to the mixed potential due to ethanol crossover. The first region of the polarization curve at high potentials is often called the activation polarization (η_{act}). The activation polarization is due to slow electron transfer (charge transfer) in the anodic and cathodic reactions. Indeed, during ethanol oxidation many undesirable intermediates and species are produced. These limit the rate of electron transfer between the solution and electrode. Therefore, the rate determining step is sluggish and an overpotential beyond the equilibrium potential is needed to overcome this step. The overpotential (η_{act}) that is required to drive anodic and/or cathodic reactions can be positive or negative. Here, the $\eta_{act} > 0$ for an anodic reaction (in this case, oxidation of ethanol), and the $\eta_{act} < 0$ for a cathodic reaction (in this case, reduction of oxygen). For a better understanding of η_{act} , it is good to introduce some electrochemical theory.

The overpotential for oxidation of ethanol at the anode (η_{act}) can be described by the Tafel equation (e.g 1.32),

$$\eta_{act} = b \ln\left(\frac{i}{i_0}\right) \quad (1.32)$$

Where, i_0 is the exchange current. Generally, the exchange current, is the current when the reaction is at equilibrium ($E = E_{eq}$) and it is equal to the anodic and cathodic currents ($i_0 = i_a = i_c$). The i_0 for a common redox system can range from $10^{-6} \mu\text{A}$ to 1 A. In the Tafel equation, the parameter b is,

$$b = \frac{RT}{n\alpha F} \quad (1.33)$$

In this equation, R is the ideal gas constant, T is temperature in Kelvin, n is the number of electrons transferred during electrochemical rate limiting step, F is the Faraday constant and α is the charge transfer coefficient. The constant α reflects the symmetry of the free energy curve for the electrochemical reaction. It varies from zero to unity ($0 < \alpha < 1$). The theoretical current vs. overpotential curve for a generic electrochemical reaction (eq. 1.34) with $\alpha = 0.5$ is shown,

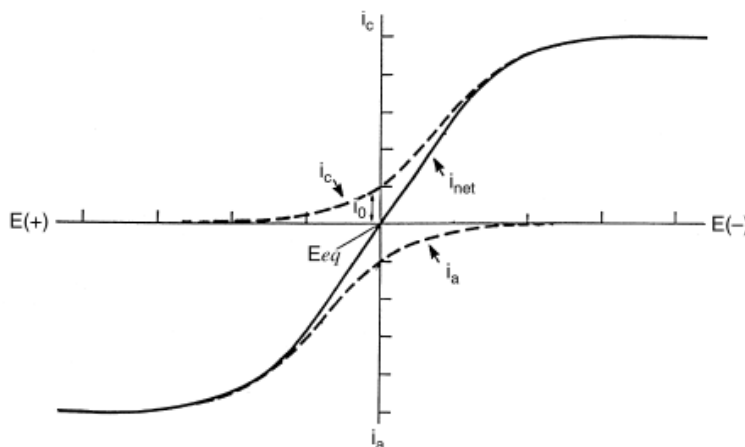


Figure. 1.11 Theoretical current-potential curve for reaction 1.34, assuming $\alpha=0.5$.¹¹³

A plot of η_{act} vs. \log of i (equation 1.32 (the Tafel equation)), known as a Tafel plot, can give us important information about the kinetics of an electrochemical reaction. Examples are shown in Figure 1.12.

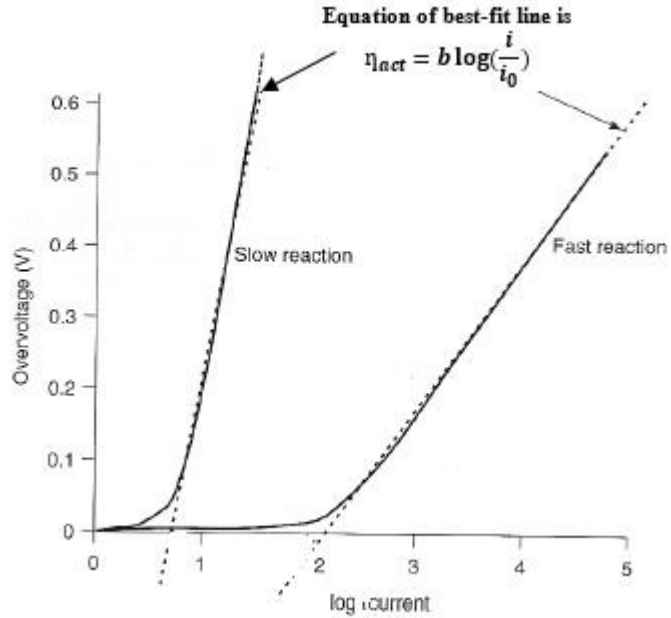


Figure. 1.12 Tafel plots for fast and slow electrochemical reactions.¹¹⁴

The exchange current represents the rate of the forward reaction (e.g. oxidation of ethanol) equilibrium potential. Thus, faster electrochemical reactions have higher values of i_0 which leads to lower activation overpotentials (η_{act}). It is important to note that in the case of DEFCs, sluggish electrochemical oxidation/reduction of ethanol and oxygen at the anode and cathode leads to very low exchange currents. Thus, high anodic and cathodic overpotentials are needed to drive these slow electrochemical reactions. This can be offset by raising the cell temperature or using more effective catalysts.³⁵

The second region in figure 1.10 is called ohmic polarization or ohmic loss. Ohmic loss is a common issue in all electronic devices. This loss is mainly due to the resistance to flow of current (electrons) and movement of protons (proton conduction) in the membrane. As

can be seen from the figure, ohmic loss results in a linear relation between the current and potential of the cell. The magnitude the ohmic loss can be calculated from Ohm's law (equation 1.39);¹¹³

$$V = iR \quad (1.39)$$

Where i is the current and R is the resistance of the cell. To reduce ohmic loss it is necessary to increase the conductivity of the electrodes, increase the conductivity of membrane, and/or to decrease the distance between the electrodes.

The last region in the figure 1.10 is called concentration polarization. Here, the main reason for the loss of potential is slow mass transfer of reactants to the electrode surfaces. For a better understanding, it is preferable to simplify the discussion by focusing on the oxidation of ethanol at the anode. The electrochemical oxidation of ethanol occurs within the anode catalyst layer, and causes a concentration gradient of methanol within the porous carbon fiber paper backing layer. This stagnant thin layer is called the diffusion layer (Nernst diffusion layer) and is shown as δ in figure 1.13. The concentration of ethanol at the surface of the electrode (concentration of ethanol between the electrode surface and the diffusion layer) is shown as $C_{\text{EtOH}(x=0)}$, where x is the distance from the electrode surface). The concentration of ethanol in the bulk solution, beyond δ , is shown as C_{bulk} .

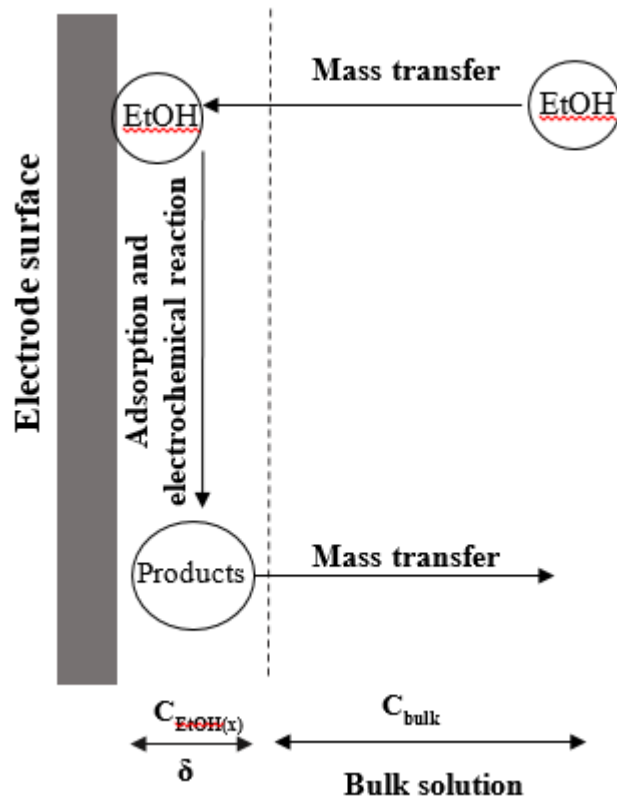


Figure. 1.13 Schematic of the electrode reactions

In electrochemistry, current can be calculated by,

$$i = n F A f \quad (1.40)$$

Where A is the area of the electrode and f is the flux of molecules (ethanol molecules in this case). The flux (f) has the unit of $\text{mol cm}^{-2} \text{s}^{-1}$. The flux can be calculated from equation

1.41,¹¹⁰

$$f = D \frac{\Delta C_{EtOH(x)}}{\delta} \quad (1.41)$$

Where, D is the diffusion coefficient with unit of $\text{cm}^2 \text{s}^{-1}$ and $\frac{\Delta C_{EtOH}(x)}{\delta}$ is the concentration gradient of ethanol at the distance x from the electrode. Now, with rearrangement of equations 1.40 and 1.41, current will be given by equation 1.42,

$$\frac{i}{nFA} = D \frac{\Delta C_{EtOH}(x)}{\delta} \quad (1.42)$$

Here,

$$\Delta C_{EtOH}(x) = C_{bulk} - C_{EtOH(x=0)} \quad (1.43)$$

When, the rate of electrochemical oxidation of ethanol is limited by the diffusion of ethanol to the anode, $C_{EtOH(x=0)} = 0$ (or more accurately, $C_{EtOH(x=0)} \ll C_{bulk}$) and $\Delta C_{EtOH}(x > \delta) \approx C_{bulk}$. The current under this condition is called the limiting current, where,

$$i_{lim} = nFAfD \frac{C_{bulk}}{\delta} \quad (1.44)$$

At the limiting current, the rate of ethanol mass transfer from the bulk solution to the electrode surface is at its maximum value. Therefore, increasing the overpotential can not increase the current beyond the limiting current value.

1.6 Project goal

The first objective of this project was to improve the efficiency of an ethanol electrolysis cell. This was achieved by the use of different types of potential waveforms (cyclic and linear sweep potentials). It is very important to find a suitable potential wave form to increase the oxidation of adsorbed carbon monoxide to carbon dioxide.

The second goal of this project was to improve the efficiency of a DEFC by using sinusoidal (AC) potential cycling conditions and elevated temperatures. It has been clearly shown that applying a sinusoidal potential waveform improves the cell efficiency and oxidation of carbon monoxide to carbon dioxide and can increase the cell efficiency.

The third object of the project was to develop a simple and novel method to determine the average number of electrons transferred during electrochemical oxidation of ethanol, and any other fuel, in conventional fuel cell hardware. This method is based on the fact that fuel crossing the membrane can be quantitatively electrochemically oxidized at the anode when the fuel solution is supplied to the cathode.

The final goal of this project was to validate the method for a real FC and for a cell operated in an anode polarization mode. To test the method in these modes, methanol was used as the fuel for all experiments. Furthermore, the model was extended to provide the average number of electron transferred at potential below the limiting current, and estimates of the crossover loss.

References

1. Cheng X, Shi Z, Glass N, Zhang L, Zhang J, Song D, Liu Z, Wang H, Shen J. A review of PEM hydrogen fuel cell contamination: Impacts, mechanisms, and mitigation. *J Power Sources* 2007; 165:739-56.
2. Jacobson M. Z, Colella W. G, Golden D. M. Cleaning the air and improving health with hydrogen fuel-cell vehicles. *Science* 2005; 308:1901-5.
3. Trimm D. L, Önsan Z. I. Onboard fuel conversion for hydrogen-fuel-cell-driven vehicles. *Catalysis Reviews* 2001; 43:31-84.
4. Girishkumar G, Rettker M, Underhile R, Binz D, Vinodgopal K, McGinn P, Kamat P. Single-wall carbon nanotube-based proton exchange membrane assembly for hydrogen fuel cells. *Langmuir* 2005; 21:8487-94.
5. Wasmus S, Küver A. Methanol oxidation and direct methanol fuel cells: A selective review. *J Electroanal Chem* 1999; 461:14-31.
6. Schultz T, Zhou S, Sundmacher K. Current status of and recent developments in the direct methanol fuel cell. *Chem Eng Technol* 2001; 24:1223-33.
7. Hamnett A. Mechanism and electrocatalysis in the direct methanol fuel cell. *Catalysis Today* 1997; 38:445-57.
8. Liu H, Song C, Zhang L, Zhang J, Wang H, Wilkinson D. P. A review of anode catalysis in the direct methanol fuel cell. *J Power Sources* 2006; 155:95-110.
9. Berg H, Libergreen A. Direct ethanol fuel cells. 2015.
10. Lamy C, Rousseau S, Belgsir E, Coutanceau C, Léger J. Recent progress in the direct ethanol fuel cell: Development of new platinum–tin electrocatalysts. *Electrochim Acta*

- 2004; 49:3901-8.
11. Rousseau S, Coutanceau C, Lamy C, Léger J. Direct ethanol fuel cell (DEFC): Electrical performances and reaction products distribution under operating conditions with different platinum-based anodes. *J Power Sources* 2006; 158:18-24.
 12. O'Hayre R. P, Cha S, Colella W, Prinz F. B. *Fuel cell fundamentals*. John Wiley & Sons New York; 2006.
 13. Revankar S. T, Majumdar P. *Fuel cells: Principles, design, and analysis*. CRC Press; 2014.
 14. Pukrushpan J. T, Stefanopoulou A. G, Peng H. *Control of fuel cell power systems: Principle modeling, analysis and feedback design*. Springer Science & Business Media; 2004.
 15. Prater K. The renaissance of the solid polymer fuel cell. *J Power Sources* 1990; 29:239-50.
 16. Li X, Fields L, Way G. Principles of fuel cells. *Platinum Metals Rev* 2006; 50:200-1.
 17. Dodds P. E, Staffell I, Hawkes A. D, Li F, Grünewald P, McDowall W, Ekins P. Hydrogen and fuel cell technologies for heating: A review. *Int J Hydrogen Energy* 2015; 40:2065-83.
 18. Steele B. C, Heinzl A. Materials for fuel-cell technologies. *Nature* 2001; 414:345-52.
 19. Mauritz K. A, Moore R. B. State of understanding of nafion. *Chem Rev* 2004; 104:4535-86.
 20. Tiwari R, Garcia E. The state of understanding of ionic polymer metal composite architecture: A review. *Smart Mater Struct* 2011; 20:083001.
 21. Lamy C, Belgsir E, Leger J. Electrocatalytic oxidation of aliphatic alcohols: Application to the direct alcohol fuel cell (DAFC). *J Appl Electrochem* 2001; 31:799-809.
 22. Johnston B, Mayo M. C, Khare A. *Hydrogen: The energy source for the 21st century*. Technovation 2005; 25:569-85.

23. Hua T, Ahluwalia R, Eudy L, Singer G, Jermer B, Asselin-Miller N, Wessel S, Patterson T, Marcinkoski J. Status of hydrogen fuel cell electric buses worldwide. *J Power Sources* 2014; 269:975-93.
24. Simmons K, Guezennec Y, Onori S. Modeling and energy management control design for a fuel cell hybrid passenger bus. *J Power Sources* 2014; 246:736-46.
25. Livshits V, Peled E. Progress in the development of a high-power, direct ethylene glycol fuel cell (DEGFC). *J Power Sources* 2006; 161:1187-91.
26. Peled E, Livshits V, Duvdevani T. High-power direct ethylene glycol fuel cell (DEGFC) based on nanoporous proton-conducting membrane (NP-PCM). *J. Power Sources* 2002; 106:245-8.
27. Livshits V, Philosoph M, Peled E. Direct ethylene glycol fuel-cell stack—Study of oxidation intermediate products. *J Power Sources* 2008; 178:687-91.
28. Kamarudin S. K, Achmad F, Daud W. R. W. Overview on the application of direct methanol fuel cell (DMFC) for portable electronic devices. *Int J Hydrogen Energy* 2009; 34:6902-16.
29. Li X, Faghri A. Review and advances of direct methanol fuel cells (DMFCs) part I: Design, fabrication, and testing with high concentration methanol solutions. *J Power Sources* 2013; 226:223-40.
30. Iwasita T. Electrocatalysis of methanol oxidation. *Electrochim Acta* 2002; 47:3663-74.
31. Bouzek K, Mangold K, Jüttner K. Electrocatalytic activity of platinum modified polypyrrole films for the methanol oxidation reaction. *J Appl Electrochem* 2001; 31:501-7.
32. Haner A. N, Ross P. N. Electrochemical oxidation of methanol on tin-modified platinum single-crystal surfaces. *J Phys Chem* 1991; 95:3740-6.

33. Kabbabi A, Faure R, Durand R, Beden B, Hahn F, Leger J, Lamy C. In situ FTIRS study of the electrocatalytic oxidation of carbon monoxide and methanol at platinum–ruthenium bulk alloy electrodes. *J Electroanal Chem* 1998; 444:41-53.
34. Laborde H, Leger J, Lamy C. Electrocatalytic oxidation of methanol and C₁ molecules on highly dispersed electrodes part 1: Platinum in polyaniline. *J Appl Electrochem* 1994; 24:219-26.
35. Chrzanowski W, Wieckowski A. Surface structure effects in platinum/ruthenium methanol oxidation electrocatalysis. *Langmuir* 1998; 14:1967-70.
36. Gasteiger H. A, Markovic N, Ross Jr P. N, Cairns E. J. Methanol electrooxidation on well-characterized platinum-ruthenium bulk alloys. *J Phys Chem* 1993; 97:12020-9.
37. Cathro K. The oxidation of Water-Soluble organic fuels using Platinum-Tin catalysts. *J Electrochem Soc* 1969; 116:1608-11.
38. Katayama A. Electrooxidation of methanol on a platinum-tin oxide catalyst. *J Phys Chem* 1980; 84:376-81.
39. De Souza J, Queiroz S, Bergamaski K, Gonzalez E, Nart F. Electro-oxidation of ethanol on Pt, Rh, and Pt/Rh electrodes. A study using DEMS and in-situ FTIR techniques. *The Journal of Physical Chemistry B* 2002;1 06:9825-30.
40. Williams C. T, Takoudis C. G, Weaver M. J. Methanol oxidation on rhodium as probed by surface-enhanced Raman and mass spectroscopies: Adsorbate stability, reactivity, and catalytic relevance. *The Journal of Physical Chemistry B* 1998; 102:406-16.
41. Kruse J. Methanol poisoning. *Intensive Care Med* 1992; 18:391-7.
42. Antolini E. Catalysts for direct ethanol fuel cells. *J Power Sources* 2007; 170:1-12.
43. Camara G, Iwasita T. Parallel pathways of ethanol oxidation: The effect of ethanol

- concentration. *J Electroanal Chem* 2005; 578:315-21.
44. Wang H, Abruna H. D. Electrocatalysis of direct alcohol fuel cells: Quantitative DEMS studies. In: *Fuel cells and hydrogen storage*. Springer; 2011.
 45. Guillén-Villafuerte O, García G, Arévalo M. C, Rodríguez JL, Pastor E. New insights on the electrochemical oxidation of ethanol on carbon-supported Pt electrode by a novel electrochemical mass spectrometry configuration. *Electrochemistry Communications* 2016; 63:48-51.
 46. Kirubakaran A, Jain S, Nema R. A review on fuel cell technologies and power electronic interface. *Renewable and Sustainable Energy Reviews* 2009; 13:2430-40.
 47. Pichonat T, Gauthier-Manuel B. Recent developments in MEMS-based miniature fuel cells. *Microsystem Technologies* 2007; 13:1671-8.
 48. Akhairi M, Kamarudin S. K. Catalysts in direct ethanol fuel cell (DEFC): An overview. *Int J Hydrogen Energy* 2016; 41:4214-28.
 49. Wang X, Zhu F, He Y, Wang M, Zhang Z, Ma Z, Li R. Highly active carbon supported ternary Pd.Sn.Pt_x (x= 0.1–0.7) catalysts for ethanol electro-oxidation in alkaline and acid media. *J Colloid Interface Sci* 2016; 468:200-10.
 50. Zignani S, Baglio V, Sebastián D, Siracusano S, Aricò A. Enhancing ethanol oxidation rate at Pt.Ru electro-catalysts using metal-oxide additives. *Electrochim Acta* 2016; 191:183-91.
 51. Song S, Zhou W, Tian J, Cai R, Sun G, Xin Q, Kontou S, Tsiakaras P. Ethanol crossover phenomena and its influence on the performance of DEFC. *J Power Sources* 2005; 145:266-71.
 52. Vigier F, Rousseau S, Coutanceau C, Leger J, Lamy C. Electrocatalysis for the direct

- alcohol fuel cell. *Topics in Catalysis* 2006; 40:111-21.
53. Sopian K, Daud W. R. W. Challenges and future developments in proton exchange membrane fuel cells. *Renewable Energy* 2006;31(5):719-27.
54. Bi W, Gray G. E, Fuller T. F. PEM fuel cell Pt/C dissolution and deposition in Nafion electrolyte. *Electrochemical and Solid-State Letters* 2007; 10:101-4.
55. Nafion® membranes: Molecular diffusion, proton conductivity and proton conduction mechanism. *MRS proceedings* Cambridge Univ Press; 1992.
56. Curtin DE, Lousenberg R. D, Henry T. J, Tangeman P. C, Tisack ME. Advanced materials for improved PEMFC performance and life. *J Power Sources* 2004; 131:41-8.
57. Gamburgzev S, Appleby A.J. Recent progress in performance improvement of the proton exchange membrane fuel cell (PEMFC). *J Power Sources* 2002; 107:5-12.
58. Bose S, Kuila T, Nguyen T. X. H, Kim N. H, Lau K, Lee J. H. Polymer membranes for high temperature proton exchange membrane fuel cell: Recent advances and challenges. *Progress in Polymer Science* 2011; 36:813-43.
59. Agmon N. The grotthuss mechanism. *Chemical Physics Letters* 1995; 244:456-62.
60. Cukierman S. Et tu, grotthuss! and other unfinished stories. *Biochimica Et Biophysica Acta (BBA)-Bioenergetics* 2006; 1757:876-85.
61. Sone Y, Ekdunge P, Simonsson D. Proton conductivity of nafion 117 as measured by a four-electrode AC impedance method. *J Electrochem Soc* 1996; 143:1254-9.
62. Peckham T. J, Schmeisser J, Rodgers M, Holdcroft S. Main-chain, statistically sulfonated proton exchange membranes: The relationships of acid concentration and proton mobility to water content and their effect upon proton conductivity. *Journal of Materials Chemistry* 2007; 17:3255-68.

63. Kim Y. S, Dong L, Hickner M. A, Glass T. E, Webb V, McGrath J. E. State of water in disulfonated poly (arylene ether sulfone) copolymers and a perfluorosulfonic acid copolymer (nafion) and its effect on physical and electrochemical properties. *Macromolecules* 2003; 36:6281-5.
64. Paddison S. The modeling of molecular structure and ion transport in sulfonic acid based ionomer membranes. *Journal of New Materials for Electrochemical Systems* 2001;4(4):197-208.
65. Kreuer K. On the development of proton conducting polymer membranes for hydrogen and methanol fuel cells. *J Membr Sci* 2001; 185:29-39.
66. Kreuer K. On the development of proton conducting polymer membranes for hydrogen and methanol fuel cells. *J Membr Sci* 2001; 185:29-39.
67. Peighambardoust S, Rowshanzamir S, Amjadi M. Review of the proton exchange membranes for fuel cell applications. *Int J Hydrogen Energy* 2010; 35:9349-84.
68. Morris DR, Sun X. Water-sorption and transport properties of Nafion 117 H. *J Appl Polym Sci* 1993; 50:1445-52.
69. Slade S, Campbell S, Ralph T, Walsh F. Ionic conductivity of an extruded Nafion 1100 EW series of membranes. *J Electrochem Soc* 2002; 149: A1556-64.
70. Tsampas M, Pikos A, Brosda S, Katsaounis A, Vayenas C. The effect of membrane thickness on the conductivity of Nafion. *Electrochim Acta* 2006; 51:2743-55.
71. Thomas C, James B. D, Lomax F. D, Kuhn I. F. Fuel options for the fuel cell vehicle: Hydrogen, methanol or gasoline? *Int J Hydrogen Energy* 2000; 25:551-67.
72. Ross D. Hydrogen storage: The major technological barrier to the development of hydrogen fuel cell cars. *Vacuum* 2006; 80:1084-9.

73. Ogden J. M, Steinbugler M. M, Kreutz T. G. A comparison of hydrogen, methanol and gasoline as fuels for fuel cell vehicles: Implications for vehicle design and infrastructure development. *J Power Sources* 1999; 79:143-68.
74. Liu Z, Ling X. Y, Su X, Lee J. Y. Carbon-supported Pt and PtRu nanoparticles as catalysts for a direct methanol fuel cell. *The Journal of Physical Chemistry B* 2004; 108:8234-40.
75. Stalnionis G, Tamašauskaitė-Tamašiūnaitė L, Pautienienė V, Jusys Z. Modification of a Pt surface by spontaneous Sn deposition for electrocatalytic applications, oxidation of CO, formaldehyde, formic acid, and methanol. *Journal of Solid State Electrochemistry* 2004; 8:900-7.
76. Zakaria Z, Kamarudin SK, Timmiati S. Membranes for direct ethanol fuel cells: An overview. *Appl Energy* 2016; 163:334-42.
77. Zhou W, Song S. Q, Li W. Z, Zhou Z. H, Sun G, Xin Q, Douvartzides S, Tsiakaras P. Direct ethanol fuel cells based on PtSn anodes: The effect of sn content on the fuel cell performance. *J Power Sources* 2005; 140:50-8.
78. Vigier F, Coutanceau C, Hahn F, Belgsir E, Lamy C. On the mechanism of ethanol electro-oxidation on Pt and PtSn catalysts: Electrochemical and in situ IR reflectance spectroscopy studies. *J Electroanal Chem* 2004; 563:81-9.
79. Lankiang S, Chiwata M, Baranton S, Uchida H, Coutanceau C. Oxygen reduction reaction at binary and ternary nanocatalysts based on Pt, Pd and Au. *Electrochim Acta* 2015; 182:131-42.
80. Deng Y, Wiberg GKH, Zana A, Arenz M. On the oxygen reduction reaction in phosphoric acid electrolyte: Evidence of significantly increased inhibition at steady state conditions. *Electrochim Acta* 2016; 204:78-83.

81. Marković N, Gasteiger H, Grgur B, Ross P. Oxygen reduction reaction on Pt (111): Effects of bromide. *J Electroanal Chem* 1999; 467:157-63.
82. Park J, Zhang L, Choi S, Roling L. T, Lu N, Herron J. A, Xie S, Wang J, Kim M. J, Mavrikakis M. Atomic layer-by-layer deposition of platinum on palladium octahedra for enhanced catalysts toward the oxygen reduction reaction. *ACS Nano* 2015; 9:2635-47.
83. Yeo Y, Vattuone L, King D. Calorimetric heats for CO and oxygen adsorption and for the catalytic CO oxidation reaction on Pt (111). *J Chem Phys* 1997; 106:392-401.
84. Zhang J. PEM fuel cell electrocatalysts and catalyst layers: Fundamentals and applications. Springer Science & Business Media; 2008.
85. Hwang BJ, Kumar SMS, Chen C, Monalisa L, Cheng M, Liu D, Lee J. An investigation of structure-catalytic activity relationship for Pt-Co/C bimetallic nanoparticles toward the oxygen reduction reaction. *The Journal of Physical Chemistry C* 2007; 111:15267-76.
86. Mukerjee S, Srinivasan S, Soriaga M. P, McBreen J. Effect of preparation conditions of Pt alloys on their electronic, structural, and electrocatalytic activities for oxygen reduction-XRD, XAS, and electrochemical studies. *J Phys Chem* 1995; 99:4577-89.
87. Stamenkovic V, Schmidt T, Ross P, Markovic N. Surface composition effects in electrocatalysis: Kinetics of oxygen reduction on well-defined Pt₃Ni and Pt₃Co alloy surfaces. *The Journal of Physical Chemistry B* 2002; 106:11970-9.
88. Hitmi H, Belgsir E, Léger J, Lamy C, Lezna R. A kinetic analysis of the electro-oxidation of ethanol at a platinum electrode in acid medium. *Electrochim Acta* 1994; 39:407-15.
89. Wang Y, Zou S, Cai W. Recent advances on electro-oxidation of ethanol on Pt-and Pd based catalysts: From reaction mechanisms to catalytic materials. *Catalysts* 2015; 5:1507

90. Nonaka H, Matsumura Y. Electrochemical oxidation of carbon monoxide, methanol, formic acid, ethanol, and acetic acid on a platinum electrode under hot aqueous conditions. *J Electroanal Chem* 2002; 520:101-10.
91. Antolini E. Catalysts for direct ethanol fuel cells. *J Power Sources* 2007; 170:1-12.
92. Fujiwara N, Friedrich K, Stimming U. Ethanol oxidation on PtRu electrodes studied by differential electrochemical mass spectrometry. *J Electroanal Chem* 1999; 472:120-5.
93. Ma Y, Wang H, Ji S, Linkov V, Wang R. PtSn/C catalysts for ethanol oxidation: The effect of stabilizers on the morphology and particle distribution. *J Power Sources* 2014; 247:142-50.
94. Vigier F, Coutanceau C, Hahn F, Belgsir E, Lamy C. On the mechanism of ethanol electro-oxidation on Pt and PtSn catalysts: Electrochemical and in situ IR reflectance spectroscopy studies. *J Electroanal Chem* 2004; 563:81-9.
95. Beyhan S, Léger J, Kadirgan F. Understanding the influence of Ni, Co, Rh and Pd addition to PtSn/C catalyst for the oxidation of ethanol by in situ Fourier transform infrared spectroscopy. *Applied Catalysis B: Environmental* 2014; 144:66-74.
96. Cantane D, Ambrosio W, Chatenet M, Lima, Fabio Henrique Barros de. Electro-oxidation of ethanol on Pt/C, Rh/C, and Pt/Rh/C-based electrocatalysis investigated by on-line DEMS. *J Electroanal Chem* 2012; 681:56-65.
97. Wong YT, Hoffmann R. Chemisorption of carbon monoxide on three metal surfaces: Nickel (111), palladium (111), and platinum (111): A comparative study. *J Phys Chem* 1991; 95:859-67.
98. Brouzgou A, Podias A, Tsiakaras P. PEMFCs and AEMFCs directly fed with ethanol: A current status comparative review. *J Appl Electrochem* 2013; 43:119-36.

99. Xu Y, Zhang B. Recent advances in porous Pt-based nanostructures: Synthesis and electrochemical applications. *Chem Soc Rev* 2014; 43:2439-50.
100. Pereira M Jimenez M, Elizalde M, Robledo A, Alonso A, Study of the electrooxidation of ethanol on hydrophobic electrodes by DEMS and HPLC, *Electrochimica Acta* 2004; 49:3917–3925.
101. Neto A, Giz M, Perez J, Ticianelli E, Gonzalez E, The electro-oxidation of ethanol on Pt/Ru and Pt/Mo particles supported on high-surface-area carbon, *Journal of the Electrochemical Society* 2002; 109:272–279.
102. Dos Anjos A, Hahn F, Leger J, Kokoh K. B, Tremiliosi G, Feliu J, Herrero E, Waszczuk P, Crown A, Mitrovski K, Wieckowski A, In situ FTIRS studies of the electrocatalytic oxidation of ethanol on Pt alloy electrodes, *Journal of Solid State Electrochemistry* 2007; 11: 58-64.
103. Altawraneh R, Pickup P. G, *Journal of Electrochemical Society* 2017; 164:861-865.
104. Rousseau S, Coutanceau C, Lamy C, Léger J. Direct ethanol fuel cell (DEFC): Electrical performances and reaction products distribution under operating conditions with different platinum-based anodes. *J Power Sources* 2006; 158:18-24
105. Kim I, Han O. H, Chae S, Paik Y, Kwon S.H, Lee K, Sung Y. E, H. Kim, Catalytic reaction in direct ethanol fuel cell, *Chem. Int. Ed. Engl.* 2011; 50:2270-2274.
106. Wang H, Jusys W, Behm R. J, Ethanol electrooxidation on carbon-supported Pt, Pt/Ru and Pt/Sn₃, *J. Power Sources* 2006; 154: 351-359.
107. Taneda K, Yamazaki Y, Study of direct ethanol fuel cell *Electrochim. Acta* 2006; 52: 1627-1631.
108. Simoes F. C, Dos Anjos D. M, Vigier F, Leger J.M, Hahn F, Coutanceau C, Gonzalez

- E.R, Tremiliosi G, de Andrade A, Olivi P, Kokoh P, Electroactivity of tin modified platinum electrodes for ethanol electrooxidation *J. Power Sources* 2007; 167:1-5
109. Liu J, Zhao T, Chen R, Wong C. The effect of methanol concentration on the performance of a passive DMFC. *Electrochemistry Communications* 2005;7: 288-94.
110. Scott K, Taama W, Argyropoulos P, Sundmacher K. The impact of mass transport and methanol crossover on the direct methanol fuel cell. *J Power Sources* 1999; 83:204-16.
111. Luan Y, Zhang H, Zhang Y, Li L, Li H, Liu Y. Study on structural evolution of perfluorosulfonic ionomer from concentrated DMF-based solution to membranes. *Membr Sci* 2008; 319:91-101.
112. Guenot B, Cretin M, Lamy C. Clean hydrogen generation from the electrocatalytic oxidation of methanol inside a proton exchange membrane electrolysis cell (PEMEC): Effect of methanol concentration and working temperature. *J Appl Electrochem* 2015; 45:973-81.
113. Rayment C, Sherwin S. Introduction to fuel cell technology. Department of Aerospace and Mechanical Engineering, University of Notre Dame, Notre Dame, IN 2003; 46556:11-2.
114. Wang J. Electrochemical glucose biosensors. *Chem Rev* 2008; 108:814-25.

CHAPTER 2

Experimental

2.1. Chemicals and Materials

Chemicals used include: anhydrous ethanol (Commercial Alcohols Inc.), methanol (Fisher Scientific), sodium hydroxide (Sigma-Aldrich), formaldehyde (Fisher-Aldrich), formic Acid, hydrochloric acid (Sigma-Aldrich), sodium citrate (Anachemia), sodium nitroprusside (Sigma-Aldrich), potassium ferricyanide (Fisher Scientific), and Nafion[®] solution (5% Dupont) Industrial grade nitrogen, oxygen and 5% H₂/N₂ from Air Liquide were used in fuel cell experiments. CO₂ (Air Liquide) was used in detector calibration.

The cell that in all of the experiments reported in this work was a 5 cm² single cell fuel cell from Fuel Cell Technology Inc. Nafion[®] 115 and 117 membranes were the only PEMs used in this work. All homemade electrodes used Toray[™] (0.26 mm) carbon fiber paper (CFP). Commercial Pt anodes and cathodes (4 mg cm⁻² loading of Pt black on Toray[™] CFP) that were used in many of the experiments were donated by Ballard Power Systems.

2.2 Preparation of electrodes and Nafion membranes

Homemade electrodes described in this work were prepared using literature methods.^{1,2}A catalyst ink was prepared by first dispersing the catalyst in sufficient 5% Nafion[®] solution (Aldrich) and the resulting mixture was sonicated for ca. 30 min. The ink was then well dispersed over a 5 cm² piece of CFP (Toray[™]). The catalyst was then allowed to dry overnight in a fumehood.

For low or room temperature (RT) experiments, MEAs were prepared by hot-pressing the electrodes and a Nafion[®] 115 membrane together at a temperature of 135 °C for 90 seconds at a pressure of 200 kg cm⁻² using a Carver laboratory press.

2.3. Electrochemical Measurements

Electrochemical measurements were carried out with a Hokuto Denko HA-301 potentiostat with sinusoidal voltage in chapter 4 generated by a Solatron 1250 frequency response analyzer.

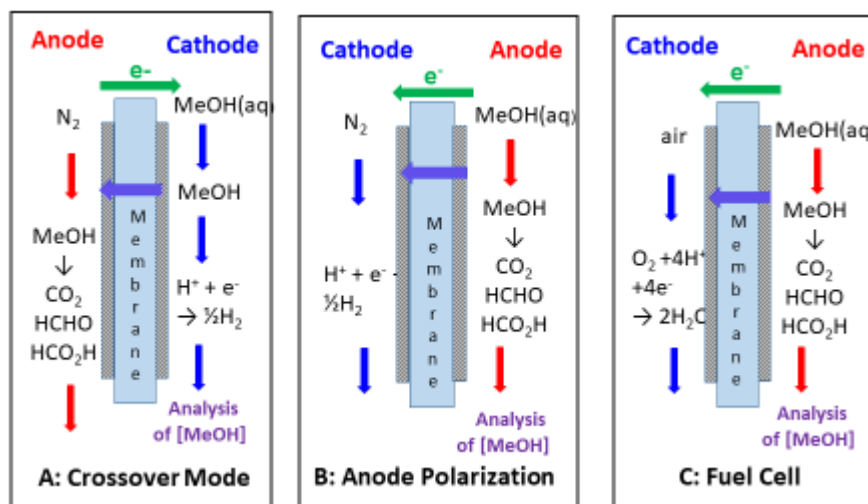


Figure 2.1. Illustration of the three modes of cell operation used in this work.

The cell was operated as an electrolysis cell and a fuel cell (Fig. 2.1). When the cell was in electrolysis mode (crossover mode (2.1 A)³ or anode polarization mode (2.1 B)⁴) oxidation of fuel (methanol or ethanol) took place at the anode (positive potential applied relative to the cathode). At the cathode, reduction of protons to hydrogen took place. In both electrolysis modes, the cathode acts as a dynamic hydrogen electrode (DHE)³. According to Ren and Gottesfeld³, at currents below 100 mA, the potential of the cathode would be less than 2 mV lower than RHE. To study the effect of crossover of fuel, the cell was operated in fuel cell mode (2.1 C). In this mode, electrochemical oxidation of fuel took place at the anode while at the cathode, oxygen was reduced to water. It is important to note that errors resulting from the IR drop of the cell ($R=0.05 \Omega$) had an insignificant effect on the applied potential.

2.4. CO₂ Analysis Instrumentation

2.4.1. Nondispersive Infrared (NDIR) Carbon Dioxide Detector⁵⁻⁷

All of the CO₂ measurements reported in this work were carried out using a commercial Telaire 7001 CO₂ detector. The detector uses a dual beam absorption infrared method with a gas flow-through inlet. It consists of an IR source which delivers light through a tube of air (Figure 2.1). The detector uses an optical filter which eliminates all wavelengths of light except for those absorbed by CO₂. When the tube is flushed with N₂, none of IR waves are absorbed and all of the light is detected at the far end of the tube. Once CO₂ is introduced into the detector, the IR waves are absorbed by the CO₂, leading to a decrease in light detected. The difference in IR light detected (CO₂/N₂ to N₂) is used to determine the concentration of CO₂ present in the detector. Beer's law represents the correlation between the analyzed concentration and intensity of light by the following:

$$\frac{I}{I_0} = e^{-kC} \quad (2.1)$$

where I is the intensity of the light striking the detector, I_0 is the measured intensity of the light in the empty gas chamber, k is a system dependent constant and C is the

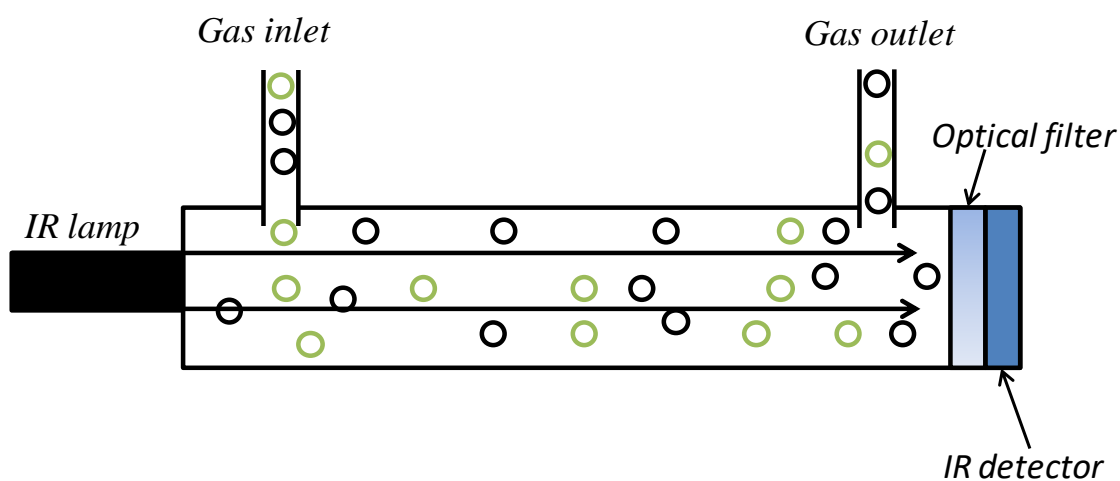


Figure 2.2 Gas chamber tube of a NDIR CO₂ monitor consisting of an IR lamp, optical filter and IR detector.

concentration of the gas to be measured. CO₂ calibration gasses are used to obtain k for the device. Logger Pro3 software was used for recording CO₂ detector signals.

2.5 Methanol analysis

The concentration of methanol in the cell exhaust was measured by UV-Visible spectroscopy. Methanol concentration was determined according to Zhan et al.⁸ According to their method, ionization of methanol to methoxy anions can occur in an alkaline solution, as shown in equation 2.2.



Then due to exchange between CH_3O^- and the OH^- adduct ($[Fe(CN)_5NO_2H]^{3-}$) of sodium nitroprusside ($[Fe^{III}(CN)_5NO]^{2-}$), $[Fe(CN)_5NO_2CH_3]^{3-}$ can be formed according equation 2.3.



The concentration of $[Fe(CN)_5NO_2CH_3]^{3-}$ can be determined by UV-Visible spectroscopy. An Agilent Technologies Cary 100 UV-Vis Spectrophotometer was used for measurement of methanol concentration.

UV-Visible spectroscopy is an analytical technique for measurement of chemical compounds by absorption of electromagnetic radiation. UV-Visible spectroscopy is based on measurement of the transmittance of the light beam when an electromagnetic light beam passes through a solution that contains analyte.

References,

1. Majidi P, Pickup P.G. Improving carbon dioxide yields and cell efficiencies for ethanol oxidation by potential scanning. *J Power Sources*. 2014; 269:173-179.
2. Majidi P, Pickup P.G. Sinusoidal potential cycling operation of a direct ethanol fuel cell to improve carbon dioxide yields. *J Power Sources*. 2014; 268:439-442.
3. Ren X, Springer T. E, Gottesfeld S, Water and methanol uptakes in Nafion membrane and membrane effects on direct methanol fuel cell performance 2000; 147:92-98
4. Li G, Pickup P. G, Measurement of single electrode potentials and impedances in hydrogen and direct methanol PEM fuel cells, *Electrochimica Acta* 2004; 49:4119–4126.
5. Lopez F, De Frutos J. Multispectral interference filters and their application to the design of compact non-dispersive infrared gas analysers for pollution control. *Sensors and Actuators A: Physical*. 1993; 37:502-506.
6. Gibson D, MacGregor C. A novel solid state non-dispersive infrared CO₂ gas sensor compatible with wireless and portable deployment. *Sensors*. 2013; 13:7079-7103.
7. Lessure H. S, Simizu S, Denes L. J, Guzman A. M. Non-dispersive infrared gas analyzer with interfering gas correction. 1999.
8. Zhan Y, Zhang Y, Li Q, Du X. A novel visible spectrophotometric method for the determination of methanol using sodium nitroprusside as spectroscopic probe. *J Chin Chem Soc*. 2010; 57:230-235.

Chapter 3

Improving Carbon Dioxide Yields and Cell Efficiencies for Ethanol Oxidation by Potential Scanning

All the experiments of this chapter were performed by Pasha Majidi.

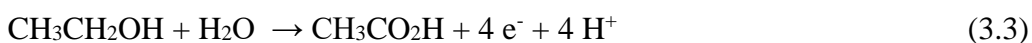
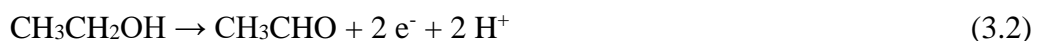
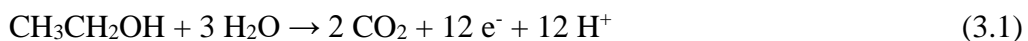
Data analysis was performed by Pasha Majidi and Dr. Peter Pickup.

This chapter has been published as (Majidi P, Pickup P. G. Improving carbon dioxide yields and cell efficiencies for ethanol oxidation by potential scanning. *J Power Sources*. 2014; 269:173-179) , which was written primarily by Dr. Peter Pickup.

3.1 Introduction

With the heavy demand for sustainable fuel sources instead of fossil fuels, fuel cells employing alcohols are becoming very attractive.¹⁻⁷ In comparison to methanol, ethanol has important advantages but also presents much more difficult challenges. First and foremost, there is already a well-developed infrastructure for renewable production of ethanol, and it is less toxic than methanol. Furthermore, the energy density of ethanol (8.0 kWh kg⁻¹) is greater than that of methanol (6.0 kWh kg⁻¹) and closer to the energy density of gasoline (10 kWh kg⁻¹). Consequently, there is rapidly growing development of direct ethanol fuel cells (DEFCs) based on proton exchange membrane technology.⁵⁻⁸

The main challenge in the development of DEFCs is that their efficiencies are very low relative to the theoretical value of 97%,³ and relative to efficiencies that can be achieved with hydrogen, methanol, and formic acid. The overall energy efficiency of a DEFC is determined by its electrochemical efficiency (theoretical efficiency \times cell potential/reversible cell potential), the ethanol oxidation efficiency (i.e. the average number of electrons passed per molecule (n_{av}) relative to the maximum available ($n_{max} = 12$ for ethanol)), and the loss of ethanol to crossover.⁹ The complete oxidation of ethanol involves the transfer of 12 electrons (eq. 3.1), while incomplete oxidation of ethanol to acetaldehyde ($n = 2$; eq. 3.2) or acetic acid ($n = 4$; eq. 3.3) will reduce the efficiency of the fuel cell considerably.



The electrochemical efficiency (voltage efficiency) is determined by the cell voltage, and so is strongly influenced by the activity of the anode catalyst. Much effort has therefore been applied to understanding the mechanism of the anodic oxidation of ethanol,^{8,10-14} and the development of more active electrocatalysts.^{8,15} PtRu, PtSn, PtRuSn, and PtRuRh based catalysts have been found to be particularly active and many other combinations of Pt with other metals and oxides have shown high activity.¹⁵ One of the key issues limiting the performance of the anode catalyst during ethanol oxidation is poisoning of the anode by strongly adsorbed CO and other intermediates (collectively referred to as CO_{ads} herein) on the catalyst surface. Thus, to increase the efficiency and performance of DEFCs, the formation of CO_{ads} should be inhibited and/or the catalyst should efficiently oxidize CO_{ads} to CO₂.

The ethanol oxidation efficiency (chemical efficiency; $n_{av}/12$) depends on the completeness of the ethanol oxidation reaction, and is determined by the weighted average yields (%_{product}) of all of the products. If it is assumed that CH₃CHO, CH₃CO₂H, and CO₂ are the only products, n_{av} is given by eq. 3.4 (note that one molecule of ethanol produces two molecules of CO₂).

$$n_{av} = (2x\%_{CH_3CHO} + 4x\%_{CH_3CO_2H} + 6x\%_{CO_2}) / (\%_{CH_3CHO} + \%_{CH_3CO_2H} + \%_{CO_2}/2) \quad (3.4)$$

It is clear from this relationship that chemical efficiency can be greatly increased by increasing the yield of CO₂. This has been achieved mainly by increasing the operating temperature of the cell,¹⁶⁻²² which promotes cleavage of the C-C bond and has the added benefit of increasing the activity of the catalyst (increased voltage efficiency). However, operation of PEM type DEFCs is limited to ca. 90 °C by the durability of the membrane and boiling point of ethanol.

Previously, we have shown that the yield of CO₂ produced from ethanol oxidation can be greatly increased by pulsing the potential or current at the anode in order to promote the oxidation of adsorbed intermediates at a high potential and allow ethanol to adsorb and dissociate at a lower potential.²³ Ethanol vapor in a nitrogen stream was used as the fuel in order to achieve a rapid response in the analysis of CO₂ using a flow through non-dispersive infrared (NDIR) CO₂ detector. That work has been extended here to conditions more representative of a DEFC. Thus an aqueous ethanol solution (0.1 M) was fed to the anode, the cell was operated at temperatures up to 80 °C, and Pt and PtRu anode catalysts were compared. However, nitrogen was used at the cathode, rather than air, so that the anode potential could be more accurately controlled and CO₂ was not produced by the chemical reaction of ethanol with O₂ either at the cathode²⁴ or anode.²⁵ Under these conditions, the cathode acts as a dynamic hydrogen pseudo reference electrode (DHE). A previously reported experimental set-up²⁴ was modified as illustrated in Fig 3.1. The CO₂ concentration in the combined anode and cathode exhausts was monitored so that the results were not impacted by crossover losses.²⁴⁻²⁶

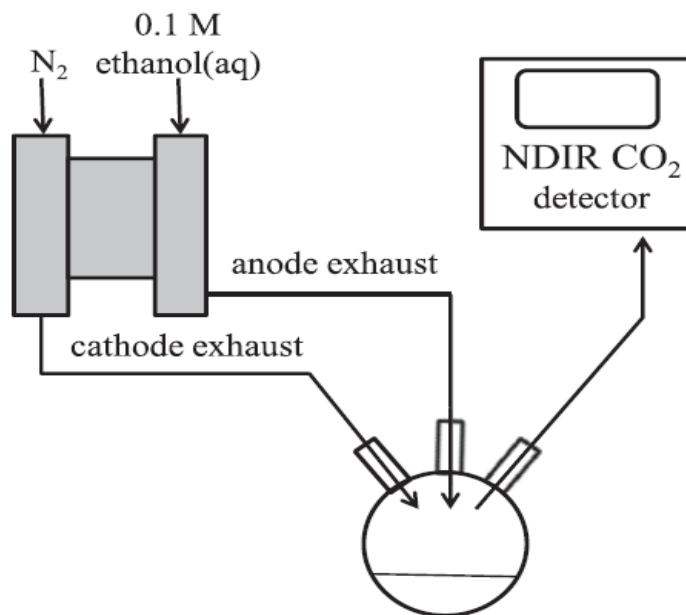


Figure 3.1. Schematic diagram of the electrolysis cell and CO₂ analysis system.

Potential cycling at a fixed sweep rate was employed here, rather than current or voltage pulses or AC perturbations, because this is a standard and widely used electroanalytical method. This provides more useful diagnostic information and allows comparisons with the extensive literature on ethanol voltammetry. The cell was operated with a dynamic hydrogen cathode (DHE) to provide a stable reference potential for the voltammetric (current vs. potential) measurements. The potential cycling results are compared with sweep and hold experiments in which a linear potential sweep was applied, and then the potential was held at the upper limit for the rest of the experiment. This mimics the initial forward scan in the corresponding cycling experiments, avoids the large current spike that accompanies a potential step, and represents constant potential behavior after the 30-80 s for the initial sweep.

The primary goals of this work were to determine whether the previously demonstrated strategy of adsorbing ethanol at low potentials and oxidatively stripping adsorbed

intermediates (primarily CO) at higher potentials would be effective at higher temperatures and with a PtRu anode catalyst, and to begin to explore how the efficiency of CO₂ production depends on the potentials employed. From a practical perspective, this knowledge could be used to improve the efficiency of DEFCs and ethanol electrolysis cells (EEC) which have recently been reported for producing clean hydrogen from ethanol.²⁷ Although, our experimental configuration is essentially an EEC, since H₂ is produced at the cathode, the dependence of CO₂ yields on anode potentials, temperature and catalyst should also provide a good guide to the behavior of a DEFC. Pulsed current, triangle, sawtooth, trapezoidal, and AC waveforms have been reported to prolonging the run time and life cycle of batteries.²⁸ Also, pulsing has been used to improve the performance of methanol fuel cells²⁹ and CO tolerance of hydrogen fuel cells,³⁰ and to decouple the parallel routes for the electrochemical oxidation of methanol.³⁰ Similar studies with DEFCs and EECs are therefore very pertinent.

3.2 Experimental

3.2.1 Chemicals and materials

Anhydrous ethanol (Commercial Alcohols Inc.) was used as received and double distilled water was used throughout all experiments. Cathodes and Pt anodes consisted of 4 mg cm⁻² Pt black on TorayTM carbon fiber paper. PtRu anodes consisted of 5.5 mg cm⁻² PtRu black on TorayTM carbon fiber paper. NafionTM 115 membranes (Ion Power) were cleaned at 80 °C in 3% H₂O₂(aq) and 1 M H₂SO₄(aq), rinsed with water, and stored in water.

3.2.2 *The cell*

A 5 cm² commercial fuel cell (Fuel Cell Technology Inc.) was used. The anode inlet and outlet were both modified to prevent the ethanol solution from contacting any metal parts of the hardware. Membrane and electrode assemblies were prepared by pressing a 5 cm² anode and a 5 cm² cathode onto a Nafion™ 115 membrane in the cell. The cell was operated with an anode feed of 0.10 mol L⁻¹ ethanol solution at 0.69 mL min⁻¹. The cathode feed was N₂ at typically ca. 0.8 mL s⁻¹. The cell was operated with a Hokuto Denko HA-301 potentiostat and HB-104 function generator.

3.2.3 *CO₂ analysis*

Both the anode solution and the cathode gas (N₂) were passed into a 125 mL flask to collect the liquid. The N₂ stream exiting the flask was passed through a Telaire 7001 non-dispersive infrared CO₂ detector. The quantity of CO₂ detected over a specified period was calculated from the integral of the CO₂ concentration (ppm) readings ($\text{moles CO}_2 = \int (\text{ppm}_{\text{CO}_2} \cdot \dot{n} / 10^6) dt$, where \dot{n} is the N₂ flow rate in mol s⁻¹). The flow rate of N₂ reaching the detector was measured for each set of experiments and was typically ca. 0.8 mL s⁻¹ ($\sim 3 \times 10^{-5}$ mol s⁻¹). No corrections were made for the amount of CO₂ remaining in the liquid in the collection flask because based on Henry's Law they would be too small (ca. 2% or lower) to significantly influence the estimated CO₂ yields. However, CO₂ retention does contribute to the slow response seen in the CO₂ concentration plots (see below).

The CO₂ detector was calibrated daily using CO₂ in N₂ standards prepared by injecting pure CO₂ in to an N₂ stream. The precision and accuracy of the system has been evaluated in a previous study, with relative standard deviations typically 5-10% at the CO₂ concentrations measured in this work.²⁶ The start times of the CO₂ traces reported here have been corrected for the minimum time required for the CO₂ to reach the detector. This causes the CO₂ collection time to be 50-100 s shorter than the cell run time.

3.3 Results and discussion

3.3.1 Potential cycling vs. fixed potential at ambient temperature

Figs. 3.2 and 3.3 illustrate how the current and production of CO₂ varied for two different potential waveforms, linear sweep with the potential held at the upper limit of 0.9 V, and potential cycling between 0.1 and 0.9 V. In both cases, the cell was operated for a total of 30 min. The sharp initial rise in the current in both experiments can be attributed mainly to the oxidation of adsorbed ethanol and partially oxidized intermediates (pre-adsorbed species).³¹ Since adsorbed CO is the primary intermediate, and the direct precursor to CO₂, all of the pre-adsorbed species are collectively referred to as CO_{ads} in this paper.

In the sweep and hold experiment, the current began to decay when the potential was held at 0.9 V, and reached an approximately steady value. In contrast, the current continued to be modulated in the potential cycling experiment, with the current decreasing during the reverse scans (0.9 to 0.1 V) and increasing on the forward scans (0.1 to 0.9 V). Apart from short periods at the end of each cycle due to discharging of the double layer (and possibly a small amount of methane production¹⁷), the current remained positive (oxidation of ethanol at

the anode). The amplitude of the current response initially decreased with cycling, but then became reasonably steady.

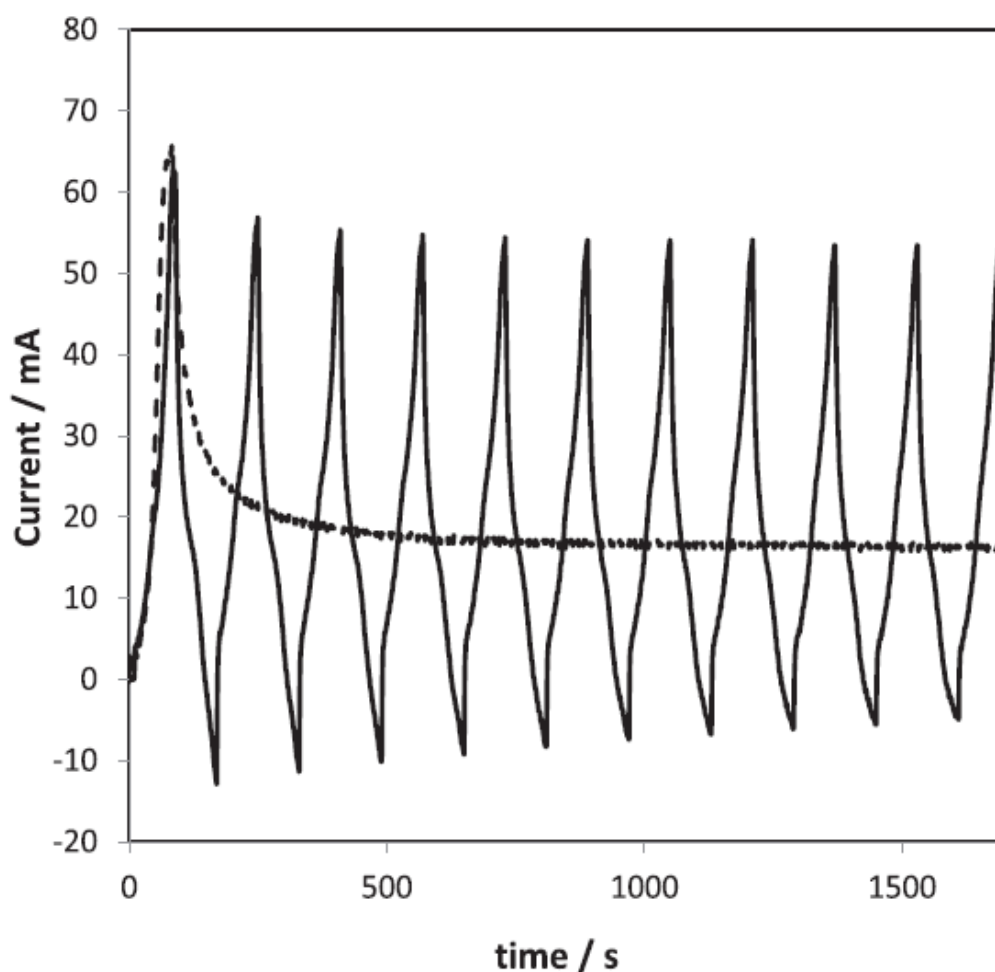


Figure 3.2. Current vs. time plots for electrolysis of 0.1 M ethanol at ambient temperature at Pt black anode using a linear potential sweep from 0.1 V vs. DHE with a potential hold at the upper limit of 0.9 V (dashed), and potential cycling between 0.1 and 0.9 V (solid). Sweep rate = 10 mV s^{-1} .

As previously reported,²³ the initial potential scan to 0.9 V produced a burst of CO_2 that can be attributed mainly to the oxidation of pre-adsorbed species (CO_{ads}). In the sweep

and hold experiment, there was only transient CO₂ production, while cycling the potential continuously between 0.1 V and 0.9 V resulted in sustained CO₂ production. As previously reported for pulsed operation of a cell,²³ the sustained CO₂ production in the potential cycling experiment can be attributed to the formation of a new layer of CO_{ads} at the lower potentials of each potential scan.

Analysis of the transient CO₂ response for the sweep and hold experiment provides important information on the response time of the CO₂ analysis system and the amount of CO_{ads}. Previous work with ethanol vapor indicated that the oxidation of CO_{ads} is much faster than the timescale in Fig. 3.3, as would be expected at 0.9 V.

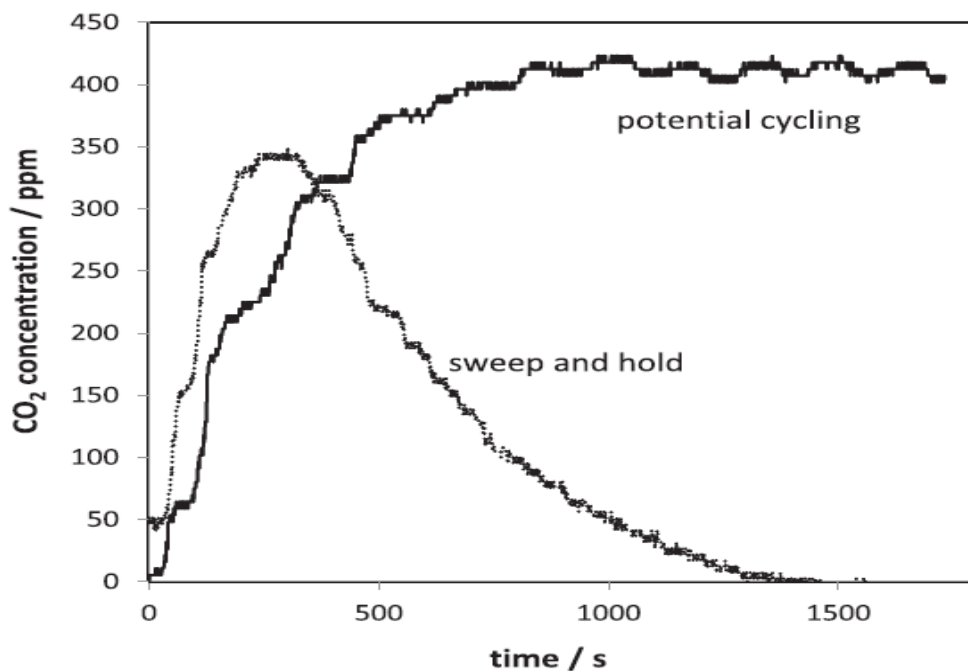


Figure 3.3. CO₂ concentration vs. time plots for the electrolyses shown in Fig. 2. Data for sweep and hold (dotted) and potential cycling (solid) are shown. Lower potential = 0.1 V; Upper potential = 0.9 V.

The breadth of the transient CO₂ response in Figure 3.3 for the sweep and hold experiment can therefore be taken as representative of the signal broadening due to the flow and collection system used here to transfer the CO₂ produced by the cell from the liquid EtOH(aq) exhaust to the N₂ stream for analysis. Much faster responses can be achieved (e.g. 20 s),²³ but the system here was designed to allow for long-term, high temperature operation of the cell with liquid EtOH(aq) rather than for a fast response.

Since the CO₂ reading dropped to zero in the sweep and hold experiment, it is a reasonable approximation to assume that most of the CO₂ produced in this experiment was due to the oxidation of CO_{ads}, and not from oxidation of ethanol diffusing to the electrode from the anode solution. Integration of this CO₂ transient provides the number of moles of CO₂ produced, 3.8 μmol, which should be a reasonable estimate of the number of moles of CO_{ads} (stripping of pure CO adsorbed on the type of anode used here produced ca. 6.2 μmol of CO₂, corresponding to an active Pt area of ca. 2500 cm²).

The potential cycling experiment shown in Fig. 3.3 produced 11.3 μmol of CO₂. Of this, ca. 4 μmol would have been due to CO_{ads}, as in the sweep and hold experiment, leaving > 7 μmol due to sustained ethanol oxidation. Since there may have also been some oxidation of ethanol from solution in the sweep and hold experiment, this is taken to represent a lower limit on the ethanol oxidized during the cycling experiment.

The important distinction that we are making here is between the oxidation of species already adsorbed on the electrode surface before the start of the experiment (i.e. CO_{ads}) and the oxidation of ethanol that diffuses to the electrode (from the solution) during the experiment. We have done this by showing that CO₂ production at constant potential is dominated by the

former. This has very important implications in the determination of faradaic yields for ethanol oxidation, and the result at constant potential allows us to make a correction to account for the effects of the pre-adsorbed species.

Of central importance in the development of DEFC technology is the faradaic yield for CO₂ production (CO₂ yield), which is defined by eq. 3.5.

$$\text{CO}_2 \text{ yield} = 6F \text{mol}_{\text{CO}_2} / Q \quad (3.5)$$

Here, mol_{CO_2} is the measured moles of CO₂ and Q is the charge passed by the cell. Application of this equation to the data from Figs. 3.2 and 3.3 produces apparent CO₂ yields of 6.1% and 21.6%, for the sweep and hold and potential cycling experiments, respectively. These are “apparent” yields because it is clear that much of the CO₂ is derived from CO_{ads} rather than ethanol from the solution, and so eq. 3.5 is inaccurate in this situation. If all of the CO₂ was from CO_{ads} in the sweep and hold experiment, the actual CO₂ yield from ethanol would have been zero.

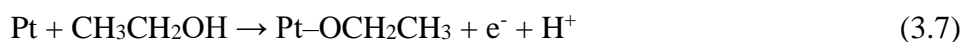
To obtain more accurate yields of CO₂ for the potential cycling experiment, corrections should be made to account for both the CO₂ produced from CO_{ads} (mol_{ads}) and the charge required to oxidize the CO_{ads} to CO₂, as shown in eq. 3.6.

$$\text{CO}_2 \text{ yield} = 6F(\text{mol}_{\text{CO}_2} - \text{mol}_{\text{ads}}) / (Q - nF\text{mol}_{\text{ads}}) \quad (3.6)$$

Here, n is the average number of electrons required to produce CO₂ from the adsorbed species. It can range from 2 for adsorbed CO to 6 for adsorbed ethanol. The amount of CO₂ produced in the sweep and hold experiment is assumed to provide a reasonable estimate of mol_{ads} . Since the value of n is unknown, we report here the values for the two extremes, which are 14.7%

for $n = 2$ and 15.5% for $n = 6$. These are average values for the whole 30 min experiment depicted in Figs. 2 and 3. However, it is clear from the comparison of the sweep and hold and cycling CO₂ profiles that the yield of CO₂ must have increased substantially over the first half of the cycling experiment. From an operational perspective, the sustained higher yield in the 2nd half of the experiment is more relevant. This can easily be estimated by applying eq. 3.5 to the region of approximately steady state CO₂ production after ca. 900 s, where the effects of the transient CO₂ from CO_{ads} would have been minor. The CO₂ yield was thus calculated to be 26.5%, which should be a good estimate of the sustained production of CO₂ from ethanol being fed to the cell.

In considering which of the above methods is most appropriate for calculation of CO₂ yields, we must consider the origin of the adsorbates. When ethanol is introduced into the cell, it will spontaneously adsorb onto the Pt anode catalyst and there will be some electron transfer to the Pt as C-H and C-C bonds are oxidized. A first step is illustrated by eq. 7.



This reaction and parallel/subsequent oxidation steps will cause the anode open circuit potential to decrease and produce a variety of adsorbates in various oxidation states.³¹ In addition, traces of oxygen in the system will contribute to the oxidation of the adsorbates without changing the anode potential. Since these processes result in partial oxidation of a substantial amount of ethanol without any charge being passed by the cell, including products from the adsorbates in the calculations of yields will produce large errors. These would be extremely difficult to accurately correct for, and so the most accurate approach is to apply eq.

3.5 (and similar equations for other products) to data (charges and product amounts) collected after the products from the adsorbates have been flushed from the analysis system.

These results and considerations illustrate the complexities of trying to define and measure product yields from ethanol oxidation. Even with product collection over a 30 min period, the effects of pre-adsorbed intermediates are large, and many hours could be required to produce acceptable accuracy in some cases. The error can be minimized, however, by beginning product collection after a delay to avoid the collection of products from adsorbed species. An alternative method would be to carry out a pre-conditioning to remove (oxidize) the adsorbates. However, we have found this to be unsatisfactory because a fresh layer of adsorbates form when the cell is returned to the initial potential, or the anode is allowed to return to its open circuit potential. The charges passed during these processes would then have to be accounted for in determining the true CO₂ yield.

3.3.2 Effects of potential limits at ambient temperature

For most efficient operation of a DEFC, in addition to high levels of conversion of ethanol to CO₂, the cell potential should be as high as possible at the power output required for the application. In the experiments described here, the cell potential is the anode potential vs. DHE. Therefore low cell potentials in this work would correspond to high efficiencies in a fuel cell and also in an ethanol electrolysis cell (EEC) producing hydrogen at the cathode.²⁷

The results in Fig. 3.3 show that CO₂ yields can be increased greatly and sustained by potential cycling, and this increases the chemical efficiency of the cell. In order to optimize the operation of either a DEFC or EEC, maximization of the yield of CO₂ should be balanced

against minimizing the average anode potential and maximizing the power output of the cell (which increases with increasing anode potential to a certain point). To this end, experiments were run in potential cycling mode with various upper and lower limits (i.e. various average anode potentials and average power usage) to explore how the CO₂ yield depends on the voltage efficiency and power. The potential sweep rate was maintained at 10 mV s⁻¹ for these experiments. Since long term performances are of interest here, CO₂ yields were determined by applying eq. 5 to just the final 800 s of each experiment, although other parameters are reported for averages (current and power) or integrals (total CO₂) over the full duration of each experiment.

Table 3.1 summarizes results for a series of experiments in which the lower potential limit was set at 0.1 V while the upper limit was varied from 0.6 V to 0.9 V. The power can only be calculated for an EEC, since the cell was not operated as a fuel cell.

Table 3.1. Summary of data for the electrolysis of 0.1 M ethanol at ambient temperature at a Pt black anode under potential cycling conditions. The lower potential limit was 0.1 V.

| Upper potential / V | Average current / mA | Total CO ₂ / μmol | Average CO ₂ yield after 900 s | Average power ^a / mW |
|------------------------|-------------------------|---------------------------------|--|------------------------------------|
| 0.6 | 4.1 | 0 | 0 | 2.0 |
| 0.7 | 8.7 | 1.6 | 8.4% | 4.9 |
| 0.8 | 13.4 | 9.1 | 21.3% | 8.6 |
| 0.9 | 17.0 | 11.3 | 26.5% | 11.6 |

^a Power consumption for an EEC.

It is clear from the data in Table 3.1 that significant production of CO₂ from ethanol in solution can only be achieved with an upper potential of at least 0.8 V, and even then the CO₂ produced was found to decline (not shown) from a peak of 400 ppm at ca. 300 s to 240 ppm at 1700 s. It should be noted that the total CO₂ produced when the upper potential was 0.7 V was less than the CO₂ that could be produced from pre-adsorbed species (3.8 μmol), indicating that the actual CO₂ yield was much less than the value of 8.4% reported in Table 3.1. These results can be explained by the high potentials required to oxidize adsorbed CO. At Pt, this reaction occurs primarily over the range of ca. 0.6-0.8 V vs. RHE,³² which corresponds approximately with the observation of CO₂ evolution reported in Table 3.1.

From the data in Table 3.1 it can be shown, using eq. 3.4, that increasing the upper potential from 0.8 V to 0.9 V increases the chemical efficiency by 5-11% depending on the CH₃CHO/CH₃CO₂H ratio. However, this is negated in the overall cell efficiency by the 14%

increase in the average cell voltage required (or decreased cell voltage for a fuel cell).

Nonetheless, this could still be of net benefit for an EEC because of the high current and therefore higher rate of hydrogen production. This would not likely be the case for a DEFC, however, where the very low cell potential at the upper anode potential limit (if attainable) would lead to very low overall efficiencies.

Table 3.2 summarizes results for a series of experiments in which the upper potential limit was set at 0.9 V while the lower limit was varied from -0.2 V to +0.6 V.

Table 3.2. Summary of data for the electrolysis of 0.1 M ethanol at ambient temperature at a Pt black anode under potential cycling conditions. The upper potential limit was 0.9 V.

| Lower potential / V | Average current / mA | Total CO ₂ / μmol | Average CO ₂ yield after 900 s | Average power ^a / mW |
|------------------------|-------------------------|---------------------------------|--|------------------------------------|
| -0.2 | 14.6 | 2.6 | 6.6% | - |
| -0.1 | 16.5 | 7.4 | 14.7% | - |
| 0 | 14.9 | 7.2 | 16.6% | 10.1 |
| 0.1 ^b | 15.1 | 7.0 | 18.3% | 10.3 |
| 0.2 | 16.3 | 8.6 | 21.2% | 11.3 |
| 0.3 | 15.5 | 7.6 | 18.5% | 10.7 |
| 0.4 | 18.4 | 9.3 | 19.9% | 13.0 |
| 0.5 | 16.9 | 6.5 | 12.1% | 12.3 |
| 0.6 | 16.3 | 1.8 | 1.9% | 12.5 |

^a Power consumption for an EEC. Not meaningful when negative cell potentials were employed. ^b Values differ from those in Table 3.1 because this is a different data set for a different MEA.

Although the use of negative potentials has little relevance to the operation of a fuel cell, it is relevant to an EEC where the anode could possibly be activated at such potentials. However, it can be seen from the results that low potentials were not beneficial, with CO₂ yields falling slightly for lower potential limits below 0.2 V and then sharply at -0.2 V. The lower yields in these cases may be due to adsorption of hydrogen atoms which can interfere with ethanol adsorption and dissociation. In light of these results, and the benefits of running

the cell at high average current and power, the lower potential limit should be set to the highest value that does not compromise selectivity for the complete oxidation to CO₂. From the data in Table 3.2, this is 0.4 V (since the slightly higher yield at 0.2 V is within the experimental uncertainty). This potential is clearly sufficiently low for dissociative adsorption and oxidation of ethanol to occur on the time scale of the cycling, while 0.5 V is not low enough for these processes to occur efficiently.

3.3.3 Operation at elevated temperatures

Although the results presented in the previous sections are scientifically significant, the practical benefits of dissociative oxidation of ethanol to CO₂ at ambient temperature may be only minor. Of key technological importance is whether the benefits of potential cycling are maintained at the higher temperatures employed in applications, and whether lower anode potentials can be employed at higher temperatures. To explore this, experiments akin to those described above were run at 50 °C and 80 °C. The lower potential limit was maintained at 0.1 V in these experiments in order to allow comparison with the upper limit effects in Table 3.1, and to ensure that the lower potential did not begin to limit ethanol absorption when the sweep rate was increased.

Fig. 3.4 depicts apparent CO₂ yields versus time for potential cycling between 0.1 V and 0.7 V at ambient temperature, 50 °C and 80 °C. These CO₂ yields were calculated by using eq. 3.1 for each CO₂ ppm reading (converted to mol s⁻¹) and the average current (C s⁻¹) over the experiment. Although this results in significant errors in the actual yield at each point, it

preserves the form of the CO₂ meter response (i.e. it provides a scaling of the CO₂ readings based on the charge passed at each temperature), which is informative.

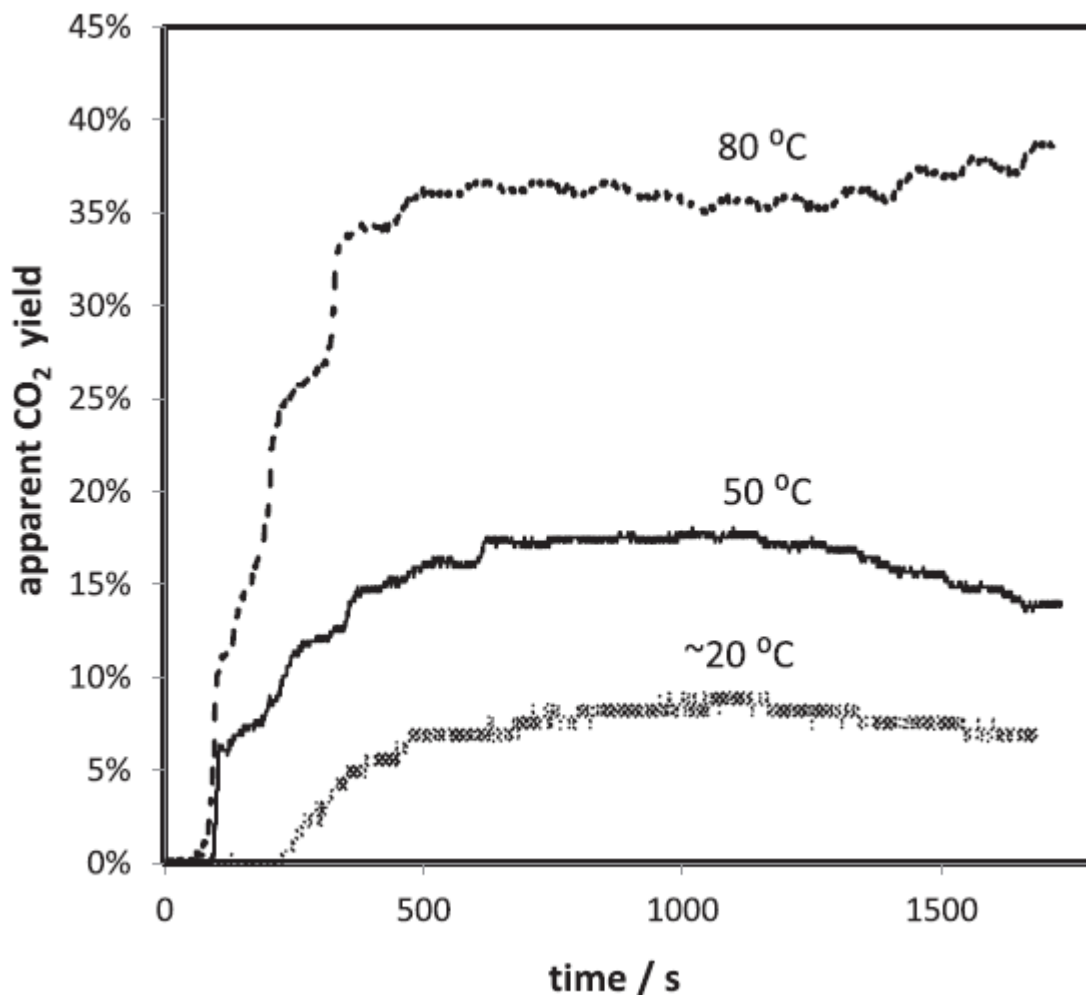


Figure. 3.4. Apparent CO₂ yields vs. time for electrolysis of 0.1 M ethanol at a Pt black anode during potential cycling between 0.1 V and 0.7 V at ambient temperature, 50 °C and 80 °C.

An upper limit of 0.7 V was selected for Fig. 3.4 because it best illustrates the benefits of increasing the temperature. As seen in Table 3.1, an upper limit of 0.7 V was insufficient

for complete adsorbate removal at ambient temperature, resulting in a large drop in CO₂ yield relative to an upper limit of 0.8 V, and a decreasing yield at long times (Fig. 3.4). However, increasing the temperature resulted in large increases in CO₂ yield (Fig. 3.4) and at 80 °C the CO₂ production was sustained for the duration of the experiment. In addition, increasing the temperature increased the average currents and power greatly, and much more CO₂ was produced (Table 3.3).

Table 3.3. Effects of temperature on cell performance parameters for the electrolysis of 0.1 M ethanol at ambient temperature at a Pt black anode for potential cycling between 0.1 V and 0.7 V at 10 mV s⁻¹

| Temperature / °C | Average current / mA | Total CO ₂ / μmol | Average CO ₂ yield after 900 s | Average power ^a / mW |
|------------------|----------------------|------------------------------|---|---------------------------------|
| Ambient | 8.7 | 1.6 | 8.4% | 4.9 |
| 50 | 25.4 | 11.0 | 16.0% | 14.6 |
| 80 | 50.8 | 48.2 | 31.9% | 28.7 |

Since complete oxidation of ethanol to CO₂ requires the cleavage of the strong C-C bond, higher temperatures generally increases CO₂ yields, and this has been well documented.¹⁶⁻²² In addition, CO oxidation is promoted by higher temperature. Both of these effects are expected to decrease the benefits of potential cycling relative to its effects at ambient temperature. To explore this, potential cycling and sweep and hold experiments at 80 °C were compared. At this temperature, a sweep rate of 100 mV s⁻¹ during potential cycling was found to provide higher CO₂ yields than 10 mV s⁻¹, and so only the 100 mV s⁻¹ data are reported here.

It is clear from the data in Table 3.4 that even at 80 °C higher CO₂ yields can be obtained at higher average currents when potential cycling is employed.

Table 3.4. Average currents and CO₂ yields for the electrolysis of 0.1 M ethanol at 80 °C at a Pt black anode under sweep (10 mV s⁻¹) and hold, and potential cycling (100 mV s⁻¹) conditions. The lower potential limit was 0.1 V. (-) results too uncertain to report.

| Upper potential / V | Average current after 900 s / mA | | Average CO ₂ yield after 900 s | |
|---------------------|----------------------------------|---------|---|---------|
| | Sweep and hold | cycling | Sweep and hold | cycling |
| 0.4 | 21.4 | - | 45.6% | - |
| 0.5 | 65.5 | - | 34.3% | - |
| 0.6 | 83.5 | 28.4 | 33.5% | 35.1% |
| 0.7 | 82.5 | 53.1 | 28.4% | 44.6% |
| 0.8 | 69.9 | 82.7 | 23.2% | 65.0% |
| 0.9 | 74.9 | 121 | 11.9% | 45.8% |

The yield of 65% obtained for potential cycling is one of the highest reported for ethanol oxidation at 80 °C. For example, a value of 35% was measured by liquid chromatography for a DEFC with a Pt anode operated at 80 °C and a current density of 8 mA cm⁻²,²⁵ while a maximum of 50% at 70 °C was reported for a differential electrochemical mass spectrometry (DEMS) study of ethanol oxidation (0.1 M) at a gas diffusion electrode containing 4.3 mg cm⁻² Pt black.¹⁷

The decrease in yield seen in Table 3.4 as the potential was increased in the sweep and hold experiments is consistent with the trend reported in other studies [e.g.^{21,23}], which is due to a decreasing tendency for C-C bond breaking and increasing oxygen coverage.¹⁹ The opposite trend was observed from 0.6 to 0.8 V in the cycling experiments, which illustrates the benefits of using higher potentials to periodically strip adsorbates from the electrode.

3.3.4 PtRu Anode Catalyst

The results for cycling between 0.1 V and 0.8 V shown in Table 3.4 are attractive for operation of an EEC but not of practical value for a DEFC because the potential required to strip CO_{ads} from anode is too high to be produced by the cell. A Pt black anode catalyst was used in all experiments reported to this point. However, in practical applications, bi- or tri-metallic catalysts with higher activities and which can oxidize adsorbed CO at lower potentials are normally preferred.^{8,15} PtRu was chosen here because it provides higher cell potentials than Pt in DEFCs, and allows adsorbed CO to be stripped at significantly lower potentials. It therefore offers the realistic possibility of increasing yields in a DEFC under potential cycling conditions. In addition, it should increase the efficiency of EECs.

Figs. 3.5 and 3.6 show current and CO₂ concentration traces for ethanol oxidation at 80 °C at a PtRu anode for cycling and sweep and hold experiments with an upper potential limit of 0.6 V.

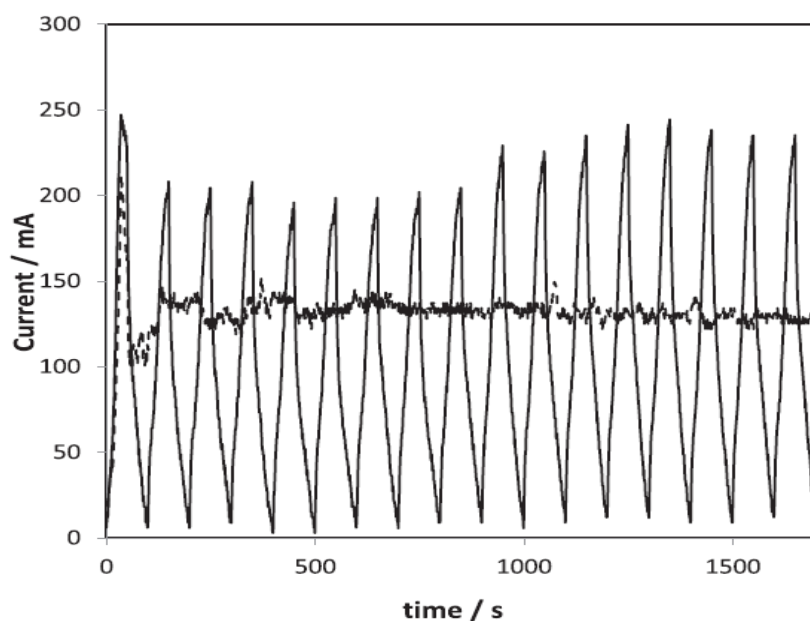


Figure 3.5. Current vs. time plots for electrolysis of 0.1 M ethanol at 80 °C at a PtRu black anode using a linear potential sweep from 0.1 V vs. DHE with a potential hold at the upper limit of 0.6 V (dashed), and potential cycling between 0.1 and 0.6 V (solid). Sweep rate = 10 mV s⁻¹

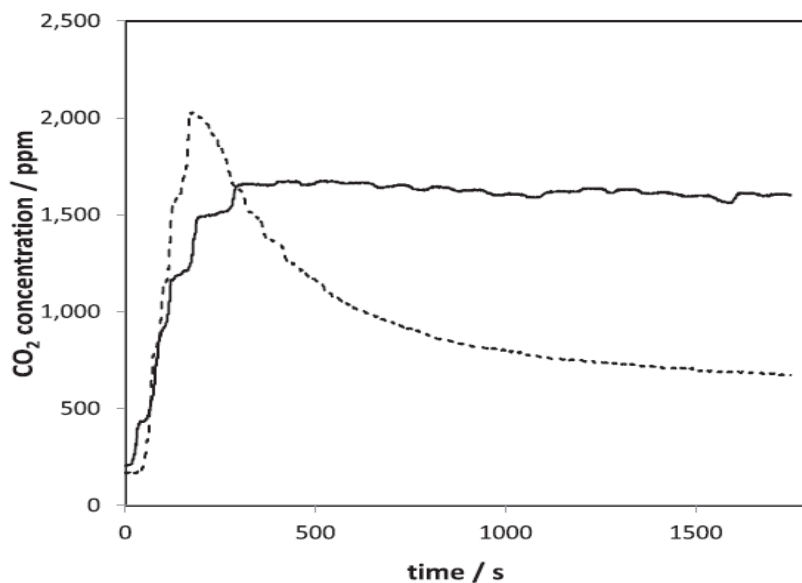


Figure 3.6. CO₂ concentration vs. time plots for the electrolyses shown in Fig. 5. Data for sweep and hold (dashed) and potential cycling (solid) are shown. Lower potential = 0.1 V; Upper potential = 0.6 V.

Average currents and CO₂ yields for these experiments and others with different upper potential limits are presented in Table 3.5.

Table 3.5. Average currents and CO₂ yields for the electrolysis of 0.1 M ethanol at 80 °C at a PtR black anode under sweep (10 mV s⁻¹) and hold, and potential cycling (10 mV s⁻¹) conditions. The lower potential limit was 0.1 V.

| Upper potential / V | Average current after 900 s / mA | | Average CO ₂ yield after 900 s | |
|---------------------|----------------------------------|---------|---|---------|
| | Sweep and hold | cycling | Sweep and hold | cycling |
| 0.4 | 103 | 34.4 | 13.2% | 17.3% |
| 0.5 | 133 | 73.3 | 13.2% | 23.3% |
| 0.6 | 131 | 110 | 11.2% | 27.1% |
| 0.7 | 121 | 111 | 7.8% | 32.4% |
| 0.8 | 132 | 130 | 4.6% | 28.3% |

As expected,^{22,26} CO₂ yields were generally lower with the PtRu catalyst relative to Pt under the same conditions. However, higher currents were obtained at lower potentials, demonstrating the higher activity of PtRu for ethanol oxidation, and potential cycling was still very effective at increasing CO₂ yields. In addition, less positive upper anode potentials were required to obtain the benefits of cycling, as required for a DEFC. For example, cycling between 0.1 V and 0.6 V produced an average current of 110 mA, which was slightly higher

than the 103 mA produced at a constant potential of 0.4 V, while the CO₂ yield during cycling was more than double (27.1%) that at constant potential (13.2%). The same cycling experiment with a Pt anode produced a higher CO₂ yield of 35.1% but a much lower average current of 28.4 mA (Table 3.4). These comparisons, and others based on the data in Tables 3.4 and 3.5 illustrate the trade-off required between efficiency (determined mainly by the anode potential and CO₂ yield) and power.

3.4 Conclusions

Previous observations that potential modulation can increase the chemical efficiency of ethanol oxidation by promoting CO₂ production have been extended to the electrolysis of ethanol in aqueous solution. The effects of potential limits, temperature and Pt vs. PtRu anode catalysts have been explored. In all cases, cycling the potential has been shown to increase the yield of CO₂ and in many cases the effects are substantial. For example, at ambient temperature with a Pt anode the yield has been increased from << 6.4% to 26%, while a yield 65% has been achieved at 80 °C. PtRu provides lower CO₂ yields than Pt, but significantly decreases the anode potential required. At 80 °C a maximum yield of 32.4% was obtained under cycling conditions, while the best yield at constant potential was only 13.2%.

These results demonstrate how the efficiency of direct ethanol fuel cells and ethanol electrolysis cells can be improved by employing potential modulation techniques. It can be anticipated that further optimization of the operational parameters (potential waveform and limits, sweep rate, temperature) will lead to higher efficiencies, and that efficient oxidation of ethanol can be sustained indefinitely.

References,

1. Majidi P, Pickup P. G. Improving carbon dioxide yields and cell efficiencies for ethanol oxidation by potential scanning. *J Power Sources*. 2014; 269:173-179.
2. Vigier F, Coutanceau C, Perrard A, Belgsir E, Lamy C. Development of anode catalysts for a direct ethanol fuel cell. *J Appl Electrochem*. 2004; 34:439-446.
3. Demirci U. B. Direct liquid-feed fuel cells: Thermodynamic and environmental concerns. *J Power Sources*. 2007; 169:239-246.
4. Li X, Faghri A. Review and advances of direct methanol fuel cells (DMFCs) part I: Design, fabrication, and testing with high concentration methanol solutions. *J Power Sources*. 2013; 226:223-240.
5. Brouzgou A, Podias A, Tsiakaras P. PEMFCs and AEMFCs directly fed with ethanol: A current status comparative review. *J Appl Electrochem*. 2013; 43:119-136.
6. Braunschweig B, Hibbitts D, Neurock M, Wieckowski A. Electrocatalysis: A direct alcohol fuel cell and surface science perspective. *Catalysis today*. 2013; 202:197-209.
7. Kamarudin M, Kamarudin S. K, Masdar M, Daud W. R. W. Review: Direct ethanol fuel cells. *Int J Hydrogen Energy*. 2013; 38:9438-9453.
8. Friedl J, Stimming U. Model catalyst studies on hydrogen and ethanol oxidation for fuel cells. *Electrochim Acta*. 2013; 101:41-58.
9. Vigier F, Rousseau S, Coutanceau C, Leger J, Lamy C. Electrocatalysis for the direct alcohol fuel cell. *Topics in Catalysis*. 2006; 40:111-121.
10. Kutz R. B, Braunschweig B, Mukherjee P, Behrens R. L, Dlott D. D, Wieckowski A. Reaction pathways of ethanol electrooxidation on polycrystalline platinum catalysts in

- acidic electrolytes. *Journal of Catalysis*. 2011; 278:181-188.
11. Evarts S. E, Kendrick I, Wallstrom B. L, et al. Ensemble site requirements for oxidative adsorption of methanol and ethanol on Pt membrane electrode assemblies. *ACS Catalysis*. 2012; 2:701-707.
 12. Kavanagh R, Cao X, Lin W, Hardacre C, Hu P. Acetaldehyde production in the direct ethanol fuel cell: Mechanistic elucidation by density functional theory. *The Journal of Physical Chemistry C*. 2012; 116:7185-7188.
 13. Melke J, Schoekel A, Gerteisen D, et al. Electrooxidation of ethanol on Pt. An in-situ and time-resolved XANES study. *The Journal of Physical Chemistry C*. 2012; 116:2838-2849.
 14. Gomes J. F, Bergamaski K, Pinto M. F, Miranda P. B. Reaction intermediates of ethanol electro-oxidation on platinum investigated by SFG spectroscopy. *Journal of catalysis*. 2013; 302:67-82.
 15. Antolini E. Catalysts for direct ethanol fuel cells. *J Power Sources*. 2007; 170:1-12.
 16. Arico A, Creti P, Antonucci P, Antonucci V. Comparison of ethanol and methanol oxidation in a liquid-feed solid polymer electrolyte fuel cell at high temperature. *Electrochemical and Solid-State Letters*. 1998; 1:66-68.
 17. Rao V, Cremers C, Stimming U, et al. Electro-oxidation of ethanol at gas diffusion electrodes a DEMS study. *J Electrochem Soc*. 2007; 154:1138-B1147.
 18. Ghumman A, Pickup P. G. Efficient electrochemical oxidation of ethanol to carbon dioxide in a fuel cell at ambient temperature. *J Power Sources*. 2008; 179:280-285.
 19. Sun S, Halseid M. C, Heinen M, Jusys Z, Behm R. Ethanol electrooxidation on a carbon-supported Pt catalyst at elevated temperature and pressure: A high-temperature/high-pressure DEMS study. *J Power Sources*. 2009; 190:2-13.

20. Cantane D, Ambrosio W, Chatenet M, Lima, Fabio Henrique Barros de. Electro-oxidation of ethanol on Pt/C, Rh/C, and Pt/Rh/C-based electrocatalysts investigated by on-line DEMS. *J Electroanal Chem.* 2012; 681:56-65.
21. Seweryn J, Lewera A. High selectivity of ethanol electrooxidation to carbon dioxide on platinum nanoparticles in low temperature polymer electrolyte membrane direct ethanol fuel cell. *Applied Catalysis B: Environmental.* 2014; 144:129-134.
22. Linares J. J, Zignani S. C, Rocha T. A, Gonzalez E. R. Ethanol oxidation on a high temperature PBI-based DEFC using Pt/C, PtRu/C and Pt₃Sn/C as catalysts. *J Appl Electrochem.* 2013; 43:147-158.
23. Ghumman A, Li G, Bennett D. V, Pickup P. G. Online analysis of carbon dioxide from a direct ethanol fuel cell. *J Power Sources.* 2009; 194:286-290.
24. James D. D, Pickup P. G. Effects of crossover on product yields measured for direct ethanol fuel cells. *Electrochim Acta.* 2010; 55:3824-3829.
25. Jablonski A, Kulesza P. J, Lewera A. Oxygen permeation through Nafion 117 membrane and its impact on efficiency of polymer membrane ethanol fuel cell. *J Power Sources.* 2011; 196:4714-4718.
26. James D. D, Pickup P. G. Measurement of carbon dioxide yields for ethanol oxidation by operation of a direct ethanol fuel cell in crossover mode. *Electrochim Acta.* 2012; 78:274-278.
27. Lamy C, Jaubert T, Baranton S, Coutanceau C. Clean hydrogen generation through the electrocatalytic oxidation of ethanol in a proton exchange membrane electrolysis cell (PEMEC): Effect of the nature and structure of the catalytic anode. *J Power Sources.* 2014; 245:927-936.

28. Chen L, Chen J, Ho C, Wu S, Shieh D. Improvement of li-ion battery discharging performance by pulse and sinusoidal current strategies. *IEEE Trans Ind Electron.* 2013; 60:5620-5628.
29. Neergat M, Seiler T, Savinova E, Stimming U. Improvement of the performance of a direct methanol fuel cell using a pulse technique. *J Electrochem Soc.* 2006; 153:997-A1003.
30. Carrette L, Friedrich K, Huber M, Stimming U. Improvement of CO tolerance of proton exchange membrane (PEM) fuel cells by a pulsing technique. *Physical Chemistry Chemical Physics.* 2001; 3:320-324.
31. Léger J. Mechanistic aspects of methanol oxidation on platinum-based electrocatalysts. *J Appl Electrochem.* 2001; 31:767-771.
32. Urchaga P, Baranton S, Coutanceau C, Jerkiewicz G. Electro-oxidation of CO on Pt nanosurfaces: Solution of the peak multiplicity puzzle. *Langmuir.* 2011; 28:3658-3663.

Chapter 4

Sinusoidal Potential Cycling Operation of a Direct Ethanol Fuel Cell to Improve Carbon Dioxide Yields

All the experiments of this chapter were performed by Pasha Majidi.

Data analysis was performed by Pasha Majidi and Dr. Peter Pickup.

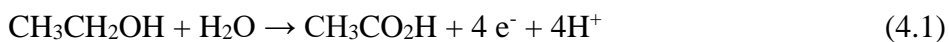
This chapter has been published as (Majidi P, Pickup P. G. Sinusoidal potential cyclin operation of a direct ethanol fuel cell to improving carbon dioxide yields. J Power Sources

2014; 268:439-442.)¹, which was written primarily by Dr. Peter Pickup.

4.1 Introduction

Direct ethanol fuel cells (DEFCs) based on proton exchange membrane (PEM) technology are attractive as part of a long-term renewable energy strategy because of their high theoretical efficiency (97%)² together with the ready availability and high energy density of bioethanol.^{3,4} However, their high anode overpotentials, crossover of ethanol to the cathode, and incomplete oxidation of ethanol to acetaldehyde and acetic acid currently make them impractical.

The most serious of these issues is the formation of acetic acid, which cannot be oxidized further under PEM DEFC operating conditions.⁵ This decreases the energy efficiency greatly because only 4 electrons are passed per ethanol molecule (eq. 4.1) relative to 12 for the complete oxidation to CO₂ (eq. 4.2).



The efficiency for the complete oxidation can be monitored and assessed by measuring the faradaic yield of CO₂ produced by the cell, given by eq. 4.3,

$$\text{CO}_2 \text{ yield} = 6F \text{mol}_{\text{CO}_2} / Q \quad (4.3)$$

where mol_{CO_2} is the moles of CO₂ produced and Q is the charge passed. The yield of CO₂ has been found to depend strongly on the catalyst employed, temperature, ethanol concentration, and current (or cell potential).^{3,5,6} The yield of CO₂ increases with increasing temperature, decreases as the ethanol concentration is increased, and generally has been found to decrease with increasing current (decreasing cell potential).⁶ It has been reported that pulsing of the current applied to an ethanol electrolysis cell can increase the CO₂ yield by promoting the

oxidation of adsorbed intermediates at a high current while ethanol adsorbs and dissociates at open circuit.⁷ Pulsing has also been applied to hydrogen⁸ and methanol fuel cells⁹ to mitigate CO poisoning. That principle has been applied here to the operation of a PEM DEFC by using a sinusoidal (AC) potential waveform.

4.2 Experimental

Anhydrous ethanol (Commercial Alcohols Inc.) was used as received and double distilled water was used throughout all experiments. Cathodes consisted of 4 mg cm⁻² Pt black on TorayTM carbon fiber paper; anodes consisted of 5.5 mg cm⁻² PtRu black on TorayTM carbon fiber paper. NafionTM 117 membranes (Dupont) were cleaned at 80 °C in 3% H₂O₂(aq) and 1 M H₂SO₄(aq), rinsed with water, and stored in water.

A 5 cm² commercial fuel cell (Fuel Cell Technology Inc.) was used. Membrane and electrode assemblies were prepared by pressing (room temperature; ca. 1.5 MPa) a 5 cm² anode and a 5 cm² cathode onto a NafionTM 117 membrane in the cell.¹⁰ The cell was operated with an anode feed of 0.10 mol L⁻¹ ethanol solution at 0.69 mL min⁻¹. The cathode feed was air at 20 mL min⁻¹. The cell was operated with a Hokuto Denko HA-301 potentiostat with the sinusoidal voltage generated by a Solartron 1250 frequency response analyzer. For CO₂ analysis both the anode solution and the cathode gas were passed into a 125 mL flask to collect the liquid. The gas stream exiting the flask was passed through a Telaire 7001 non-dispersive infrared CO₂ detector.¹¹ The CO₂ traces have been corrected for the delay in the detector response due to tubing and flask, and the background reading prior to passing current

though the cell, due to CO_2 produced by the chemical reaction of ethanol and O_2 arising from crossover of both through the membrane.^{12,13}

4.3 Results and discussion

Fig. 4.1. shows how the cell voltage was varied, and the corresponding current as a function of time, in an experiment at a bias potential of 0.4 V, frequency of 0.1 Hz, and amplitude (rms) of 0.1 V. An expanded section towards the end of the experiment is shown, to illustrate the steady state behavior. The average current over this period was 73 mA, while an average of 79 mA was obtained over the full 1200 s of the experiment.

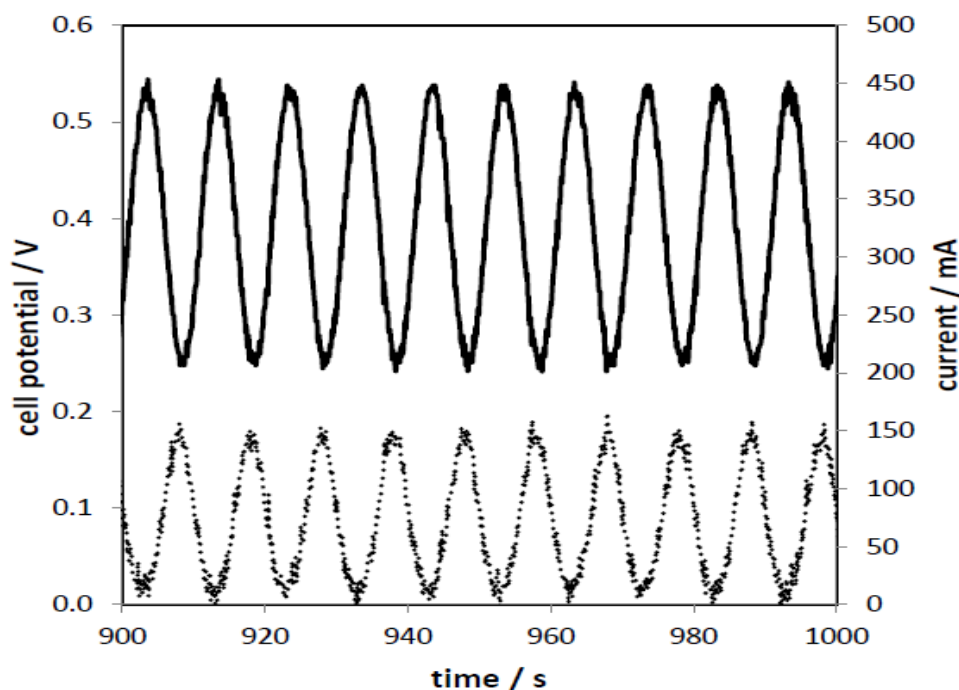


Figure 4.1. Cell potential (solid) and current (dotted) vs. time plots for operation of a DEFC at 80 °C under AC potential cycling conditions. Potential bias = 0.4 V; frequency = 0.1 Hz; amplitude = 0.1 V rms.

It can be seen from Fig. 4.1 that the current dropped to close to zero at the cell potential peaks. During this part of the cycle, ethanol will adsorb and dissociate on the electrode with limited production of undesirable products (acetaldehyde and acetic acid) because the current is low. At the minima in the cell potential, the current was high with a significant contribution due the oxidation of adsorbed CO, as demonstrated by *in situ* infrared spectroscopy¹⁴ and mass spectrometry.¹⁵ This leads to enhanced selectivity for the complete oxidation of ethanol to CO₂ as illustrated in Fig. 4.2, which compares CO₂ vs. time traces for operation of the cell as in Fig. 4.1 and for operation at a constant potential of 0.4 V.

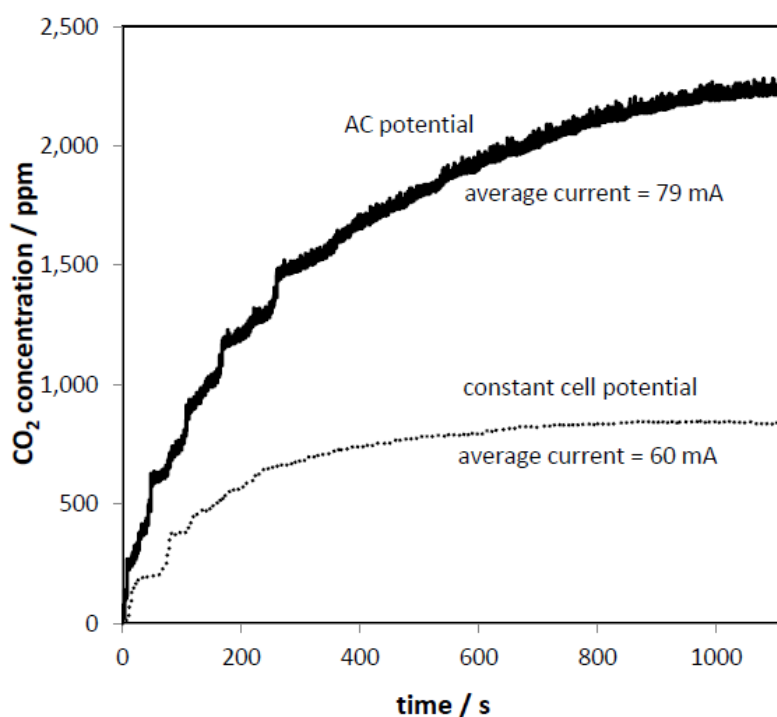


Figure 4.2. CO₂ concentration vs. time plots for the combined anode and cathode exhaust streams from a DEFC at 80 °C at a constant potential of 0.4 V (dotted) and under AC potential cycling conditions (solid; bias = 0.4 V; frequency = 0.1 Hz; amplitude = 0.1 V rms).

Here, the much higher concentration of CO₂ exiting the cell during AC potential cycling indicates that more ethanol was oxidized completely to CO₂. Although the average current was slightly lower in the constant potential experiment (60 mA vs. 79 mA), it is very clear from the data in Fig. 4.2 that the CO₂ yield was significantly higher in the AC experiment. Based on the charge passed and the moles of CO₂ produced (moles CO₂ = $\int(\text{ppm}_{\text{CO}_2} \cdot \dot{n} / 10^6) dt$, where \dot{n} is the N₂ flow rate in mol s⁻¹) over the full runs, the average CO₂ yields calculated using eq. 4.3 were 17.8% for AC operation and 9.8% at constant potential. However, these values are underestimated because of the long time (ca. 600-800 s) required for the CO₂ level in the collection flask to approach equilibrium. More accurate steady-state yields of 25.6% for AC operation and 11.6% at constant potential were therefore estimated (eq. 4.3) by integrating the current (Fig. 4.1) and CO₂ readings (Fig. 4.2) over just the final 200 s (i.e. 900 to 1100 s). The much higher steady-state CO₂ yield obtained under AC operation indicates that a higher fraction of the ethanol consumed underwent the complete 12 electron oxidation to CO₂. Consequently, it can be inferred that a lower fraction was oxidized to the acetaldehyde and acetic acid byproducts. Although these results do not provide any direct mechanistic information, it can be inferred from previous mechanistic studies^{14,15} that oxidation of adsorbed CO contributed significantly to the enhanced CO₂ yield. During each potential cycle, this CO would have been replenished at high cell potentials by partial oxidation of ethanol flowing through the cell.⁷

The mechanism of the electrochemical oxidation of ethanol at Pt based electrodes is still under intensive experimental^{16,17} and theoretical¹⁸ investigation.⁶ The main initial pathway involves partial oxidation of adsorbed ethanol to adsorbed acetaldehyde, which can desorb as

the first product.¹⁵ However, further oxidation (dehydrogenation) can easily occur to an adsorbed acetyl species ($\text{CH}_3\text{CO}_{\text{ads}}$), which is the common intermediate for both acetic acid and CO_2 formation.^{18,19} One of these theoretical studies¹⁸ “highlights the need for careful control of oxidant surface coverage that will allow facile C-C bond cleavage while still providing sufficient levels of CO oxidation”. The results shown in Fig. 4.2 demonstrate that this can be achieved to a significant extent by potential cycling.

A series of additional experiments were performed in order to explore whether higher yields could be obtained under other AC operation conditions, and to check whether the difference in the average current contributed to the difference in CO_2 yields between the two sets of data in Fig. 4.2. Bias potentials from 0.3-0.4 V were used because this is the optimum operating potential range. At higher potentials the current is too low to be very useful, while lower potentials are not very useful and produce much lower cell efficiencies. The results are summarized in Table 1. It can be seen from these results that decreasing the DC potential increased the average current, but did not have a significant effect on the CO_2 yield. AC operation of the cell at a lower bias potential and lower frequency resulted in lower CO_2 yields, although they were still significantly higher than any obtained at constant potential. Changing the amplitude at 0.35 V did not change the average current nor CO_2 yield significantly. These experiments, and a number of others that are not reported here, indicated that the cycling conditions in Fig. 4.1 were close to optimum for the cell and other operating conditions employed in this work.

Fig. 4.3 compares a polarization curve for the cell with current and voltage data from Fig. 1. The current during AC operation doesn't track the steady-state current exactly because of the charging current due to the double layer capacitance of the electrodes.

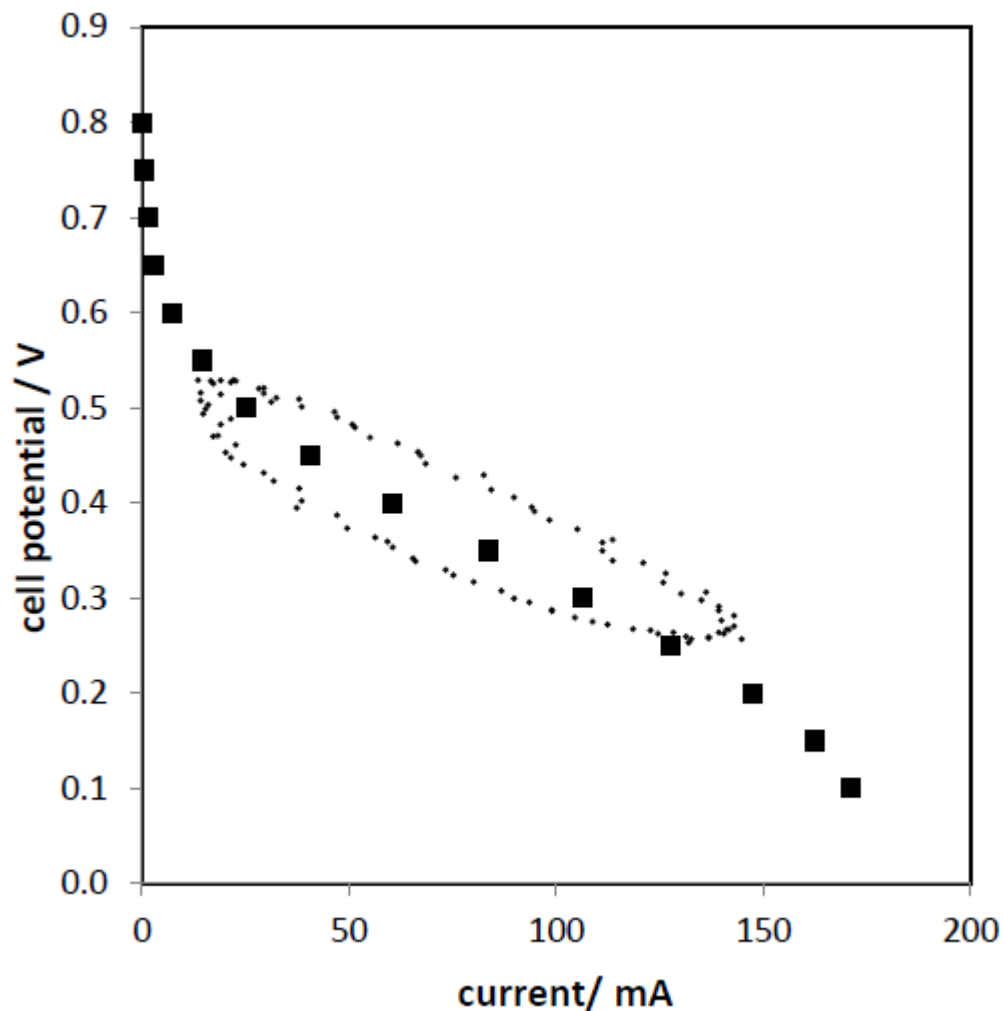


Figure. 4.3. Polarization curve (■; current averaged over 1 min after 4 min at each potential) and current vs. potential for AC potential cycling (dotted; potential bias = 0.4 V; frequency = 0.1 Hz; amplitude = 0.1 V rms).

The average current at most potentials is slightly higher under AC operation indicating improved cell performance under cycling conditions. This is most notable at high currents, while the cell underperforms at low currents during AC cycling.

The highest percentage increase in CO₂ yield obtained in this work was 121%, for the experiments at 0.4 V shown in Figs. 4.1 and 4.2. Although this appears to be substantial, its effect on the efficiency of the cell is much lower because of the nature of the relationship between CO₂ yield and efficiency, and also because AC operation of the cell decreases the potential efficiency. If we neglect the effects of crossover, the overall efficiency (ϵ_{cell}) of a DEFC is given by eq. 4.4,¹⁴

$$\epsilon_{\text{cell}} = \epsilon_{\text{rev}} \times \epsilon_{\text{E}} \times \epsilon_{\text{F}} \quad (4.4)$$

Where ϵ_{rev} is the theoretical efficiency (97%), ϵ_{E} is the potential efficiency ($E_{\text{cell}}/E_{\text{rev}}$ where E_{rev} is the reversible cell potential of 1.14 V under the conditions used here), and ϵ_{F} is the faradaic efficiency given by eq. 4.5,

$$\epsilon_{\text{F}} = 100 / (\% \text{CO}_2 + 3 \times \% \text{CH}_3\text{CO}_2\text{H} + 6 \times \% \text{CH}_3\text{CHO}) \quad (4.5)$$

where the % terms are the faradaic yields of each of the three major products.

Faradaic efficiencies calculated using eq. 4.5 are plotted in Fig. 4.4 as a function of the CO₂ yield for various ratio of acetaldehyde to acetic acid.

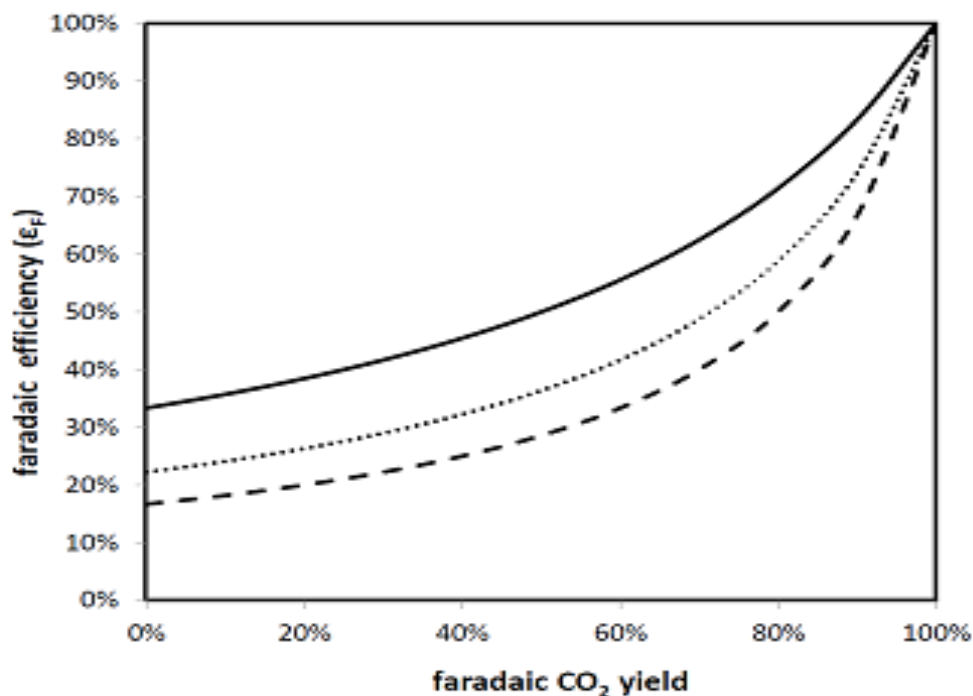


Figure 4.4. Theoretical relationships between faradaic efficiency and CO₂ yield at acetaldehyde (AL): acetic acid (AA) ratios of 1.0 (solid), 0.5 (dotted), and 0 (dashed).

It can be seen that increasing the yield of CO₂ has a much greater effect on the cell efficiency at high CO₂ yields. For the data in Table 4.1 at 0.4 V, and assuming a faradaic acetic acid yield of 50%,^{11,12} ϵ_F was 25.5% at constant potential and increased to 31.1% under AC cycling. However, the potential efficiency (weighted for the moles of ethanol converted at each potential during cycling) decreased from 35.0% to 29.4% when the potential was cycled because more ethanol was oxidized at lower cell potentials. Overall, cycling increased the cell efficiency (eq. 4.4) from 8.7% to 8.9%. Although not large, this 2% increase in cell efficiency was achieved with a 25% increase in the average current (Table 4.1) and a 4.3% increase in average power.

Table 4.1. Summary of data for operation of a DEFC at 80 °C at constant potential and under AC potential cycling conditions. Currents and yields are averages after 900 s of operation.

| DC potential / V | Frequency / Hz | Amplitude / V | Average current / mA | Average CO ₂ yield |
|---------------------|-------------------|------------------|-------------------------|----------------------------------|
| 0.30 | no AC | | 106 | 13.0% |
| 0.30 | 0.05 | 0.12 | 131 | 14.5% |
| 0.35 | 0.03 | 0.12 | 93.1 | 16.4% |
| 0.35 | 0.03 | 0.13 | 89.8 | 17.9% |
| 0.35 | 0.03 | 0.15 | 103 | 16.8% |
| 0.40 | no AC | | 57.5 | 11.6% |
| 0.40 | 0.1 | 0.1 | 72.0 | 25.6% |

From a practical point of view, the PtRu catalyst used here is not suitable for use in DEFCs because of the low yields of CO₂ that it produces. Pure Pt produces much higher CO₂ yields than PtRu because it promotes C-C bond cleavage, but its potential efficiency is lower because higher potentials are needed to oxidize CO.^{6,20} Other alloy catalysts such as PtSn can deliver higher potential efficiency as well as improved CO₂ yields.⁶ Fig. 4.4 shows that the benefits of AC cycling would high for such catalysts because of the higher slopes at higher CO₂ yields. Increasing the cell temperature would also increase CO₂ yields³ and this should also increase the benefits of AC cycling.

4.4 Conclusions

It has been demonstrated that potential cycling with a sinusoidal waveform can greatly increase the yield of CO₂ produced by a DEFC, and that this leads to a significant increase in the faradaic efficiency of the cell. Although this is partially offset by a decrease in potential efficiency, there can be a net benefit in overall cell efficiency, and/or power density. It is demonstrated, in theory, that AC cycling (or other potential modulation) of DEFCs with better catalysts has the potential to significantly enhance their efficiencies. This could be a significant factor in their commercialization.

References

1. Majidi P, Pickup P. G. Sinusoidal potential cycling operation of a direct ethanol fuel cell to improving carbon dioxide yields. *J Power Sources*. 2014; 268:439-442.
2. Demirci U. B. Direct liquid-feed fuel cells: Thermodynamic and environmental concerns. *J Power Sources*. 2007; 169:239-246.
3. Kamarudin M, Kamarudin S. K, Masdar M, Daud W. R. W. Review: Direct ethanol fuel cells. *Int J Hydrogen Energy*. 2013; 38:9438-9453.
4. Brouzgou A, Podias A, Tsiakaras P. PEMFCs and AEMFCs directly fed with ethanol: A current status comparative review. *J Appl Electrochem*. 2013;43(2):119-136.
5. Rao V, Cremers C, Stimming U, et al. Electro-oxidation of ethanol at gas diffusion electrodes a DEMS study. *J Electrochem Soc*. 2007; 154:1138-B1147.
6. Friedl J, Stimming U. Model catalyst studies on hydrogen and ethanol oxidation for fuel cells. *Electrochim Acta*. 2013; 101:41-58.
7. Ghumman A, Pickup P. G. Efficient electrochemical oxidation of ethanol to carbon dioxide in a fuel cell at ambient temperature. *J Power Sources*. 2008; 179:280-285.
8. Carrette L, Friedrich K, Huber M, Stimming U. Improvement of CO tolerance of proton exchange membrane (PEM) fuel cells by a pulsing technique. *Physical Chemistry Chemical Physics*. 2001; 3:320-324.
9. Neergat M, Seiler T, Savinova E, Stimming U. Improvement of the performance of a direct methanol fuel cell using a pulse technique. *J Electrochem Soc*. 2006; 153:997-1003.
10. Song C, Pickup P. Effect of hot pressing on the performance of direct methanol fuel cells. *J Appl Electrochem*. 2004; 34:1065-1070.

11. James D. D, Pickup P. G. Effects of crossover on product yields measured for direct ethanol fuel cells. *Electrochim Acta*. 2010; 55:3824-3829.
12. James D. D, Pickup P. G. Measurement of carbon dioxide yields for ethanol oxidation by operation of a direct ethanol fuel cell in crossover mode. *Electrochim Acta*. 2012; 78:274-278.
13. Jablonski A, Kulesza PJ, Lewera A. Oxygen permeation through Nafion 117 membrane and its impact on efficiency of polymer membrane ethanol fuel cell. *J Power Sources*. 2011; 196:4714-4718.
14. Vigier F, Rousseau S, Coutanceau C, Leger J, Lamy C. Electrocatalysis for the direct alcohol fuel cell. *Topics in Catalysis*. 2006; 40:111-121.
15. Wang H, Liu Z. Comprehensive mechanism and structure-sensitivity of ethanol oxidation on platinum: New transition-state searching method for resolving the complex reaction network. *J Am Chem Soc*. 2008; 130:10996-11004.
16. Kutz R. B, Braunschweig B, Mukherjee P, Behrens RL, Dlott D. D, Wieckowski A. Reaction pathways of ethanol electrooxidation on polycrystalline platinum catalysts in acidic electrolytes. *Journal of Catalysis*. 2011; 278:181-188.
17. Gomes J. F, Bergamaski K, Pinto MF, Miranda P. B. Reaction intermediates of ethanol electro-oxidation on platinum investigated by SFG spectroscopy. *Journal of catalysis*. 2013; 302:67-82.
18. Kavanagh R, Cao X, Lin W, Hardacre C, Hu P. Origin of low CO₂ selectivity on platinum in the direct ethanol fuel cell. *Angewandte Chemie International Edition*. 2012; 51:1572-1575.
19. Wang H, Jusys Z, Behm R. Ethanol electro-oxidation on carbon-supported Pt, PtRu and

Pt₃Sn catalysts: A quantitative DEMS study. *J Power Sources*. 2006; 154:351-359.

20. Ghumman A, Li G, Bennett D. V, Pickup P. G. Online analysis of carbon dioxide from a direct ethanol fuel cell. *J Power Sources*. 2009; 194:286-290.

Chapter 5

Determination of the Average Number of Electrons Released During the Oxidation of Ethanol in a Direct Ethanol Fuel Cell

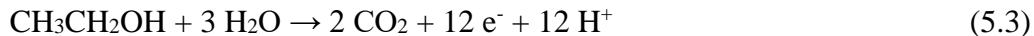
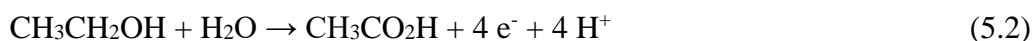
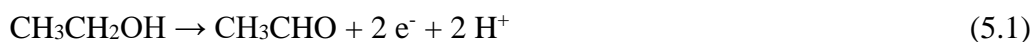
All the experiments of this chapter were performed by Pasha Majidi.

Data analysis was performed by Pasha Majidi and Dr. Peter Pickup.

This chapter has been published as (Majidi P, Pickup P. G. Determination of the average number of electrons released during the oxidation of ethanol in a direct ethanol fuel cell. *Electrochim Acta*. 2015; 182:856-860)¹, which was written primarily by Dr. Peter Pickup.

5.1. Introduction

The high theoretical efficiency (97%)² of direct ethanol fuel cells (DEFCs) together with their zero theoretical net carbon dioxide emission when operated with bioethanol,^{3,4} make them attractive as power sources. However, the formation of acetaldehyde and acetic acid in proton exchange membrane (PEM) DEFCs greatly decreases the energy efficiency and increases emissions. Oxidation of ethanol to acetaldehyde produces only two electrons per molecule (eq. 1; $n = 2$), while oxidation to acetic acid produces four electrons (eq. 5.2; $n = 4$), and the complete oxidation to CO₂ produces twelve ($n = 12$; eq. 3).



If we neglect the effects of fuel crossover through the membrane, the overall efficiency (ϵ_{cell}) of a DEFC is given by eq. 5.4,⁵

$$\epsilon_{\text{cell}} = \epsilon_{\text{rev}} \times \epsilon_{\text{E}} \times \epsilon_{\text{F}} \quad (5.4)$$

Where ϵ_{rev} is the theoretical efficiency (97%), ϵ_{E} is the potential efficiency ($E_{\text{cell}}/E_{\text{rev}}$ where E_{rev} is the reversible cell potential of ca. 1.14 V), and ϵ_{F} is the faradaic efficiency. The faradaic efficiency is the ratio of the average number of electrons obtained per molecule of ethanol (n_{av}) to the theoretical value of 12 ($\epsilon_{\text{F}} = n_{\text{av}}/12$). It can be estimated by analysis of the products exiting the DEFC by using eq. 5.5.⁶⁻⁸

$$\epsilon_F = 100/(\%CO_2 + 3 \times \%CH_3CO_2H + 6 \times \%CH_3CHO) \quad (5.5)$$

Where the % terms are the faradaic yields of each of the three major products.

The determination of n_{av} values by product analysis is time consuming and expensive, requires all products to be identified and quantified, and involves considerable sources of inaccuracy. These include a multitude of crossover effects^{9,10}, and low/uncertain product collection efficiencies. A better approach is to measure the charge for oxidation of a known amount of ethanol, as reported by Hitmi et al.¹¹ who measured the charge (Q), and concentration change (ΔC) for electrolysis of a known volume (V_0) of ethanol solution. For the electrolysis of ethanol at 0.8 V vs. RHE in 0.1 M HClO₄ at 10 °C, they obtained n_{av} values (from eq. 5.6) ranging from ca. 2 to 4 as the concentration was decreased.

$$n_{av} = Q/F\Delta CV_0 \quad (5.6)$$

These low values indicate that the main products were acetic acid at low concentrations and acetaldehyde at high concentrations.

The attraction of approaches based on eq. 5.6 is that this equation can be applied simply to any fuel without knowledge of, or analysis of, the reaction products. The difficulty, however, lies in the determination of ΔC under conditions that are relevant to fuel cells (flow conditions at elevated temperatures and with fuel and oxygen crossover). We present here a simple electrochemical methodology to determine n_{av} for ethanol, and potentially any other fuel, in conventional fuel cell hardware, without any reactant or product analysis, and without errors due to crossover. It is based on the principle that fuel crossing through the membrane can be quantitatively electrochemically oxidized at the anode when a fuel solution is passed

through the cathode compartment and N₂ is passed through the anode compartment.¹² Under these conditions, reactions 5.1-5.3 occur simultaneously at the anode while hydrogen is evolved at the cathode from protons crossing the membrane from the anode.

At high fuel flow rates, the limiting current (I_{lim}) is related to the flux (f , in mol s⁻¹) of fuel crossing the membrane by eq. 5.7.

$$I_{lim} = n_{av}Ff \quad (5.7)$$

At lower flow rates the current decreases because of depletion of the fuel as it passes through the cathode flow field. This effect is modeled here, and it is shown that the decrease in current (I) with decreasing flow rate depends on n_{av} and can be used to provide good estimates of n_{av} values. The method has been validated by using methanol, and then used to determine n_{av} values for ethanol oxidation.

5.2. Experimental

Methanol (99.8% from ACP Chemical Inc.) and anhydrous ethanol (Commercial Alcohols Inc.) were used as received and double distilled water was used throughout all experiments. Electrodes consisted of 4 mg cm⁻² Pt black on TorayTM carbon fiber paper. NafionTM 115 membranes (Dupont) were cleaned at 80 °C in 3% H₂O₂(aq) and 1 M H₂SO₄(aq), rinsed with water, and stored in water.

A 5 cm² commercial fuel cell (Fuel Cell Technology Inc.) was used. In order to use very low fuel flow rates provided by a syringe pump, this cell was modified so that a syringe needle entered directly into to the inlet on the graphite cathode flow field plate (sealed with

epoxy). Membrane and electrode assemblies (MEA) were prepared by pressing (room temperature; ca. 1.5 MPa) a 5 cm² anode and a 5 cm² cathode onto a NafionTM 115 membrane in the cell.¹³ The cell was operated with a cathode feed of aqueous ethanol or methanol solution from a syringe pump, and a cathode feed of N₂ at ca. 10 cm³ min⁻¹. Under these conditions, the cathode approximates a dynamic hydrogen electrode, since the cathode reaction is $H^+ + e^- \rightarrow \frac{1}{2}H_2$. The cell was operated at a fixed potential of 0.6 or 0.7 V with a Hokuto Denko HA-301 potentiostat.

5.3. Modeling

Fig. 5.1 shows schematic cross-sections of the channel in the fuel (cathode) flow field. The crossover of fuel to the anode generates a current ($I = n_{av}Ff$) and decreases the concentration of the fuel as it passes through the flow field. Consequently, C , f and I all decrease with distance (x) through the flow field. Although the ridges of the flow field cover a significant fraction of the MEA area, the electrodes are sufficiently porous to allow crossover through the full area. Consequently, the width parameter (w) includes these ridges. The electrodes are assumed to have a negligible influence on the flux of fuel across the membrane,¹² although this is not a necessary assumption for the determination of n_{av} .

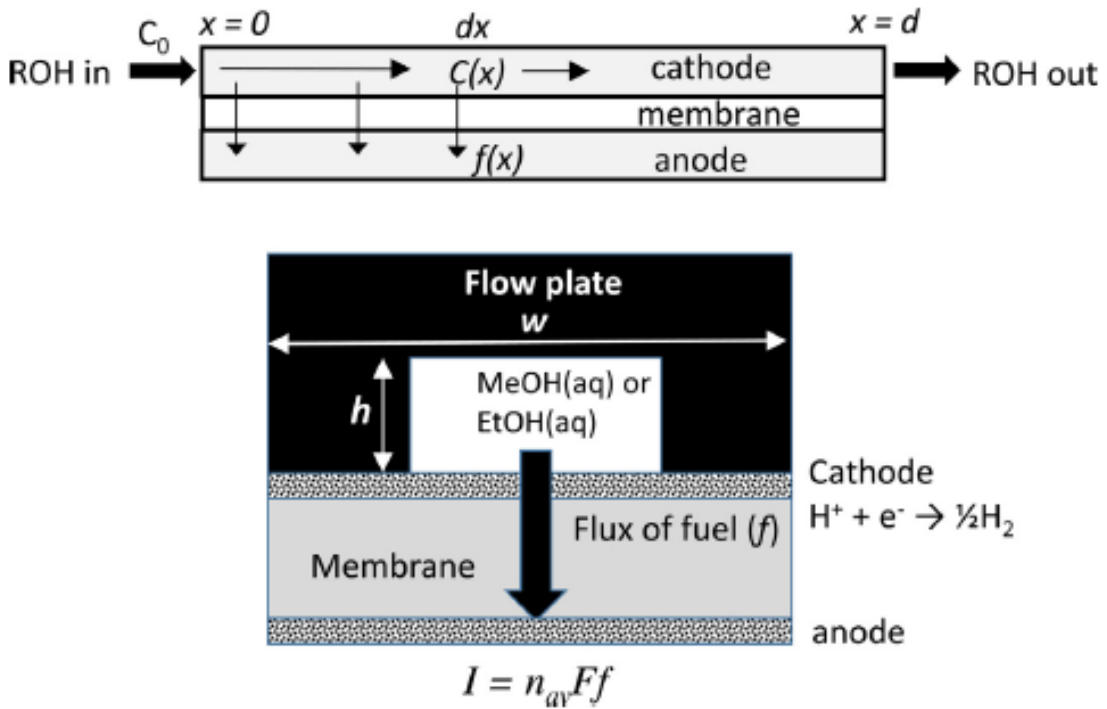


Figure 5.1 Schematic cross-sections of the cell along the fuel flow field (top) and across a channel in the fuel flow field (bottom).

Assuming steady state conditions under which there are linear concentration gradients of the fuel across the membrane,¹² concentration profiles along the fuel flow field can be obtained by integration of eq. 5.8,

$$\frac{dC(x)}{dx} = \frac{-DC(x)}{lhv} \quad (5.8)$$

Where D is the diffusion coefficient for the fuel in the membrane, l is the thickness of the membrane, h is the height of the flow channel, and v is the flow velocity (cm s^{-1}). Since, the flow velocity is u/hw , where w is the channel width and u is the volumetric flow rate ($\text{cm}^3 \text{s}^{-1}$), the resulting concentration profile can be written as eq. 5.9,

$$C(x) = C_0 \exp\left(-\frac{wDx}{lu}\right) \quad (5.9)$$

Where C_0 is the initial concentration of the fuel.

The constant D/l can be obtained from the limiting current at high flow rates by using eq. 5.10,

$$I_{lim} = \frac{n_{av}FAC_0D}{l} \quad (5.10)$$

Where A is the MEA area ($w d$, where d is the length of the flow field). A small correction (ca. 1%) for the effects of electroosmotic drag would be required to determine D/l accurately,¹² but is not needed here because this error is canceled out when eq. 5.10 is used again below to obtain eq. 5.12. There may also be an error in D/l due to the pressure drop across the membrane.

The current can be obtained by integration of the current density along the flow field using eq. 5.11.¹⁴

$$I = \int_0^d \frac{n_{av}FDC(x)w}{l} dx \quad (5.11)$$

Substitution of eqs. 5.9 and 5.10 gives eq. 5.12,

$$I = (I_{lim}/d) \int_0^d \exp\left(-\frac{I_{lim}x}{n_{av}FC_0ud}\right) dx \quad (5.12)$$

which yields eq. 5.13.

$$I = n_{av}FC_0u \left(1 - \exp \left(- \frac{I_{lim}}{n_{av}FC_0u} \right) \right) \quad (5.13)$$

This result is analogous to that for electrolysis of a solution flowing through a porous working electrode,¹⁴ since it is assumed that there are negligible concentration gradients perpendicular to the flow direction in the flow channel and cathode. It is also assumed that the effect of lateral diffusion along the flow field is negligible, which is reasonable given that at the lowest flow rate employed here (5 $\mu\text{L min}^{-1}$) lateral diffusion would be only ca. 0.4 cm along the ca. 30 cm flow channel at 80 °C.

5.4. Results and discussion

5.4.1. Methanol oxidation

Fig. 5.2 shows polarization curves for the oxidation of methanol and ethanol in crossover mode, where a constant flux of the fuel reaches the anode by diffusion across the membrane.¹² These experiments were conducted at constant potentials with a sufficiently high fuel flow rate to avoid significant changes in concentration along the flow field.

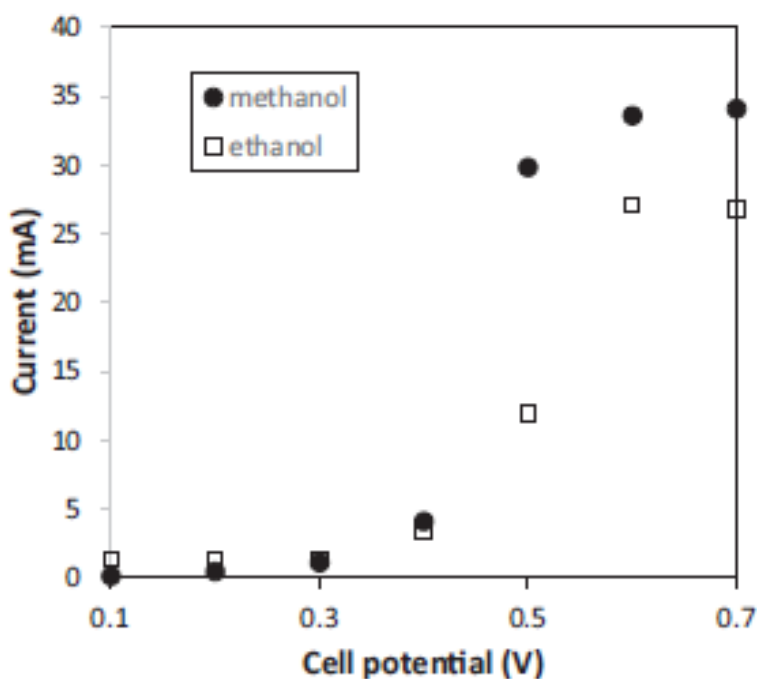


Figure 5.2 Polarization curves for oxidation of 0.1 M methanol (●) and 0.1 M ethanol (□) at 50°C.

The plateau currents at high potential (I_{lim}) result from oxidation of all of the fuel reaching the anode, which provides the maximum concentration gradient across the membrane. This limiting current provides a measure of n_{av} through eq. 5.7, if the flux is known. This requires knowledge of the diffusion coefficient (D) and membrane thickness (l).¹² Although this is potentially an excellent way to determine n_{av} values, it is not straightforward. Diffusion coefficients vary with operating conditions, and the membrane thickness can vary if the hydration level changes (e.g. with temperature). To obtain accurate results, it is necessary to determine D and l , or the flux (f), for each experiment. This is achieved here by making

multiple measurements at different fuel flow rates. Then n_{av} and I_{lim} (proportional to f) can be obtained from two or more measurements by fitting eq. 5.13 to the experimental results.

It can be seen from eq. 5.13 that the current per unit concentration of reactant (I/C_0) vs. flow rate can be described by two variables, the limiting current per unit concentration of reactant (I_{lim}/C_0) and the number of electrons passed per molecule that crosses the membrane (n_{av}). The results are independent of the length or volume of the flow field and independent of the choice of fuel (e.g. ethanol vs. methanol here).

Fig. 5.3 shows theoretical (eq. 5.13) plots of current vs. fuel flow rate together with experimental data for 0.1 M methanol at 50 °C.

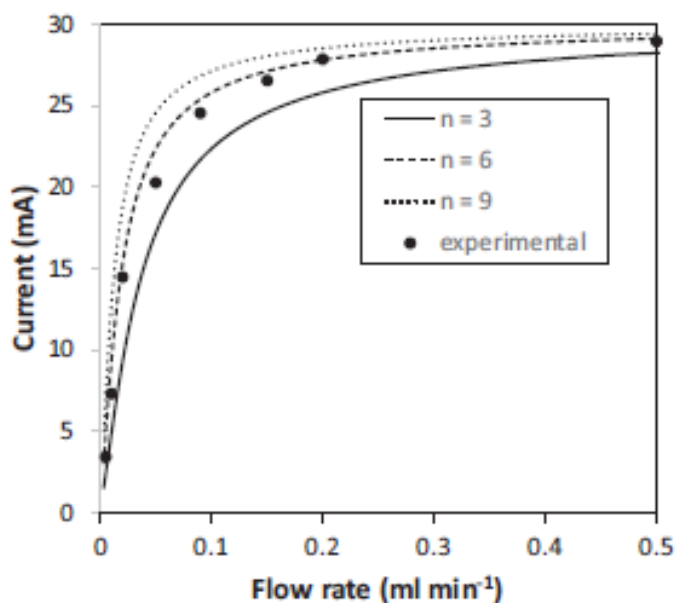


Figure 5.3 Calculated (eq. 13 with $I_{lim}/C_0 = 0.3 \text{ A M}^{-1}$) current vs. flow rate curves and experimental data for 0.1 M methanol at 50 °C.

It can be seen that for a fixed value of I_{lim}/C_0 (set at 0.3 A M^{-1} to match the experimental data) there is a systematic change in the rate of current decay as n_{av} is changed. Consequently, the theoretical plots can be used as working curves to determine n_{av} . The experimental data points for methanol oxidation in Fig. 5.3 are close to the theoretical curve for $n = 6$, as expected for complete oxidation to CO_2 . Several reports have previously shown that methanol can be oxidized to CO_2 at high faradaic efficiency at fuel cell electrodes.¹⁵⁻¹⁷ The deviation of the experimental data from the $n = 6$ curve can be accounted for by partial oxidation of some of the methanol to formaldehyde ($n = 2$) and formic acid ($n = 4$).¹⁵⁻¹⁸ Using the solver feature of Excel, a n_{av} value of 4.9 was found to give the best fit (least squares) to the experimental data in Fig. 5.3.

Fig. 5.4 shows theoretical (eq. 5.9) examples of how the concentration changes as fuel passes through the flow field at several different flow rates.

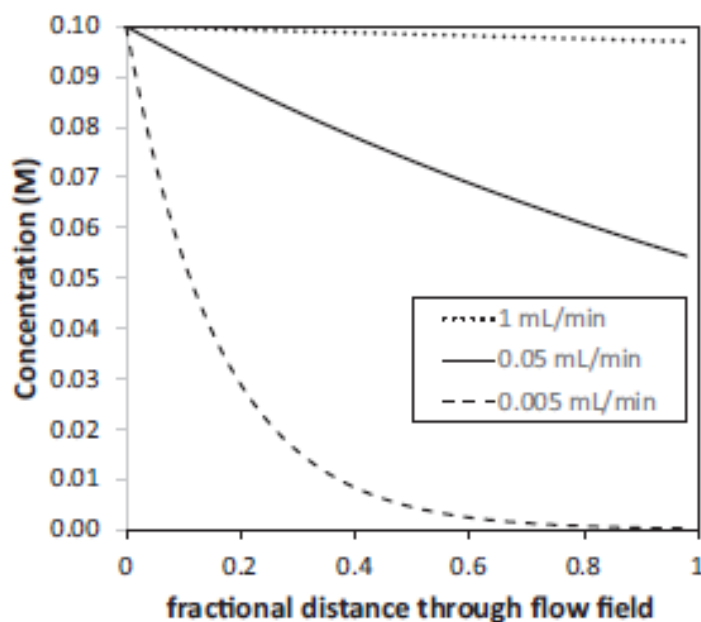


Figure 5.4 Calculated (eq. 5.9) concentration profiles for selected flow rates with $C_0 = 0.1 \text{ M}$, $I_{lim} = 30 \text{ mA}$ and $n_{av} = 6$.

In the limiting current region (e.g. 1 mL min⁻¹) there is little change in concentration, while at low flow rates (e.g. 0.005 mL min⁻¹) the concentration of fuel leaving the cell can become negligible. Under these latter conditions, the current becomes linearly dependent on the flow rate (see $n = 3$ simulation in Fig. 5.3), and n_{av} values can be obtained directly from eq. 6 with $\Delta C = C_0$. This equation can be rewritten as eq. 5.14.

$$n_{av} = I/uFC_0 \quad (5.14)$$

Although equation 14 appears to be attractive for determining n_{av} , it takes a long time to obtain steady state currents at the low flow rates required, and both random and systematic (e.g. due to fuel losses) errors can become prohibitive.

Since it is not necessary to make measurements at more than two flow rates to simultaneously determine I_{lim} and n_{av} , their values can be determined independently at each flow rate employed, with the highest flow rate measurement as the reference value to provide the closest initial estimate of I_{lim} . This allows possible changes in n_{av} with concentration (the average concentration changes with flow rate) to be identified, which is important for ethanol.¹¹⁻¹⁹ It can also provide an assessment of the quality of the data at each flow rate.

Table 5.1 shows n_{av} values (found using solver) obtained from the current at each flow rate and the current at 0.5 mL min⁻¹. The value of 6.9 at 0.2 mL min⁻¹ is clearly inaccurate because it is above the theoretical value of 6. This can be attributed to the large uncertainty arising from the small difference in the currents at 0.2 and 0.5 mL min⁻¹. The other n_{av} values are all reasonable, and give an average of 4.73 ± 0.45 . There is no indication that n_{av} changes systematically with flow rate. Based on these results, and the uncertainties and inaccuracies

than can arise at very low flow rates, it was concluded that the optimum low flow rate to use would be between ca. 0.01 and 0.05 mL min⁻¹.

Table 5.1. Apparent n_{av} values from two point fits to eq. 5.13 with a high flow rate of 0.5 mL min⁻¹ as a function of the second (lower) flow rate, for 0.1 M methanol and ethanol solutions at 50 °C.

| Lower flow rate / mL min ⁻¹ | n_{av} | |
|---|----------|---------|
| | methanol | ethanol |
| 0.20 | 6.9 | 3.3 |
| 0.15 | 4.8 | 2.4 |
| 0.09 | 4.9 | 2.8 |
| 0.05 | 4.4 | 3.4 |
| 0.02 | 5.5 | 4.0 |
| 0.01 | 4.6 | 4.5 |
| 0.005 | 4.3 | 4.6 |

Consequently, flow rates of 0.02 and 0.5 mL min⁻¹ were selected for routine determinations of I_{lim} and n_{av} . Using these two flow rates only, multiple (8) measurements with 0.1 M methanol at 50 °C over a period of months provided average values of $I_{lim} = 37.0 \pm 4.5$ mA and $n_{av} = 5.27 \pm 0.49$. The uncertainties (standard deviations) indicated here are due to

noise and drift in the current measurements as well as random variations in the characteristics of the MEA from day to day.

5.4.2. Ethanol oxidation

Fig. 5.5 shows experimental currents over a range of flow rates for the oxidation of 0.1 M ethanol supplied to the cathode side of the cell, at 50 °C, together with the best fit theoretical curve (eq. 5.13).

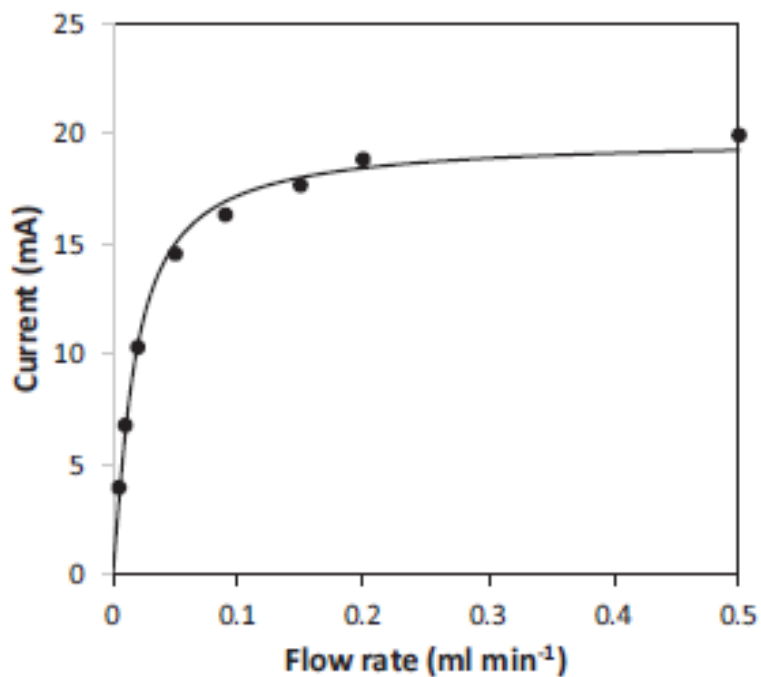


Figure 5.5 Current vs. flow rate for oxidation of 0.1 M ethanol at 50 °C (points) and best fit Curve calculated by using eq. 5.13 with $I_{lim}/C_0 = 0.198 \text{ A M}^{-1}$ and $n_{av} = 4.23$.

The best fit n_{av} for this full data set was 4.2, while using the currents at just 0.02 and 0.5 mL min⁻¹ gave a value of 4.0. These low values, relative to $n = 12$ for complete oxidation to CO₂, are consistent with the low CO₂ yields that have been reported for ethanol oxidation at

this temperature.¹⁹ Further experiments at 0.6 V (0.7 V was used for Fig. 5.5), gave $n_{av} = 4.69 \pm 0.12$. The increase with decreasing potential is consistent with a differential electrochemical mass spectrometry study¹⁹ that demonstrated higher CO₂ yields at lower potentials. However, other studies have shown that this trend can be reversed under some conditions.¹⁶⁻²⁰ Unfortunately the methodology employed here can only currently be used in the limiting current region, which means that n_{av} values at potentials below 0.6 V are not yet available.

Table 5.1 shows apparent n_{av} values obtained from the current at each flow rate in Fig. 5.5, and the current at 0.5 mL min⁻¹. In contrast to the data for methanol in Table 5.1, the apparent n_{av} values for ethanol show a clear increase with decreasing flow rate. This is consistent with reports that CO₂ yields from ethanol oxidation increase with decreasing concentration,¹⁶⁻¹⁹ since the average concentration of ethanol in the flow field decreases with decreasing flow rate (see Fig. 5.4). As for methanol, flow rates of 0.02 and 0.5 mL min⁻¹ were selected for routine determinations of I_{lim} and n_{av} for ethanol oxidation. For the data in Fig. 5.5, this provided the closest result to the full fit value of 4.2, and so provides the best “characteristic value” for assessing the effects of changing operating conditions, and in future for changing the catalyst.

Table 5.2 summarizes additional result for ethanol oxidation under a variety of operating conditions. The trends in n_{av} with temperature and ethanol concentration are consistent with trends in CO₂ yields from other studies,¹⁶⁻¹⁹ which have clearly established that CO₂ yields increase sharply with increasing temperature and decrease with increasing concentration. Based on eq. 5.5, the very high n_{av} of 9.4 for 0.1 M ethanol at 80 °C

corresponds to a faradaic CO₂ yield of between 86% and 94%, depending on the ratio of acetic acid to acetaldehyde produced as byproducts. Such high yields can be attributed to the use of mass transport limited currents here, which result in very low concentrations of ethanol at the anode catalyst surface.¹⁶

Table 5.2. n_{av} and I_{lim} results, from currents at 0.02 and 0.5 and mL min⁻¹, for ethanol oxidation under a variety of operating conditions. Averages with standard deviations are for 2 or 3 measurements on different days.

| Ethanol concentration /M | Temperature / °C | Cell potential /V | n_{av} | I_{lim} / mA |
|--------------------------|------------------|-------------------|----------|----------------|
| 0.10 | 50 | 0.6 | 4.7±0.12 | 26.1±2.9 |
| 0.10 | 50 | 0.7 | 3.9±0.11 | 25.0±6.2 |
| 0.10 | 80 | 0.7 | 9.4±0.18 | 75.8±5.2 |
| 1.00 | 50 | 0.7 | 3.0 | 94.4 |
| 1.00 | 80 | 0.7 | 6.6 | 238 |

Measurement of the CO₂ yield in a similar crossover experiment at 0.5 mL min⁻¹ gave a CO₂ yield of 65%,¹⁶ and it can be seen from the data in Table 5.1 that the CO₂ yield would have been significantly higher at 0.02 mL min⁻¹.

It is notable that the limiting currents reported in Table 5.2 for 1 M ethanol are only ca. 3-4 times higher than those for 0.1 M ethanol, while a 10 fold increase is expected for a constant n_{av} (eq. 5.10), and is observed (approximately) for methanol oxidation.^{12,21} This difference can be qualitatively accounted for by the observed decreases in n_{av} values with increasing ethanol concentration, although a quantitative comparison is complicated because the reported “characteristic” n_{av} values are higher than they would be at the limiting current.

5.5. Conclusions

Simple electrochemical methodology is presented for the determination of the average number of electrons (n_{av}) obtained from methanol, ethanol, or any other fuel, in conventional fuel cell hardware, without any reactant or product analysis, and without errors due to crossover. For methanol oxidation, the method is shown to provide n_{av} values close to the theoretical value of 6, while for ethanol oxidation n_{av} values correlate well with product distributions reported in the literature. The results validate the methodology as a useful tool for catalyst screening, and confirm previous reports that very high yields of CO₂ can be obtained with low ethanol concentrations at 80 °C. This methodology can also be applied to a DEFC operating normally, although corrections need to be made for the loss of ethanol due to crossover, including crossover of O₂ from the cathode.

References

1. Majidi P, Pickup P. G. Determination of the average number of electrons released during the oxidation of ethanol in a direct ethanol fuel cell. *Electrochim Acta*. 2015; 182:856-860.
2. Demirci U. B. Direct liquid-feed fuel cells: Thermodynamic and environmental concerns. *J Power Sources*. 2007; 169:239-246.
3. Kamarudin M, Kamarudin S. K, Masdar M, Daud W. R. W. Review: Direct ethanol fuel cells. *Int J Hydrogen Energy*. 2013; 38:9438-9453.
4. Brouzgou A, Podias A, Tsiakaras P. PEMFCs and AEMFCs directly fed with ethanol: A current status comparative review. *J Appl Electrochem*. 2013; 43:119-136.
5. Vigier F, Rousseau S, Coutanceau C, Leger J, Lamy C. Electrocatalysis for the direct alcohol fuel cell. *Topics in Catalysis*. 2006; 40:111-121
6. Majidi P, Pickup PG. Sinusoidal potential cycling operation of a direct ethanol fuel cell to improving carbon ioxide yields. *J Power Sources*. 2014; 268:439-442.
7. Wang H, Jusys Z, Behm R. Ethanol electrooxidation on a carbon-supported pt catalyst: Reaction kinetics and product yields. *The Journal of Physical Chemistry*. 2004; 108:19413-19424.
8. Lamy C, Jaubert T, Baranton S, Coutanceau C. Clean hydrogen generation through the electrocatalytic oxidation of ethanol in a proton exchange membrane electrolysis cell (PEMEC): Effect of the nature and structure of the catalytic anode. *J Power Sources*. 2014 ; 245:927-936.
9. James D. D, Pickup P. G. Effects of crossover on product yields measured for direct ethanol fuel cells. *Electrochim Acta*. 2010; 55:3824-3829.

10. Jablonski A, Kulesza PJ, Lewera A. Oxygen permeation through Nafion 117 membrane and its impact on efficiency of polymer membrane ethanol fuel cell. *J Power Sources*. 2011; 196:4714-4718.
11. Hitmi H, Belgsir E, Léger J, Lamy C, Lezna R. A kinetic analysis of the electro-oxidation of ethanol at a platinum electrode in acid medium. *Electrochim Acta*. 1994; 39:407-415.
12. Ren X, Springer T, Gottesfeld S. Water and methanol uptakes in Nafion membranes and membrane effects on direct methanol cell performance. *J Electrochem Soc*. 2000; 147:92-98.
13. Song C, Pickup P. Effect of hot pressing on the performance of direct methanol fuel cells. *J Appl Electrochem*. 2004; 34:1065-1070.
14. Bard AJ, Faulkner L. R. Fundamentals and applications. *Electrochemical Methods*, 2nd ed.; Wiley: New York. 2001.
15. Masdar M. S, Tsujiguchi T, Nakagawa N. Mass spectroscopy for the anode gas layer in a semi-passive direct methanol fuel cell using porous carbon plate: Part II. relationship between the reaction products and the methanol and water vapor pressures. *J Power Sources*. 2009; 194:618-624.
16. James D. D, Pickup P. G. Measurement of carbon dioxide yields for ethanol oxidation by operation of a direct ethanol fuel cell in crossover mode. *Electrochim Acta*. 2012; 78:274-278.
17. Gao L, Huang H, Korzeniewski C. The efficiency of methanol conversion to CO₂ on thin films of Pt and PtRu fuel cell catalysts. *Electrochim Acta*. 2004; 49:1281-1287.
18. Jusys Z, Kaiser J, Behm R. Methanol electrooxidation over Pt/C fuel cell catalysts: Dependence of product yields on catalyst loading. *Langmuir*. 2003; 19:6759-6769.

19. Sun S, Halseid M. C, Heinen M, Jusys Z, Behm R. Ethanol electrooxidation on a carbon-supported Pt catalyst at elevated temperature and pressure: A high-temperature/high-pressure DEMS study. *J Power Sources*. 2009; 190:2-13.
20. Andreadis G, Stergiopoulos V, Song S, Tsiakaras P. Direct ethanol fuel cells: The effect of the cell discharge current on the products distribution. *Applied Catalysis B: Environmental*. 2010; 100:157-164.
21. Ren X, Springer T. E, Zawodzinski T. A, Gottesfeld S. Methanol transport through nion membranes. electro-osmotic drag effects on potential step measurements. *J Electrochem Soc*. 2000; 147:466-474.

Chapter 6

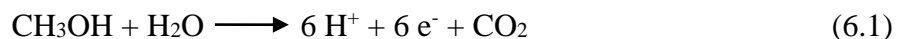
Determination of the Efficiency of Methanol Oxidation in a Direct Methanol Fuel Cell

6.1 Introduction

Wasteful harvesting, processing and consumption of fossil fuels can cause severe damages on environmental areas. Global warming which is a serious problem due to massive exploitation and purification of fossil fuels, can increase the temperature of our planet's atmosphere. As a result of global warming, polar ices start to melt down. The melt down of polar ices and glaciers lead to sea level rise and coastal flooding. These disasters can cause many ecological, economical and environmental challenges. Therefore, it is reasonable to search for alternative kinds of energy sources.

Fuel cells are attractive alternatives to fossil fuels for production of energy from renewable energy sources^{1,2}. Among all renewable energy sources, methanol and ethanol are promising fuels for production of energy for many reasons. Firstly, their energy densities (ca. 6 and 8 kWh/kg, respectively) are very close to the energy density of gasoline (ca. 10 kWh/kg).³ Secondly, ethanol can be easily produced from many feedstocks such as sugarcane, corn, grape, cotton, potato, sunflower and even biomass. Also, unlike the transportation of hydrogen, transporting methanol and ethanol is less hazardous.

In a direct methanol fuel cell (DMFC), the complete oxidation of methanol occurs at the anode according to the following reaction.



Hydrogen ions pass to the cathode through the membrane and react with oxygen. As a result, reduction of oxygen takes place at the cathode,



Thus, the total net reaction will be,



And the $\Delta E^\circ_{\text{Rxn}} = E_{\text{cathode}} - E_{\text{anode}} = 1.23 - 0.046 = 1.18 \text{ V}$.⁴ However, the actual cell voltage is lower than the theoretical value of ca. 1.18 V due to slow kinetics at both the anode and cathode, and poisoning of the platinum catalyst at the anode by adsorbed species such as CO_{ads} and CH_X_{ads} .⁵⁻⁷ Moreover, a chemical reaction of methanol with O_2 occurs at the cathode due to the crossover of methanol through the membrane, and this decreases the cell voltage and efficiency of DMFCs. Also, it has been reported that during the oxidation of methanol, formaldehyde and formic acid are produced as by-products. Oxidation of methanol to formaldehyde and formic acid generates 2 and 4 electrons, respectively.⁸⁻¹⁰ As a result of this incomplete oxidation of methanol, the cell efficiency declines drastically.

The overall efficiency of a direct methanol fuel cell can be written as eq. 6.4,¹¹

$$\epsilon_{\text{cell}} = \epsilon_{\text{rev}} \epsilon_{\text{E}} \epsilon_{\text{F}} \quad (6.4)$$

Where ϵ_{rev} is theoretical efficiency, ϵ_{E} is the potential efficiency (ϵ_{E} is equal to $E_{\text{cell}}/E_{\text{rev}}$ where E_{rev} is the reversible cell potential of 1.18 V), and ϵ_{F} is the faradic efficiency. The faradaic efficiency is the ratio of the average number of electrons obtained per molecule of methanol (n_{av}) to the theoretical value of 6 ($\epsilon_{\text{F}} = n_{\text{av}}/6$). It is important to note that n_{av} is determined by the products distribution from the oxidation of methanol at the anode. It can be determined directly from the charge required to oxidize a known amount of methanol, or indirectly from measurement of all products quantitatively. Determination of n_{av} by product analysis suffers from inaccuracies and errors caused by methanol crossover and the volatility of the products.

Hence, we have reported an electrochemical method to measure n_{av} for methanol oxidation in DMFC hardware. This method is based on the electrochemical oxidation of fuel (methanol) at the anode when it crosses through the Nafion membrane from the cathode side of the DMFC to the anode compartment. To prohibit chemical reaction between oxygen and methanol, nitrogen was passed through the anode compartment.

The mass transport limited current (I_{lim}) for oxidation of methanol when it crosses the membrane at high fuel flow rates and high overpotentials can be used to determine n_{av} ,

$$I_{lim} = n_{av}fF \quad (6.5)$$

Where F is the Faraday constant and f is the flux ($\text{mol cm}^{-2} \text{s}^{-1}$) of fuel through the membrane.

At low fuel flow rates, the fuel concentration decreases as it passes through the cathode flow field. Hence, the local mass transport limited current density decreases with distance along the cathode flow field, and the total current decreases as the fuel flow rate is decreased. It has been shown that the relationship between current and fuel flow rate follows eq. 6.6,¹²

$$I = n_{av}FC_{in}u \left(1 - \exp \left(- \frac{I_{lim}}{n_{av}FC_{in}u} \right) \right) \quad (6.6)$$

In the chapter 5.3, eq. 6.6 is used to determine n_{av} values for a cell under crossover mode of operation in which methanol and ethanol were fed to the cell. However, it is more common to operate the cell as a fuel cell or in an anode polarization mode. Anode polarization curves are used to evaluate how a catalyst performs and measuring n_{av} in this mode can provide an indication of the product distribution in the cell. When the cell is operating in fuel cell mode it can produce power for industry and domestic purposes. Therefore, it is quite

useful to test eq. 6.6 for these two modes of operation. Again, it is good to recall that fuel losses due to crossover in a fuel cell decrease the efficiency of fuel cell. As a result, this method can not only give insight about product distribution but also may reveal the losses of fuel in the various operation modes.

Moreover, in the previous chapter, eq. 6.6 was only tested for the mass transport regions where the current was at the limiting value. In a fuel cell, currents are normally lower than the limiting current and so it is important to explore the method for potentials below the limiting current region.

The purpose of the work described in this chapter was to test eq. 6.6 for the different modes of operation of the cell shown schematically in Fig. 6.1. Furthermore, to evaluate and enhance the accuracy of the method, the concentration of methanol in the cell exhaust was measured by UV-visible spectrophotometry. Parts of this work have been published.¹⁷

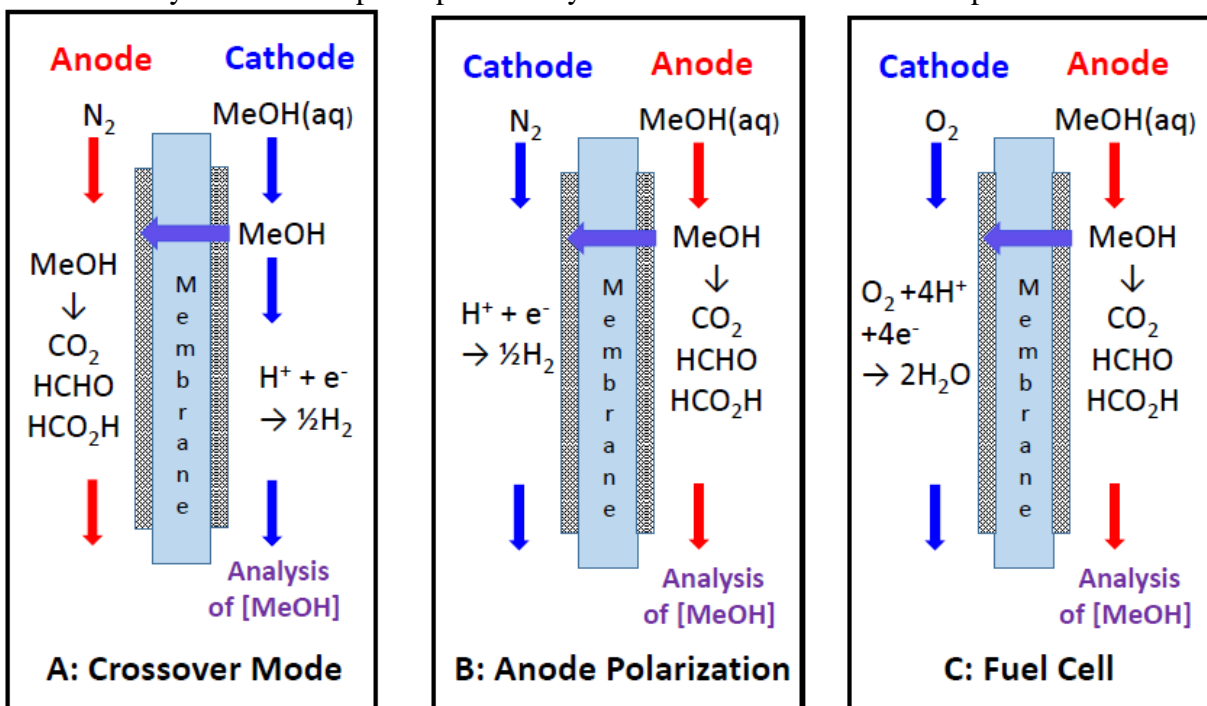


Figure 6.1. Illustration of the three modes of cell operation used in chapter 6.

6.2 Experimental

All the chemicals and apparatus that were used for experiments in this section were the same as in chapter 5.

Concentrations of methanol in the anode exhaust solution were measured spectrophotometrically with a Cary 100 UV-Visible Spectrophotometer. A sodium nitroprusside chromogenic reagent¹³ (2 mL; prepared from 100 mL sodium nitroprusside solution (10% w/v), 100 mL potassium ferricyanide solution (10% w/v), 100 mL sodium hydroxide solution (5% w/v) and 300 mL of deionized water) was added to 2 mL samples collected from the cell, and the absorbance was measured at 481 nm. Formaldehyde does not interfere at levels below 0.6 mg mL⁻¹ (20 mM) for 1.2 mg mL⁻¹ (37 mM) methanol.¹³ Based in the n_{av} values obtained in this work, the formaldehyde levels in the anode exhaust could not have exceeded 17 mM, and would have been much less due to further oxidation to formic acid, and diffusion into the cathode exhaust stream.¹⁴ Also, no interference was seen when 20 mM formic acid was added to a 50 mM solution.

6.3 Result and discussion

6.3.1 Crossover mode

In chapter 5, we described our method for determining n_{av} for the cell in crossover mode. In this mode, methanol is pumped to the cathode and the anode is supplied by N₂. Methanol diffuses from the cathode to the anode. In the anode, by imposing a potential, fuel can be oxidized to carbon dioxide, formaldehyde and formic acid (Fig 6.1 A). However, the method

for determining n_{av} would not be accurate if there was leakage of methanol from the cell or methanol was not quantitatively electrochemically oxidized in the anode. Therefore, the method may encounter errors and inaccuracies. The purpose of this section was to assess the accuracy. It is important to recall that in crossover mode, the cathode acts as a dynamic reference electrode.

To check the accuracy of the method by using measurements of methanol concentration in the cell exhaust ($C_{exhaust}$), it was necessary to calculate the theoretical concentration of methanol coming out of the cell.

In chapter 5, we showed that under steady state conditions, the concentration profile along the fuel flow field ($\frac{dC_{(x)}}{dx}$) can be written as eq. 6.7:

$$\frac{dC_{(x)}}{dx} = -\frac{D C_{(x)}}{lv} \quad (6.7)$$

D is diffusion coefficient ($\text{cm}^2 \text{s}^{-1}$), l is the thickness of the membrane, h is the height of the flow channel and v is the flow velocity (cm s^{-1}). The flow velocity can be written as,

$$v = \frac{u}{hw} \quad (6.8)$$

Where u is the volumetric flow rate ($\text{cm}^3 \text{s}^{-1}$) and w is the width of channel. Substitution of eq. 6.8 and 6.7 gives eq. 6.9,

$$\frac{dC_{(x)}}{dx} = -\frac{wDC_{(x)}}{lu} \quad (6.9)$$

The parameter D/l can be obtained from the limiting current,

$$I_{lim} = \frac{n_{av}FADC_{in}}{l} \quad (6.10)$$

Where F is the Faraday constant, A is the membrane area ($A = wd$, where d is the length of flow field), C_{in} is the initial concentration of methanol solution. Rearrangement of eq. 6.10 for D/l and then substitution of equation. 6.10 and 6.9 gives eq. 6.11,

$$\frac{dC_{(x)}}{dx} = -\frac{I_{lim}C_{(x)}}{Fn_{av}uC_{in}d} \quad (6.11)$$

Now, from the law of natural growth from calculus,

$$\frac{dC_{(x)}}{dx} = KC_{(x)} \quad (6.12)$$

By rearrangement and taking the integral of eq. 6.12,

$$\frac{dC_{(x)}}{C_{(x)}} = Kdx \quad (6.12)$$

$$\int \frac{dC_{(x)}}{C_{(x)}} = \int Kdx \quad (6.13)$$

By solving eq. 6.13,

$$\ln C_{(x)} = Kx + C \quad (6.14)$$

$$C_{(x)} = e^{Kx} \cdot e^C \quad (6.15)$$

And finally,

$$C_{(x)} = A e^{Kx} \quad (6.16)$$

the same method of calculus can be applied to eq. 6.11:

$$\int_{C_{(in)}}^{C_{(exhaust)}} \frac{dC_{(x)}}{C_{(x)}} = \int_0^d \frac{-I_{lim}}{uFn_{av}uC_{in}d} dx \quad (6.17)$$

$$\ln \frac{C_{exhaust}}{C_{in}} = - \frac{I_{lim}}{Fn_{av}uC_{in}d} d \quad (6.18)$$

With antilog from eq. 6.18,

$$\frac{C_{exhaust}}{C_{in}} = \exp\left(- \frac{I_{lim}}{Fn_{av}uC_{in}d}\right) \quad (6.19)$$

And finally,

$$C_{exhaust} = C_{in} \exp\left(- \frac{I_{lim}}{Fn_{av}uC_{in}d}\right) \quad (6.20)$$

Eq. 6.20. depicts how the concentration of methanol coming out of the cell decreases as the flow rate is decreased. In this equation, C_{in} is equal to the initial concentration of methanol pumped into the cell ($C_{in} = C_0$). Therefore, this equation can be used to calculate expected methanol concentration in the cell exhaust.

Table 6.1 shows experimental results and parameters derived from them for two different concentrations of methanol at high and low fuel flow rates (0.5 and 0.02 ml min⁻¹, respectively). As discussed in chapter 5, it is not necessary to make measurements at more than two flow rates to determine I_{lim} and n_{av} . A high flow rate can be used for estimation of the limiting current in the mass transfer region and low a flow rate is suitable for obtaining n_{av} due to the fact that the decrease in current and concentration of methanol are strongly related to n_{av} .

Also, two different concentrations of methanol (50 and 100 mM) were selected to show that the method is independent of fuel concentration. These experiments were performed at sufficiently high constant potential to make sure that the current was in the mass transport region. During the experiment, samples were collected from the cathode exhaust (Fig. 6.1A) at 0.5 and 0.02 mL min⁻¹ for analysis of the methanol concentration in the cell's exhaust by UV-visible spectrophotometry. The experimental values of current at different flow rates and concentrations of methanol were measured while the current readings were stable and free of fluctuations.

Table 6.1. Theoretical and experimental results for I_{lim} , $C_{exhaust}$ and n_{av} for 50 and 100 mM MeOH at two different flow rates at 50 °C and 0.7 V.

| C_0 (mM) | Flow rate (mL min ⁻¹) | I /mA (experimental) | I_{lim} /mA (calculated) | $C_{exhaust}$ /mM (experimental) | $C_{exhaust}$ /mM (calculated) | n_{av} |
|---------------|--------------------------------------|---------------------------|-------------------------------|-------------------------------------|-----------------------------------|----------|
| 50 | 0.5 | 18.6 | 19.4 | 46.1 | 46.0 | 5.7 |
| | 0.02 | 9.1 | | 8.4 | 6.0 | |
| 100 | 0.5 | 36.5 | 38.1 | 87.2 | 95.8 | 5.3 |
| | 0.02 | 17.2 | | 15.1 | 34.7 | |

The values of I_{lim} and n_{av} in this table were determined by simultaneously solving eq. 6.6 for the two flow rates. Then, the values of $C_{exhaust}$ (for each concentration of methanol) were determined by using results of n_{av} , I_{lim} and eq. 6.20. As can be seen from table 6.1, the experimental and calculated $C_{exhaust}$ agreed well for 50 mM methanol while discrepancies were

somewhat higher at 100 mM, but still within reasonable experimental uncertainty given that only two flow rates were employed. Since, in crossover mode, a very high potential was applied to the anode, methanol can only exit the cell from the cathode. Therefore, the reasonable agreement in the experimental C_{exhaust} (at the high flow rates) and C_0 are showing that there was no leakage of methanol in the cell.

On the other hand, the amount of methanol that crosses the membrane from the cathode to the anode, is electrochemically oxidized to products. The n_{av} values in the table 6.1 are representative of relative rates of electrochemical reactions 5.1, 5.2 or 5.3. They are close to the value of 6 for complete oxidation of methanol to carbon dioxide, however, they indicate that there was also some partial oxidation of methanol to formaldehyde and/or formic acid.

Although variation in the characteristics of the membrane (hydration level, thickness, etc.) and electrodes (e.g. accumulation and oxidation of adsorbates) during the course of experiments can effect the method, the data in the Table 6.1 shows it is valid and provides reasonable estimates of n_{av} . However, data obtained at additional flow rates should be employed to increase precision.¹⁷

6.3.2 Anode polarization mode

Evaluation of fuel cell catalyts is often performed in an anode polarization mode (Fig. 6.1 B). In this mode, the cell acts as an electrolysis cell in which fuel is pumped to the anode and N_2 supplied to the cathode. In this cell set-up, the cathode acts as a dynamic hydrogen electrode, and chemical reaction with oxygen (used as the cathode in a fuel cell) is avoided.

To check the validity of eq. 6.6 for operation of a cell in anode polarization mode, methanol was pumped to the anode (Fig. 6.1 B). Now, there are three pathways for the methanol: electrochemical oxidation at the anode, crossover from the anode to the cathode via the membrane and exhaust of unreacted methanol from the anode. Therefore, in addition to measuring the current vs. flow rate to determine n_{av} , the methanol concentration in the cell exhaust was measured by UV-visible spectrophotometry ($\lambda=481$ nm).

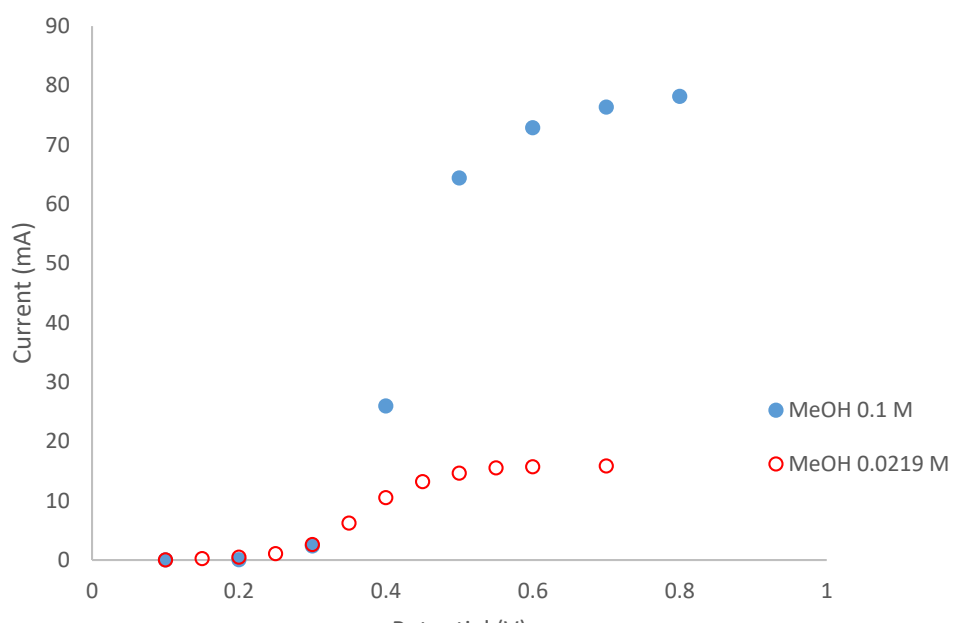


Figure 6.2. Anode polarization curves for the oxidation of 111 mM and 21.9 mM methanol at 50°C in the cell configurations in Fig. 6.1B. The methanol flow

To check the validity of eq. 6.6 for different concentrations of methanol, solutions with concentrations of 21.9 mM and 111 mM methanol were pumped to the cell in anode polarization mode. The temperature of the experiments was fixed at 50 °C. To reach the mass transport region (the limiting current value), a potential of 0.7 V was applied to the anode of the cell. Fig. 6.2 shows the polarization curves, these experiments, which were conducted at a sufficiently high flow rate (0.5 mL min⁻¹) to prevent significant changes in concentration of fuel in the flow field. The high current generation (I_{lim}) at each concentration is because of oxidation of all the fuel reaching the anode. It can be seen from this figure that the limiting current decreased when methanol concentration was decreased, from ca. 85 mA to ca. 17 mA for 111 mM methanol and 21.9 mM methanol, respectively.

Table 6.2 shows experimental currents, anode exhaust concentrations, and apparent n_{av} values for the cell in Fig. 6.2B, when the cathode was purged with nitrogen.

Table 6.2. Theoretical and experimental results for I_{lim} , $C_{exhaust}$ and n_{av} for 21.9 mM and 111 mM MeOH at two different flow rates at 50 °C and 0.7 V for the cell in anode polarization mode.

| C_0 (mM) | Flow rate (mLmin ⁻¹) | I /mA (experimental) | I_{lim} /mA | $C_{exhaust}$ /mM (experimental) | $C_{exhaust}$ /mM (calculated) | n_{av} |
|---------------|-------------------------------------|---------------------------|---------------|-------------------------------------|-----------------------------------|----------|
| 21.9 | 0.5 | 17.1 | 19.3 | 17.4 | 17.0 | 4.3 |
| | 0.02 | 3.01 | | 3.5 | 0.04 | |
| 111 | 0.5 | 84.0 | 93.2 | 85.4 | 90.0 | 5.0 |
| | 0.05 | 44.4 | | 27.7 | 13.6 | |

The measured concentration of methanol in the cell exhaust (C_{exhaust}), I_{lim} and n_{av} values in the table 6.2 were determined by simultaneously solving the eq. 6.6 and 6.20 for two different flow rates. In anode polarization mode, when the potential was in the limiting current region (the plateaus at the polarization curves in Fig. 6.2) all of the methanol reaching to the anode catalyst layer is oxidized. Therefore, crossover of methanol from the anode through the membrane can not occur. In Table 6.2, the high concentrations of methanol in the anode exhaust at the high flow rate confirms that methanol crossover was negligible. From table 6.2, the values of n_{av} were 4.3 and 5 for 21.9 and 111 mM methanol, respectively. These low electron generations indicate that methanol undergoes some partial oxidation to formaldehyde and/or formic acid under these conditions. It has been shown that partial oxidation of methanol to formaldehyde or formic acid leads to lower electron generation at the surface of platinum.¹⁵

16

As can be seen from table 6.2, there was a significant difference between the experimental and calculated C_{exhaust} values at the low fuel flow rate for 21.9 mM methanol. From the table 6.2, at the low flow rate (0.02 mL min^{-1}) for 21.9 mM methanol, the experimental C_{exhaust} (measured by UV-vis spectrophotometry) was ca. 3.5 mM, while the calculated C_{exhaust} (from eq. 6.20) is ca. 0.04 mM. This high value of the experimental C_{exhaust} can be attributed to the oxidation of the methanol molecules that had been adsorbed (during the previous experiment at 0.5 mL min^{-1}) into porous anode graphite plate. Note that the higher experimental C_{exhaust} over the calculated C_{exhaust} (27.7 mM vs. 13.6 mM) at 111 mM methanol clearly shows that crossover has not taken place in the cell.

To check eqs. 6.6 and 6.20 for a potential below the limiting current region, where crossover is inevitable, the anode potential was decreased from 0.7 V to the half-wave potential of 0.35 V. During experiments with 111 mM methanol, we became concerned that the production of carbon dioxide bubbles at high methanol concentration could cause an error in the application of eq. 6.6. Moreover, at the high concentration of fuel, the ohmic resistance of the cell becomes a significant phenomenon in the cell. Therefore, experiments were conducted only with 21.9 mM methanol.

Table 6.3 depicts the experimental and calculated results for current and C_{exhaust} of the cell in an anode polarization mode for 21.9 mM methanol, with the potential constant at 0.35 V (half-wave potential).

Table 6.3. Theoretical and experimental results for I_{lim} , C_{exhaust} and n_{av} for 21.9 mM MeOH at Different flow rates at 50 °C and 0.35 V for the cell in anode polarization mode.

| C_0 (mM) | Flow rate (mL min ⁻¹) | I/mA (experimental) | I_{lim} /mA (calculated) | C_{exhaust} /mM (experimental) | C_{exhaust} /mM (calculated) | n_{av} |
|---------------|--------------------------------------|------------------------|--------------------------------------|--|--|-----------------|
| 21.9 | 0.5 | 8.3 | 8.8 | 17.8 | 19.8 | 5.1 |
| | 0.02 | 3.6 | | 4.6 | 1.9 | |

Solving eq. 6.6 for the data in table 6.3 gave $n_{\text{av}} = 5.1$. The calculated C_{exhaust} values were determined by using calculated I_{lim} and n_{av} values. The calculated concentrations of methanol in the cell exhaust were 19.8 mM and 1.9 mM for high and low flow rates, respectively. In table 6.3, at the half-wave potential, the experimental limiting current was only ca. 50% of the current at 0.7 V. It is important to note that in the cell, electrochemical oxidation of methanol

produces a faradaic current. Crossover of methanol to the cathode results in loss of methanol that will not produce any current. The higher calculated C_{exhaust} vs. the experimental C_{exhaust} (19.8 mM vs 17.8 mM) clearly shows that there was significant crossover of fuel from the anode to the cathode.

In order to account for methanol crossover at potentials below the limiting current region, the model described in chapter 6 has been modified. The modified treatment can be found in our published paper.¹⁷

6.3.3 Operation of the cell as a fuel cell

Fuel cells are attractive energy production devices due to their many advantages over fossil fuels. However, fuel crossover from the anode to the cathode, and also oxygen crossover from the cathode to the anode can decrease the cell efficiency¹⁸⁻²⁰. Therefore, to study the effect of fuel crossing from the anode to the cathode on the use of eq. 6.6, the cell was operated in fuel cell mode (Fig. 6.1C). In this mode (galvanic cell), methanol was pumped to the anode while air was passed through the cathode. There are four pathways for the methanol: electrochemical oxidation at the anode, chemical reaction with oxygen that crosses over from cathode to the anode, crossover to the cathode and exhaust from the anode. The purpose of this section was the measurement values of n_{av} for a real fuel cell and assessment of the effect of crossover.

Fig. 6.4 shows a polarization curve for a cell operated as a fuel cell (Fig. 6.1 C). To ensure that the current reached the mass transport region, a low concentration of methanol was

pumped to the anode (21.25 mM methanol). In fuel cell mode, both the anode and the cathode potentials change as the potential is varied.

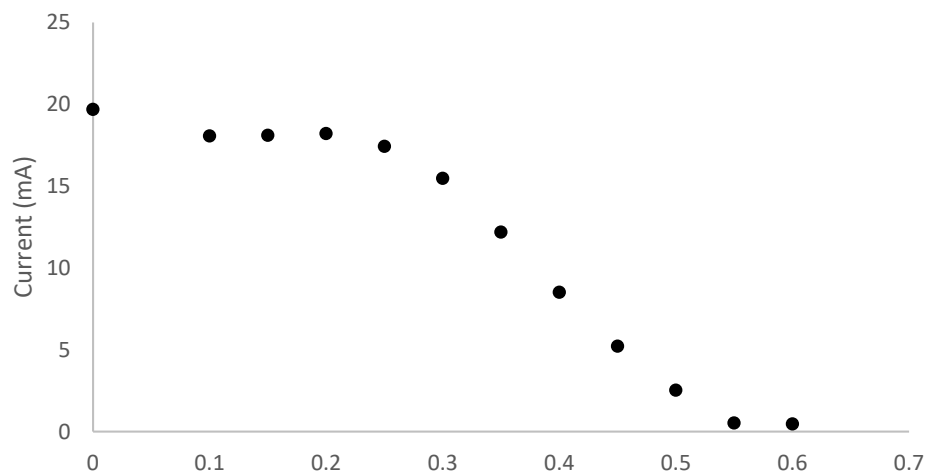


Fig. 6.3. Fuel cell polarization curves for the oxidation of 21.25 mM methanol at 50°C in the cell configuration shows in Fig. 6.1C. The methanol flow rate was 0.5 mL min⁻¹. The cathode. was purged with air.

Based on the polarization curve, two different potentials were selected for the n_{av} measurements: a constant potential of 0 V where the fuel cell is operating in the mass transport region and 0.4 V (half-wave) where crossover takes place due to the mixed diffusion and kinetic control of the current. Table 6.4 illustrates data for experiments when 21.25 mM methanol was pumped to the anode of fuel cell at low and high fuel flow rates at these two different potentials. In this table, n_{av} values were obtained by fitting the current values to equation 6.6.

In the limiting current region (0 V), where current generation is limited by the mass transport of methanol from the bulk to the anode catalyst layer, fuel crossover should not take place. The much higher value of the experimental $C_{exhaust}$ (18.8 mM) than the calculated

C_{exhaust} (15.5 mM) at the high flow rate (Table 6.4) clearly implies that methanol crossover was minimal. It also indicates that n_{av} has been underestimated by use of equation 6.6.

Table 6.4. Theoretical and experimental results for I_{lim} , C_{exhaust} and n_{av} for 21.25 mM MeOH at two different flow rates at 50°C for a fuel cell at two different potentials.

| Potential (V) | Flow rate (mL min ⁻¹) | I_{lim} /mA (experimental) | I_{lim} /mA (calculated) | C_{exhaust} /mM (experimental) | C_{exhaust} /mM (calculated) | n_{av} |
|------------------|--------------------------------------|--|--------------------------------------|--|--|-----------------|
| 0 | 0.5 | 18.4 | 21.5 | 18.8 | 15.5 | 4 |
| | 0.02 | 2.7 | | 2.5 | 0.008 | |
| 0.4 | 0.5 | 9.4 | 10.4 | 18.04 | 17.3 | 2.9 |
| | 0.02 | 2.00 | | 3.15 | 0.12 | |

Solving eq. 6.6 for the limiting current region (0 V) gave $n_{\text{av}} = 4.0$. This low value of electron generation in the mass transport region indicates a partial oxidation of methanol to formaldehyde and/or formic acid at the surface of the anode catalyst layer (complete oxidation of methanol to carbon dioxide produces 6 electrons). In fact, it has been shown that partial oxidation of methanol to formic acid can be a significant reaction in a fuel cell.^{12, 20-22}

Although oxygen crossover from the cathode could lead to chemical reaction in the anode and decrease the methanol concentration, the high concentration of methanol in the cell exhaust at the low flow rate shows that this was not significant.

In the potential region below the limiting current, crossover of methanol from the anode to the cathode is inevitable in the cell. When the potential was constant at 0.4 V, there

would have been a significant methanol concentration at the interface between the anode catalyst layer and the membrane. This would lead to loss of methanol into the cathode and chemical reaction between oxygen and fuel. As a result of this chemical reaction, the efficiency of the fuel cell would be decreased dramatically.

In table 6.4 when the potential was below the limiting current region, the calculated limiting current dropped to ca. 48% of the limiting current in the mass transfer region. Solving eq. 6.6 for the currents at a fixed potential of 0.4 V (Table 6.4) gave an n_{av} of 2.9. This low value, together with the low calculated concentration of methanol in the $C_{exhaust}$ at the high flow rate, indicates that eq. 6.6 is inaccurate here due to crossover. This was confirmed by modelling of the effects of crossover in our published paper.¹⁷

6.4 Conclusion

Measurements of mass transport limited currents for methanol oxidation in fuel cell hardware as a function of flow rate can provide an estimate of the average number of electrons obtained per methanol molecule (n_{av}). Measurements of n_{av} were performed in two different potential ranges. In the high potential region, current generation reaches the limiting current value, where mass transport of fuel to the electrode is controlled by methanol diffusion. As a result, imposing a high potential to the anode may lead to oxidation of methanol to carbon dioxide, formic acid/formaldehyde. In the lower potential region (e.g. at the half-wave potential) crossover of methanol across the membrane takes place. Methanol crossover caused errors at the lower potentials where the current was less than current in the mass transport region. Also,

it was shown that in the lower potential region, analysis of methanol concentration is necessary.

It was found that when the cell was operated in anode polarization mode, incomplete oxidation of methanol to formic acid/formaldehyde was significant in the mass transport region. It was shown that errors and inaccuracies due to crossover of methanol were significant in the lower potential region in anode polarization mode.

In the fuel cell mode, incomplete oxidation of methanol to formic acid was significant in the mass transfer region. At potentials below the limiting current region, the low value of n_{av} (2.9) indicated that fuel crossover needs to be taken into account.

Finally, it is clear that use of only two flow rates of fuel (especially with the low flow rate of 0.02 mL min^{-1}) is not enough for accurate determination of n_{av} value. Also, adsorption of fuel into the graphite plates of the cell can be caused of error in n_{av} calculation. Therefore, to obtain better results, it is necessary to use more different flow rates of fuel for determination of n_{av} value. Additionally, the cell needs to be modified to fill the pores of the graphite plates.

References

1. Akhairi M, Kamarudin SK. Catalysts in direct ethanol fuel cell (DEFC): An overview. *Int J Hydrogen Energy*. 2016; 41:4214-4228.
2. Zakaria Z, Kamarudin SK, Timmiati S. Membranes for direct ethanol fuel cells: An overview. *Appl Energy*. 2016; 163:334-342.
3. Lamy C, Belgsir E, Leger J. Electrocatalytic oxidation of aliphatic alcohols: Application to the direct alcohol fuel cell (DAFC). *J Appl Electrochem*. 2001; 31:799-809.
4. Kamarudin S. K, Achmad F, Daud W. R. W. Overview on the application of direct methanol fuel cell (DMFC) for portable electronic devices. *Int J Hydrogen Energy*. 2009;34: 6902-6916.
5. Kamarudin M, Kamarudin S. K, Masdar M, Daud W. R. W. Review: Direct ethanol fuel cells. *Int J Hydrogen Energy*. 2013; 38:9438-9453.
6. Brouzgou A, Podias A, Tsiakaras P. PEMFCs and AEMFCs directly fed with ethanol: A current status comparative review. *J Appl Electrochem*. 2013; 43:119-136.
7. Jusys Z, Kaiser J, Behm R. Methanol electrooxidation over Pt/C fuel cell catalysts: Dependence of product yields on catalyst loading. *Langmuir*. 2003; 19:6759-6769.
8. Jusys Z, Behm R. Methanol oxidation on a carbon-supported pt fuel cell catalyst a kinetic and mechanistic study by differential electrochemical mass spectrometry. *The Journal of Physical Chemistry B*. 2001; 105:10874-10883.
9. Wang H, Löffler T, Baltruschat H. Formation of intermediates during methanol oxidation: A quantitative DEMS study. *J Appl Electrochem*. 2001; 31:759-765.

10. Fan Q, Pu C, Smotkin E. In situ fourier transform Infrared-Diffuse reflection spectroscopy of direct methanol fuel cell anodes and cathodes. *J Electrochem Soc.* 1996; 143:3053-3057.
11. Coutanceau C, Brimaud S, Lamy C, et al. Review of different methods for developing nanoelectrocatalysts for the oxidation of organic compounds. *Electrochim Acta.* 2008; 53:6865-6880.
12. Majidi P, Pickup P. G. Determination of the average number of electrons released during the oxidation of ethanol in a direct ethanol fuel cell. *Electrochim Acta.* 2015; 182:856-860.
13. Zhan Y, Zhang Y, Li Q, Du X. A novel visible spectrophotometric method for the determination of methanol using sodium nitroprusside as spectroscopic probe. *J Chin Chem Soc.* 2010; 57:230-235.
14. James D. D, Pickup P. G. Effects of crossover on product yields measured for direct ethanol fuel cells. *Electrochim Acta.* 2010; 55:3824-3829.
15. Bagotzky V, Vassilyev YB. Mechanism of electro-oxidation of methanol on the platinum electrode. *Electrochim Acta.* 1967; 12:1323-1343.
16. Marković N. M, Gasteiger H. A, Ross P. N, Jiang X, Villegas I, Weaver MJ. Electro-oxidation mechanisms of methanol and formic acid on pt-ru alloy surfaces. *Electrochim Acta.* 1995; 40:91-98.
17. Majidi P, Altarawneh R. M, Ryan N. D, Pickup P. G. Determination of the efficiency of methanol oxidation in a direct methanol fuel cell. *Electrochim Acta.* 2016; 199:210-217.
18. Arico A, Srinivasan S, Antonucci V. DMFCs: From fundamental aspects to technology development. *Fuel cells.* 2001; 1:133-161.

19. Cruickshank J, Scott K. The degree and effect of methanol crossover in the direct methanol fuel cell. *J Power Sources*. 1998; 70:40-47.
20. Heinzl A, Barragan V. A review of the state-of-the-art of the methanol crossover in direct methanol fuel cells. *J Power Sources*. 1999; 84:70-74.
21. Iwasita T. Electrocatalysis of methanol oxidation. *Electrochim Acta*. 2002; 47:3663-3674.
22. Bittins-Cattaneo B, Iwasita T. Electrocatalysis of methanol oxidation by adsorbed tin on platinum. *Journal of electroanalytical chemistry and interfacial electrochemistry*. 1987; 238:151-161.

Chapter 7

Summary and future work

7.1 Summary

It was shown that potential modulation increased the chemical efficiency of a direct ethanol fuel cell and an ethanol electrolysis cell by promoting carbon dioxide production. Also, the effect of potential limits for Pt and Pt-Ru anode catalysts was explored. It was shown that when cyclic potentials were applied to the cell, the yield of carbon dioxide was more than that of the cell with linear sweep potentials. Also, with the application of cyclic potentials, the amplitude of the current was reasonably positive and stable. In contrast, the current generation decayed very quickly with use of constant potentials. The effect of temperature was investigated on the ethanol oxidation reaction. It was shown that the chemical efficiency of the ethanol oxidation reaction was increased at higher temperatures. Furthermore, it was found that although the Pt-Ru anode provided lower yields of carbon dioxide than Pt, it significantly decreased the anode potential.

An AC voltage was applied on the fuel cell. It was shown that with the sinusoidal waveform, the carbon dioxide production and current generation were increased. With the AC potential, ethanol was adsorbed and dissociated at the cell potential peaks. In the minima of the cell potential, when the current was high, adsorbed carbon monoxide was oxidized to carbon dioxide and as a result, the chemical efficiency of the ethanol oxidation reaction increased.

A new methodology for determining the average number of electrons (n_{av}) released during ethanol oxidation was developed. This method, which was independent of the type of fuel, was based on the quantitative oxidation of fuel at the anode when it passed through the membrane. It was found that the n_{av} values were related to the dependence of the cell current

on the fuel flow rate. To eliminate any error due to oxygen crossover, the anode was purged with nitrogen. Fuel (ethanol or methanol solution) was pumped to the anode (crossover mode). It was shown that in crossover mode and at high potential (the limiting potential and mass transfer region), when ethanol solution was pumped to the cathode, the n_{av} values increased with increasing in temperature of the cell. On the contrary, when the concentration of ethanol was increased, n_{av} values decreased.

To increase the accuracy of the method, the concentration of fuel in the cell exhaust was determined by UV-visible spectroscopy. Also, the method was applied on an electrolysis cell in anode polarization mode (methanol at the anode, nitrogen at the cathode). It was shown that at the mass transfer region in anode polarization mode, incomplete oxidation of methanol to formic acid/formaldehyde was a significant pathway. The method was also used for the cell in anode polarization mode for potentials below the mass transfer region where fuel crossover is inevitable.

Finally, the method was checked for a real fuel cell. The low value of n_{av} when zero potential was applied to the fuel cell, indicated that partial oxidation of methanol was significant. However, at 0.4 V an unreasonably low value of n_{av} indicates that crossover caused errors for the method. Hence, the method needed some modifications.

7.2 Future work

Based on the results obtained in this research, there are some areas that should be further explored. Other catalysts (such as Pt-Sn or Pt-Rh) should be used to investigate potential modulation on the ethanol oxidation reaction. In this work, only the chemical yield of carbon

dioxide was measured with an IR-detector. However, for better analysis, other ethanol oxidation products such as acetic acid, acetaldehyde, ethane and methane should be measured. One way is the use of *in situ* infrared spectroscopy such as subtractively normalized interfacial Fourier transform infrared spectroscopy (SNIFTIRS) or single potential alteration surface infrared spectroscopy (SPAIRS). These spectroelectrochemical techniques can provide more accurate data about EOR products.

As mentioned in the chapter 3, the response time of the carbon dioxide detector was long. Therefore, for more accurate and precise reading of carbon dioxide signal, it is necessary to develop a system with a shorter response time to the carbon dioxide signal.

Also, the method that was developed for determination of the n_{av} value needs further modification for the potentials below the mass transfer region. One way to achieve this goal is to input a new mathematical term in eq. 5.13 as a crossover parameter. Also, to enhance the accuracy of the method, the anode and the cathode exhausts of the cell in the anode polarization mode and a real fuel cell should be measured quantitatively. To achieve this, the anode and cathode exhaust should be combined and measured with a spectroscopy technique, such as NMR.

The method that we developed here, was only evaluated for the methanol and ethanol oxidation reactions at platinum catalyst. It should be further examined for other catalysts such as Pt-Ru, Pt-Sn¹⁻³ and Pt-Rh⁴ which have shown better activities toward the ethanol oxidation reaction.

References,

1. Akhairi M. A. F, Kamarudin, S. K, Catalysts in direct ethanol fuel cell (DEFC).
Int J Hydrogen Energy. 2016; 41:4214-4228.
2. Tóth M, Varga E, Oszkó A, Baán K, Kiss J. Erdőhelyi A. Partial oxidation of ethanol on supported Rh catalysts: Effect of the oxide support. Journal of Molecular Catalysis Chemical. 2016; 411:377-387.
3. Zignani, S. C, Baglio V, Sebastián D, Siracusano S, Aricò A.S, Enhancing ethanol oxidation rate at Pt/Ru electro-catalysts using metal-oxide additives. Electrochim Acta, 2016; 191:183-191.
4. Higuchi E, Takase T, Chiku M, Inoue H, Preparation of ternary Pt/Rh/SnO₂ anode catalysts for use in direct ethanol fuel cells and their electrocatalytic activity for ethanol oxidation reaction J. Power Sources, 2014; 263:280-287.

